Graduate School ETD Form 9
(Revised 12/07)

PURDUE UNIVERSITY
GRADUATE SCHOOL
Thesis/Dissertation Acceptance

This is to certify that the thesis/dissertation prepared

By Daniel Eugene Minner

Entitled
Design of Biomembrane-Mimicking Substrates of Tunable Viscosity to Regulate Cellular Mechanoresponse

For the degree of Doctor of Philosophy

Is approved by the final examining committee:

Christoph A. Naumann
Chair

Eric C. Long

Daniel Suter

Kavita Shah

To the best of my knowledge and as understood by the student in the *Research Integrity and Copyright Disclaimer (Graduate School Form 20)*, this thesis/dissertation adheres to the provisions of Purdue University's "Policy on Integrity in Research" and the use of copyrighted material.

Approved by Major Professor(s): Christoph A. Naumann

Approved by: Martin J. O'Donnell 11/30/2010
Head of the Graduate Program Date

Graduate School Form 20
(Revised 9/10)

PURDUE UNIVERSITY
GRADUATE SCHOOL

Research Integrity and Copyright Disclaimer

Title of Thesis/Dissertation:

Design of Biomembrane-Mimicking Substrates of Tunable Viscosity to Regulate Cellular Mechanoresponse

For the degree of Doctor of Philosophy

I certify that in the preparation of this thesis, I have observed the provisions of *Purdue University Executive Memorandum No. C-22,* September 6, 1991, *Policy on Integrity in Research.**

Further, I certify that this work is free of plagiarism and all materials appearing in this thesis/dissertation have been properly quoted and attributed.

I certify that all copyrighted material incorporated into this thesis/dissertation is in compliance with the United States' copyright law and that I have received written permission from the copyright owners for my use of their work, which is beyond the scope of the law. I agree to indemnify and save harmless Purdue University from any and all claims that may be asserted or that may arise from any copyright violation.

Daniel Eugene Minner

Printed Name and Signature of Candidate

11/30/2010

Date (month/day/year)

*Located at http://www.purdue.edu/policies/pages/teach_res_outreach/c_22.html

DESIGN OF BIOMEMBRANE-MIMICKING SUBSTRATES OF TUNABLE VISCOSITY TO REGULATE CELLULAR MECHANORESPONSE

A Dissertation

Submitted to the Faculty

of

Purdue University

by

Daniel Eugene Minner

In Partial Fulfillment of the

Requirements for the Degree

of

Doctor of Philosophy

December 2010

Purdue University

Indianapolis, Indiana

ACKNOWLEDGMENTS

I would like to first thank my advisor, Dr. Christoph Naumann, for providing me with such a challenging and interdisciplinary project that has afforded various collaborations and has even allowed me to study abroad. Of these collaborators, I would like to express my appreciation to the lab of Josef Käs for providing supplies and technical expertise in the live cell imaging needed to complete this research and in particular Johannes Stelzer and Philipp Rauch for their contributions to this work. Additionally, the lab of Ben Fabry and Wolfgang Goldmann donated focal transfection vectors, stably transfected cells, and provided the software and knowledge needed to complete the force traction microscopy experiments along with their student Andreas Schörnborn. I would also like to recognize Guilherme Sprowl for his hard work in performing the single particle tracking analysis for the characterization of the newly designed multibilayer substrates. Thanks go out to all the past and current members of our research lab that I have had the pleasure of working with. In particular, Mike Murcia who not only trained me in quantum dot synthesis, but got me excited about research and played a large role in my decision to pursue the Ph.D. track, and Amanda Siegel for her friendship and her enthusiasm, which I found so

motivating (I also could not have asked for a better thesis editor). I am grateful to my friends and family for all of their encouragement over the years. Lastly, I thank my wife Jacki, not only for her support and understanding, but also for instilling such confidence in me.

TABLE OF CONTENTS

Page

LIST OF TABLES

LIST OF FIGURES

Figure Page

Figure Page

Figure Page

LIST OF ABBREVIATIONS

AFM	Atomic force microscopy.
APS	Ammonium persulfate.
CDF	Cumulative distribution function.
CTF	Cellular traction force.
DGS-NTA(Ni)	1,2-dioleoyl-sn-glycero-3-[(N-(5-amino-1-carboxypentyl)-iminodiacetic acid)succinyl] (nickel salt).
DIC	Differential interference contrast microscopy.
DMEM	Dulbecco's Modified Eagle Medium.
DPPC	1,2-dipalmitoyl-sn-glycero-3-phosphocholine.
DPTE	1,2-dipalmitoyl-sn-Glycero-3-Phosphothioethanol (Sodium Salt).
D_R	Rotational diffusion.
DSF	Dorsal stress fiber.
D_T	Translational diffusion.
ECM	Extracellular matrix.
Epi	Epifluorescence.
FA	Focal adhesion.
FBS	Fetal bovine serum.

FPS	Frames per second.
FRAP	Fluorescence recovery after photobleaching.
FTM	Force traction map.
G(*t*)	Autocorrelation function.
GFP	Green fluorescent protein.
GFP-actin	Green fluorescent protein tagged actin.
GFP-FAK	Green fluorescent protein tagged focal adhesion kinase.
GMBS	(N-[g-Maleimidobutyryloxy]succinimide ester).
GUV	Giant unilamellar vesicle.
HAD	Hexadecylamine.
HEPES	4-(2-hydroxyethyl)-1-piperazineethanesulfonic acid.
HS	Horse serum.
LB	Langmuir-Blodgett.
LINC	Linker of nucleoskeleton and cytoskeleton.
LS	Langmuir-Schaefer.
MSD	Mean squared displacement.
NA	Numerical aperture.
NBD-PE	N-(7-nitrobenz-2-oxa-1,3-diazol-4-yl)-1,2-dihexadecanoyl-sn-glycero-3-phosphoethanolamine, triethylammonium salt (NBD-PE).
NGF	Nerve growth factor.
PAA	Polyacrylamide.
PBS	Phosphate buffered saline.
PEG	Polyethylene glycol.

PEG2000	1,2-distearoyl-sn-glycero-3-phosphoethanolamine-N-[methoxy-(polyethylene glycol)-2000] (ammonium salt).
PEG2000-MAL	1,2-distearoyl-sn-glycero-3-phosphoethanolamine-N-[maleimide(polyethylene glycol)-2000] (ammonium salt).
PEG2000-NHS	1,2-distearoyl-sn-glycero-3-phosphoethanolamine-N-[NHS-Active Ester(polyethylene glycol)-2000] (ammonium salt).
$PMOX_{50}$	1,2-distearoyl-sn-gycero-3-phosphoethanolamine-N-polymethyloxazoline(50).
POPC	1-palmitoyl-2-oleoyl-sn-glycero-3-phosphocholine.
QD	Quantum dot.
SDS	Sodium dodecyl sulfate.
SMFM	Single molecule fluorescence microscopy.
SMFM-TF	Total internal reflectance-based single molecule fluorescence microscopy.
SOPC	1-stearoyl-2-oleoyl-sn-glycero-3-phosphocholine.
Sulfo-Sanpah	N-Sulfosuccinimidyl-6-(4'-azido-2'-nitrophenylamino) hexanoate.
SUV	Small unilamellar vesicle.
TA	Transverse arc.
TBP	Tributylphosphine.
TEMED	N,N,N′,N′-Tetramethylethylenediamine.
TFM	Traction force microscopy.
t_{lag}	Time lag.
TOP	Trioctylphosphine.
TOPO	Trioctylphosphine Oxide.

TR-DHPE	Texas Red® 1,2-dihexadecanoyl-sn-glycero-3-phosphoethanolamine, triethylammonium salt.
TRITC	Tetramethylrhodamine isothiocyanate.
TRITC-DHPE	N-(6-tetramethylrhodaminethiocarbamoyl)-1,2-dihexadecanoyl-sn-glycero-3-phosphoethanolamine, triethylammonium salt (TRITC-DHPE).
TYPE 1	Polymer-supported phospholipid bilayer-based cell substrate.
TYPE 2	Multibilayer-based cell substrate.
VSF	Ventral stress fiber.
VF	Vesicle fusion.

ABSTRACT

Minner, Daniel Eugene. Ph.D., Purdue University, December, 2010. Design of Biomembrane-Mimicking Substrates of Tunable Viscosity to Regulate Cellular Mechanoresponse. Major Professor: Christoph Naumann.

Tissue cells display mechanosensitivity in their ability to discern and respond to changes in the viscoelastic properties of their surroundings. By anchoring and pulling, cells are capable of translating mechanical stimuli into a biological response through a process known as mechanotransduction, a pathway believed to critically impact cell adhesion, morphology and multiple cellular processes from migration to differentiation. While previous studies on polymeric gels have revealed the influence of substrate elasticity on cellular shape and function, a lack of suitable substrates (i.e. with mobile cell-substrate linkers) has hindered research on the role of substrate viscosity. This work presents the successful design and characterization of lipid-bilayer based cell substrates of tunable viscosity affecting cell-substrate linker mobility through changes in viscous drag. Here, two complementary membrane systems were employed to span a wide range of viscosity. Single polymer-tethered lipid bilayers were used to generate subtle changes in substrate viscosity while multiple, polymer-interconnected lipid bilayer stacks were capable of producing dramatic changes in substrate

viscosity. The homogeneity and integrity of these novel multibilayer systems in the presence of adherent cells was confirmed using optical microscopy techniques. Profound changes in cellular growth, phenotype and cytoskeletal organization confirm the ability of cells to sense changes in viscosity. Moreover, increased migration speeds coupled with rapid area fluctuations suggest a transition to a different migration mode in response to the dramatic changes in substrate viscosity.

CHAPTER 1. INTRODUCTION

1.1. Rationale and Objectives

An important aspect of mechanobiology is that tissue cells are anchorage-dependent and respond to viscoelastic changes in their environments. Adherent cells continually probe their surrounding environment through actomyosin generated pulling forces. Mechanical information gained in this sensing process is then translated into an appropriate biological response through a process known as mechanotransduction. Thus, mechanical properties such as substrate viscoelasticity and dimensionality are increasingly recognized as key components in cellular mechanoresponse and changes in these substrate properties have been observed to induce changes in cellular responses from phenotype to migration, and even non-localized processes such as differentiation. Moreover, with changes in tissue stiffness arising in such pathogenic states as fibrosis and cancer, many researchers have proposed a correlation between disease and mechanical stimuli [1-10]. However, despite its accepted importance, many elements of the mechanotransduction process remain elusive. While particular components have been identified, it remains largely unclear how these components orchestrate a specific cellular response

toward mechanical stimuli. A major obstacle in this area of research has been a lack of suitable cell substrates.

Traditional cell substrates such as culture glass and plastic fail to replicate a cell's native environment and often induce cellular morphologies and functions that are uncharacteristic, and at times strikingly different, than those found in tissue. The development of 2D polyacrylamide (PAA) gels and 3D collagen matrices with adjustable viscoelastic properties better replicate tissue environments and have been used to demonstrate a cell's ability to respond to changes in substrate viscoelasticity in the absence of external chemical signals. These platforms have provided insight into the process of mechanotransduction by revealing the mechanical-dependence of cell morphologies, motility, proliferation, differentiation, and more [2, 3, 8, 9, 11-17].

However, while viscoelastic properties of the aforementioned substrates can be tuned through varying the concentration of polymer crosslinkers, design aspects of these substrates predict that changes primarily impact elasticity. This is a result of the immobilized cell/substrate linkers present in these substrates. Though the degree of crosslinking in these gels does simultaneously affect the amount a cell can push/pull and remodel the substrate, the distance a cell linker can be displaced is finite. Thus, the immobilized cell linkers present in PAA gels fall short of replicating the dynamic cell-cell attachments present in the extracellular matrix (ECM) of tissue cells. Only a fluid system containing mobile

cell/substrate linkers can truly address the role of substrate viscosity in the mechanotransduction process. Viscosity is expected to influence various cell behaviors including cell morphology and migration, as these processes are closely related to the assembly and disassembly of focal adhesions or focal complexes, processes that appear to depend, at least partially, on the lateral diffusion of adhesion receptors in the plasma membrane [7, 18-22]. In order to separately investigate the contributions of substrate elasticity and viscosity, a substrate comprised of mobile cell-substrate linkers must be designed.

Herein, phospholipid bilayer-based cell substrates were designed and constructed to complement existing polymeric substrates in the study of mechanotransduction. Contrary to PAA gels, lipid bilayers represent comparatively thin substrates ill-suited for elasticity regulation. However, the fluid nature of lipids comprising artificial membranes makes them ideal candidates for studies exploring the impact of substrate viscosity. The viscosity of lipid bilayers can be regulated in a variety of ways from lipid composition to altering the degree of frictional coupling experienced by solid-supported lipid bilayers. Lipid bilayer-based systems, containing specific cell linkers of adjustable density, can be used to regulate cellular mechanoresponse through substrate viscosity affecting linker mobility, as shown in Figure 1.1.

In addition, lipid bilayers behave similarly to plasma membranes and are routinely modified with various proteins. Thus, not only can viscosity, a

mechanical aspect, be tuned, but lipid-bilayer substrates can be made to express various biological stimuli as well. This allows the fine tuning of these substrates for specific applications and extends their ability to truly mimic biological membranes in biochemical, mechanical, and dynamic aspects.

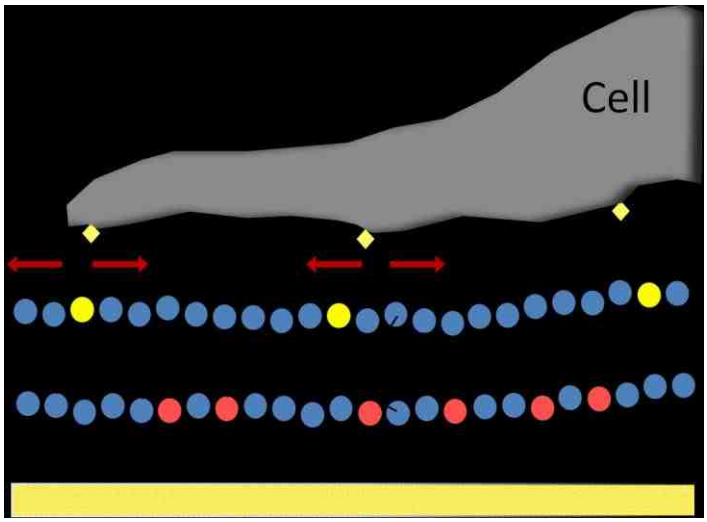

Figure 1.1. A phospholipid bilayer, which behaves as a two dimensional fluid results in mobile cell-substrate linkers.

The research described within this dissertation focuses on the development of artificial cell substrates well suited to investigate the impact of viscosity on cellular mechanoresponse. This report will be divided into four main objectives:

Objective 1: Design, fabrication, and characterization of fluid, lipid bilayer-based, biomembrane-mimicking cell substrates of adjustable viscosity

Objective 2: Confirming substrate integrity under the force of adherent cells

Objective 3: Design and fabrication of suitable cell-substrate linkers

Objective 4: Exploring the role of substrate viscosity in cellular mechanoresponse

1.2. Organization

This dissertation is organized into five chapters. The first chapter provides the rationale and key objectives of this study and describes the organizational structure of the dissertation. The second chapter introduces various methods and instrumentation utilized in this research. The second chapter also contains theoretical introductions to the structure and function of phospholipid bilayers, lipid membrane diffusion theory, and cellular mechanotransduction and motility. The third chapter details the materials and technical procedures utilized to construct cell substrates, to link cells to these substrates, to test and characterize these substrates and to identify and quantify cellular response on these substrates. The fourth chapter contains results and discussion regarding cell substrate design and characterization, including substrate integrity confirmation linker design and functionality, and cellular mechanoresponse toward substrate viscosity. Lastly, chapter five summarizes the key conclusions put forth by this research.

CHAPTER 2. BACKGROUND

2.1. Methodology

2.1.1. Langmuir-Blodgett Film Deposition

Solid supported phospholipid bilayers were assembled using previously reported Langmuir-Blodgett (LB)/Langmuir Schaefer (LS) film deposition techniques [23-25] or through the fusion of giant unilamellar vesicles (GUVs). It was desirable to have the most homogeneous, defect-free phospholipid bilayers possible to minimize any unwanted cellular interaction is the underlying glass support. While vesicle fusion techniques are straightforward and perhaps the most routinely used procedures for creating supported lipid bilayers, they are prone to more bilayer defects and are limited to the formation of symmetric bilayers. In contrast, asymmetric, polymer-tethered lipid bilayers are easily prepared using a LB/LS approach and reliably provide the well-defined, homogenous films needed for single bilayer cell substrates [26, 27], as well as a uniform starting layer for the assembly of multibilayer substrates. The ability to prepare asymmetric films using a LB/LS technique comes from the two-part procedure depicted in Figure

2.1, where the inner and outer leaflets of lipid bilayers are deposited sequentially. Using this technique, the inner leaflet of an asymmetric (or symmetric) bilayer is first prepared through LB transfer, Figure 2.1 (A), where a glass substrate is submerged in a Teflon-coated trough and a lipid mixture is spread. Lipids are then compressed via a motorized barrier arm to a surface pressure of 30mN, as monitored by a surface pressure detector. The amphiphilic character of lipids causes them to properly self-orient at the air-water interface so that the hydrophobic lipid tails are exposed to air and the hydrophilic head groups (including the polymer moieties of lipopolymers in this case) interact with the water. A lipid monolayer is deposited onto a glass substrate by attaching the glass substrate to a motorized dipper arm and raising the assembly through the aqueous subphase, while the motorized barrier maintains a constant surface pressure.

The outer leaflet of an asymmetric (or symmetric) bilayer is completed using the LS procedure shown in Figure 2.1 (B). In a similar approach, a lipid mixture is spread and compressed. However, here the LB-monolayer is deposited onto the LS monolayer, to form a complete bilayer, by pressing the glass substrate through the air-water interface.

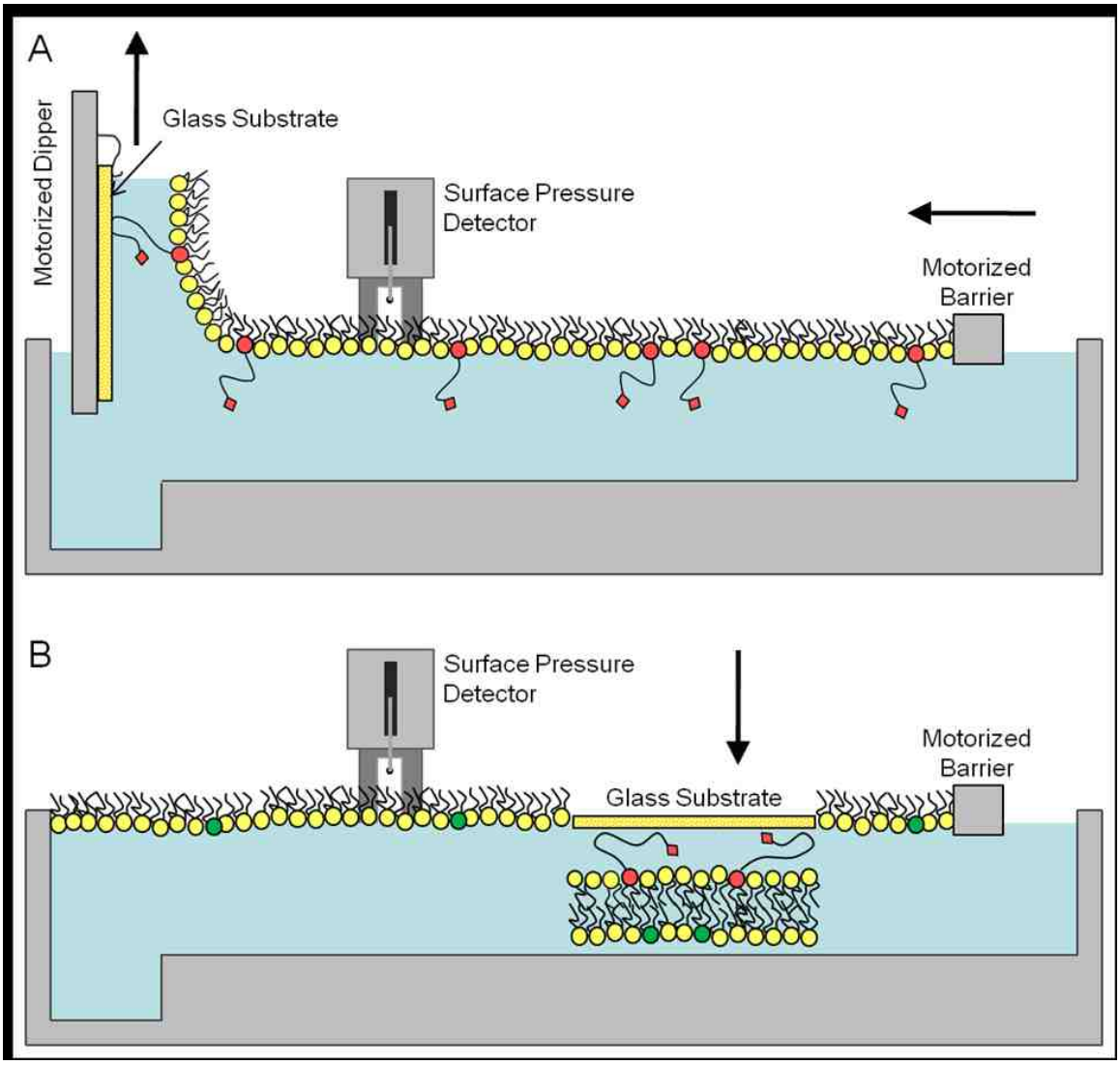

Figure 2.1. Phospholipid bilayer fabrication with the use of a Langmuir trough and LB (A) and LS (B) techniques.

2.1.2. Single Molecule Fluorescence Microscopy

Single molecule fluorescence microscopy (SMFM) is an experimental technique used to determine the position of fluorescent molecules at a sub-diffraction resolution. Thus, this technique is ideal for studying the dynamic properties of small, nanometer-sized molecules (e.g. dye-labeled lipids in phospholipid bilayers). Moreover, this technique which has increased resolving power over ensemble averaging techniques such as fluorescence recovery after photobleaching, FRAP, provides a more accurate depiction of diffusion properties. While diffraction-limited techniques like FRAP are readily used to obtain lateral diffusion coefficients of lipid bilayers, the information acquired represents the average diffusion characteristics of a large population of lipids. In contrast, imaging and tracking through SMFM provides a detailed account of an individual fluorophore's movement over time. SMFM is particularly superior in describing diffusion in heterogeneous systems as SMFM imparts the ability to see subpopulations with different diffusion properties, as well as specific types of diffusion (e.g. confined, directed, anomalous), information which is lost in the ensemble techniques, but that proves valuable in understanding diffusion within a complex biological system such as a plasma membrane of cells. Here subpopulations with differing diffusion properties (e.g. domains) are anticipated and bilayer fluidity is thought to serve a role in regulating biological functions within biomembranes.

Two forms of SMFM were employed in the experiments conducted within this thesis, namely SMFM using wide-field fluorescence and SMFM using total internal reflectance (SMFM-TF). While both methods allow for accurate SMFM, one can prove advantageous over the other depending on the properties of the sample to be imaged. More traditional wide-field techniques are well suited for imaging applications on thicker samples, samples requiring longer working distance objectives, and samples where autofluorescence is not a concern. Wide-field SMFM was used to characterize the fluidity of the newly designed phospholipid bilayer-based cell substrates, as these samples do not display any autofluorescent properties. However, TIRF-based SMFM (SMFM-TF) was used in the characterization of QD-based cell-substrate linkers. Here QD-tagged lipids were tracked in live cell membranes, making cellular autofluorescence an obvious issue. TIRF images result in improved signal-to-noise by reducing background. By directing light to a sample at an extremely oblique angle, TIRF is capable of illuminating thin planes. Here, evanescent waves selectively excite fluorophores present in this plane and with the evanescent field decaying rapidly, out of plane fluorescence is largely eliminated. In the case of studying dynamics within the cellular plasma membrane, TIRF proves beneficial in reducing background caused by cellular autofluorescence. SMFM imaging and tracking analysis are described, in detail, in Chapters 3.2.2 and 3.2.7.

2.1.3. Fluorescence Correlation Spectroscopy

Fluorescence Correlation Spectroscopy (FCS) is a confocal technique capable of measuring the diffusion time, brightness, and size (hydrodynamic radius) of fluorophores at the single molecule level. Its application to the characterization of quantum dots can reveal the aggregation state, emission intensity, and concentration of these nanoparticles. The concept of FCS is outlined in Figure 2.2.

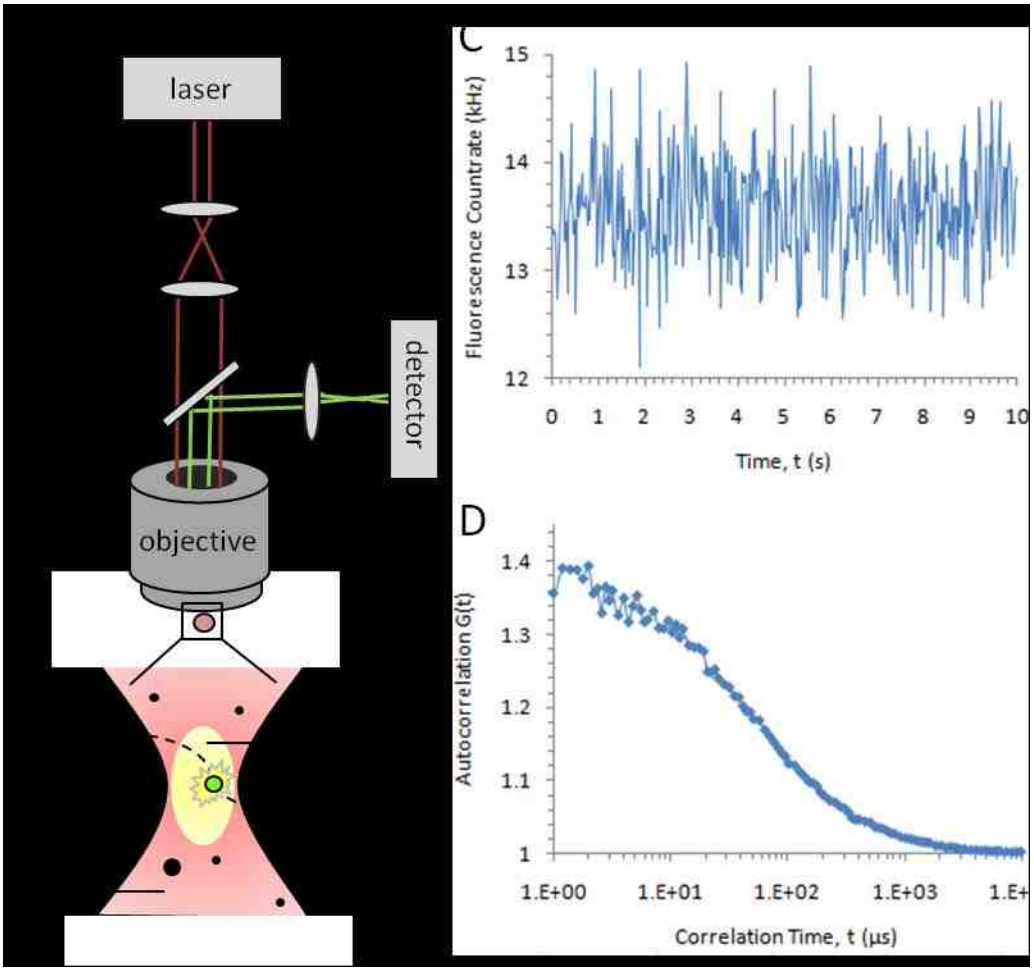

Figure 2.2. Schematic of FCS instrumental setup (A) and the confocal volume created (B). Fluorescent fluctuations (C) are recorded as fluorophores diffuse through the confocal volume and are used to calculate an autocorrelation curve (D).

In Figure 2.2, (a) represents a general schematic for a FCS microscope where a laser beam is expanded and then focused onto a fluorescent sample which, in this case, is a bulk solution. Fluorescent signal from the sample is then reflected by a dichroic mirror and is eventually passed through a confocal aperture before reaching avalanche photodiode detectors. The confocal aperture blocks out of plane fluorescence to create a small, discrete confocal volume, as shown in Figure 2.2. (b). The observation volume depicted in Figure 2.2 (b) represents the actual confocal volume, on the order of a femtoliter, in which fluorescent particles are excited and detected.

Fluctuations in the fluorescence signal, resulting from fluorophores diffusing through the confocal volume, are recorded over time as shown in Figure 2.2. (c). These fluctuations along with the average fluorescent signal, F(*t*), are then translated into an autocorrelation function using computer software, Figure 2.2. (d). Here, the fluorescent fluctuation from the average intensity, δF(*t*), is correlated to a later time, (*t*+ τ), to produce an autocorrelation function, G(*t*), shown below.

$$G(\tau) = 1 + \frac{\langle \delta F(t) \delta F(t+\tau) \rangle}{\langle F(t) \rangle^2} \qquad \text{Eq. 2.1}$$

The confocal excitation volume is best described as 3D Gaussian volume, and setting Eq. 2.1 equal to the autocorrelation function of a 3D Gaussian allows specific fluorophore properties such as diffusion times, average single particle intensities, and the number of particles present in the confocal volume to be

extracted. A detailed description of FCS data analysis, and how it can be used to determine nanoparticle aggregation state and concentration, is found in Chapter 3.2.6

.

2.1.4. Differential Interference and Phase Contrast Microscopy

Brightfield microscopy, which simply requires a basic light microscope, relies on differences in light absorption to produce contrast. However, absorbance differences among transparent cellular components are subtle. Differential Interference Contrast (DIC) and Phase Contrast microscopy are complementary techniques used to add contrast to cellular images, allowing organelles and other cellular components to be observed. Both techniques rely on changes in the phase shift of light passing through a sample.

Phase contrast microscopy amplifies these changes in light phase by inserting a phase annulus (or phase ring) with a matched objective containing a phase plate into the light path. The phase plate contains a centered, ring-shaped area, which matches the annulus, and that retards light exactly a quarter-wavelength. A light source is directed through the annulus, the sample, and then the objective before hitting the phase plate. If the annulus is properly aligned with the phase plate, direct (non-diffracted, or background) light is passed through the phase plate and is retarded in phase by a quarter-wavelength, before it reaches the eyepiece (or camera). However, light that passes through the sample is diffracted due to

differences in thickness and refractive index within the specimen. This light, when passing through the phase plate, is retarded by up to an additional quarter-wavelength. Light from both diffracted and non-diffracted light interact at the image plane to create interference. Here, the interference resulting from differences in phase create bright and dark regions within the specimen (i.e. constructive and destructive interference). One disadvantage of phase contrast, depending on its application, is the formation of “phase halos” or glowing edges along the boundaries of specimen and background. These are a consequence of the phase-retarding ring of the phase plate also transmitting small amounts of the light diffracted from the specimen.

While similar to phase contrast, DIC uses a more sophisticated light path containing polarizing filters and prisms to transform changes in the refractive index of cellular components into visible contrast in the image. A key benefit to this technique is the disappearance of phase halo artifacts present in phase contrast images. Additionally, eliminating the masking effects of the phase annuli raises the working numerical aperture and adds resolution. With DIC, polarized light is passed through a Wollaston prism where it is separated into a sampling ray and a reference ray that are then focused on a condenser lens, which in effect supplies the sample with two light sources roughly 0.2µm apart. As the two rays penetrate the sample, their optical path is determined by changes in the refractive index of various components within the cell sample and their phase becomes different. Upon exciting the sample, the two rays are recombined via a

second Wollaston prism. However, their phase differences result in interference at the prism, which is revealed as brighter or darker areas. When imaging thicker cells with DIC, it is important to note that any dimensionality seen in the images is a merely a result of optical, not true geometrical, topographical changes. This is a result of DIC using differences in optical path to add contrast. In fact, even thin cells are given an artificial 3D appearance. However, DIC proves extremely valuable when analyzing adherent cells for information such as cellular phenotype, cellular area, migration, and more. With DIC being an interference technique, the edges of cell shapes are easily visualized when compared to phase contrast images where more 3D (i.e. thicker) cells appear to have "glowing" edges (i.e. phase halos). Instead, resulting DIC images are typically characterized by dark edges and bright cell shapes against a dark grey background.

2.1.5. Epi and Confocal Microscopy

Fluorescence microscopy holds several advantages over conventional light microscopy. Primarily, it allows imaging of specific components within a sample, through the addition of fluorescent markers to regions of interest. Unlike conventional light microscopy, fluorescent microscopy uses a higher intensity light source to excite specific fluorophores, which in turn, emit a distinct wavelength longer than that of the excitation source. This fluorophore property, known as the Stoke's shift, enables excitation light to be separated from emitted

light, using specific optical filters, to create a fluorescent image. In the case of Epi microscopy, a mercury arc-discharge lamp is commonly used as a low wavelength excitation source that is passed through a set of excitation filters that allow only a specific window of wavelengths to proceed to a dichroic mirror, through the objective, and onto the sample; proper excitation filters are chosen based on the specific absorption properties of the fluorophore used. Light emitted by the sample is then directed back through the objective, dichroic mirror, and through a set of emission filters before reaching the detector (or camera). Emission filters are used to remove excitation light, or background, from the image by allowing only a specific window of wavelengths (characteristic to the fluorophore) to pass. Thus, properly chosen filter sets also allow for dual labeling and imaging of multiple components. While Epi microscopy creates bright, vibrant fluorescent images through the use of a high intensity lamp generating a large excitation volume, this factor may prove disadvantageous depending on the properties of the sample. Epi microscopy may be ill-suited in studies with low signal, and where photobleaching is a concern. Moreover, resolution is lost in thicker samples due to a large excitation volume exciting out-of-plane fluorophores. Such samples are better candidates for confocal microscopy.

Confocal microscopy operates in a similar manner to Epi microscopy, but the addition of a monochromatic excitation source and a confocal aperture aid in eliminating out of plane (background) fluorescence. Here, the excitation lamp is replaced by a laser, which scans the sample. The use of a scanning laser results

in smaller excitation volumes which help to eliminate background by exciting only a thin plane through x-y scanning; this difference is depicted in Figure 2.3. Additionally, a confocal aperture, added before the detector, blocks out-of-focus light, resulting in a sharper image. In this system, a camera is no longer used to capture images. Instead, images are reconstructed by computer from intensity information acquired point by point through scanning. With these components in place, resolution in x-y, and z are enhanced. In the case of thicker samples, the ability to image optical sections with reduced background fluorescence results in clearer fluorescent images throughout a sample and allows for 3D rendering. Additionally, different scanning modes can be used to simultaneously acquire multi-labeled images, while eliminating fluorophore cross talk much more efficiently than Epi microscopy.

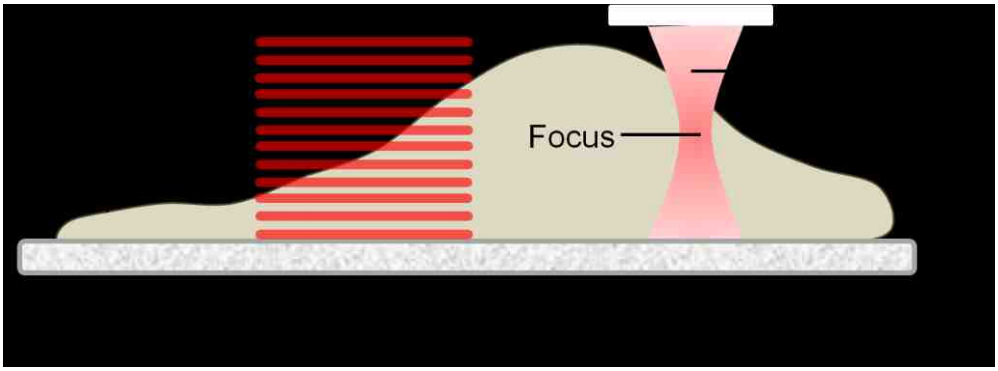

Figure 2.3. Comparison of the excitation volumes created using confocal and wide-field illumination techniques.

2.1.6. Traction Force Microscopy

Many cell types, including fibroblasts, are anchorage dependent and require adhesion to a substrate to survive [28-30]. Following attachment, such cells generate internal pulling forces that trigger various biological responses through the process of mechanotransduction, which is discussed in detail in Chapter 2.4. Cellular traction forces (CTFs) play roles in key processes including inflammation, wound healing, embryogenesis, angiogenesis, metastasis, and more [29]. The biological relevance of CTFs has prompted various methods designed to measure these forces.

Early methods of measuring CTFs consisted of embedding cells within collagen gels. Here, a reduction in the diameter of the collagen disk, resulting from cells pulling, could be used to estimate the CTFs exerted by the embedded cells [29, 31]. However, this method suffers from being an ensemble averaging technique unable to provide CTF information for individual cells. In an effort to obtain such data, thin silicone membranes were designed to wrinkle under the stress of individual, adherent cells. However, while wrinkling was easily observed, determining the amount of force required to generate these wrinkles posed a problem; this information was approximated by determining the amount of force needed for a flexible microneedle to reverse the effect [29, 32]. Another approach has involved the creation of micromachined cantilever arrays [33]. In this system CTFs of individual cells are determined through beam deflection as

the cantilevers are displaced. However, only deflection changes in a single direction can be monitored.

The limitations of these techniques have led to the development of traction force microscopy (TFM). Here, substrate designs including micropatterned elastomers [18] and microneedle-like posts [34] have been created to measure CTFs on individual cells. In these techniques, displacements of micropatterned designs are visualized through brightfield microscopy and used to deduce CTFs. Yet, while designs such as this are elegant and capable of providing CTF information for individual cells in all directions, these methods have their disadvantages. Aside from fabrication aspects, these substrates are only applicable for certain cell types because the elasticity of the stiffer elastomers used can only be varied over a small range and cannot be adjusted low enough to capture small deformations [29]. Thus, these techniques are ill-suited for the study of cells which generate low CTFs (e.g. neurons). Moreover, the use of brightfield techniques, which lack the resolution of fluorescence imaging, further fail to provide information on smaller CTFs.

The use of PAA gels as TFM substrates has addressed many of the limitations described above. These gels can be tuned over a physiologically relevant range of 100Pa to 100kPa [35]. Furthermore, micron-sized fluorescent beads are easily embedded in these substrates and allow substrate displacements to be visualized, at high resolution, through fluorescence microscopy [36-40]. As in the

previous methods, cells are plated and allowed to adhere and spread. A high resolution fluorescent image is then taken underneath an adherent cell to acquire a “force-loaded” image. Cells are then detached from the substrate and a second fluorescent snapshot is taken as a “null-force” image [30]. The “null force” images represent the positions of the fluorophores prior to the adhesion of cells and because PAA gels are also linearly elastic in response to forces, the deformations resulting from CTFs are completely recovered upon removal of the force [8, 41].

After obtaining “null-force” and “force-loaded” images, three main methods have been used to determine the displacement of the fluorescent beads. The methods include the Butler, et al. method [38], the Dembo Wang method [39, 42], and the Yang, et al. method [30]. Using these methods, bead placement is identified based on pixel intensity values in the “null force” and “force-loaded” fluorescent images. The above methods represent different tracking algorithms used to identify the displacement of individual beads. With bead displacements known, the force required to induce such displacement can be calculated based on the elastic modulus of the PAA gel. Computer software such as Matlab provides an important tool capable of efficiently determining bead displacement and calculating CTFs.

2.2. Solid-Supported Phospholipid Bilayer Systems

2.2.1. Solid-Supported Phospholipid Bilayer

In biological systems, membranes not only function to compartmentalize cellular components, but also host much of the machinery for cellular communication and transport across the membrane [43]. Despite being only nanometers thick, cellular membranes are dynamic, complex, and take the form of a two dimensional fluid (created by the hydrophobic interactions of lipid molecules) with embedded and transiently associated membrane proteins that are free to diffuse about [44]. Although fluid, biological membranes are highly ordered in the membrane plane as first described by the fluid mosaic [45, 46], which is largely a result of the diffusion properties of these systems. For example, the lateral diffusion of constituent lipids across the membrane is rapid while flip-flop (or transverse) diffusion occurs on a much slower time scale [47]; this property imparts the ability to establish asymmetry across the two leaflets of a membrane [45]. Moreover, phase separation between various lipid components can create protein rich environments (i.e. lipid rafts) which organize proteins laterally across the membrane.

For these reasons, the lipid bilayer represents one of the most important self-assembled structures in nature and was accepted as the basic principle of design for biological membranes more than 40 years ago [43, 45]. Since this time,

interest in the lateral structure of membranes and the way they regulate the activity of constituent membrane proteins has prompted the design of cell mimetic surfaces [48]. The application of solid support phospholipid bilayers as artificial cell membrane systems in the study of biomembrane structure and function was a logical progression. While free lipid bilayers mimic the dynamic processes of biological membranes, the planar geometry of solid supported bilayers allowed for the study of biological membranes with analytical instrumentation [43]. Since their development in the early 1980s, solid supported bilayers have been used as artificial membranes to study lipid phase behavior and domain formation; membrane protein structure, localization and function; membrane receptors, pores, and channels; and more [44, 45]. In fact, some of the earliest implementations of solid supported membranes were for purposes of live cell studies, and this continues to be a promising area of growth [48, 49].

The amphipathic properties of phospholipids, resulting from their hydrophilic headgroup and hydrophobic tails, cause their spontaneous self-assembly into a variety of supramolecular assemblies when hydrated [50]. In an effort to minimize energetically unfavorable interactions with water molecules, hydrophobic tails aggregate (towards the interior of the membrane) and orient hydrophilic headgroups towards the aqueous surroundings [50]. Taking advantage of this self assembly process, supported lipid bilayers are fabricated by one of the following three methods: the Langmuir-Blodgett(LB)/Langmuir-Schaefer(LS) technique, vesicle fusion (VF) techniques, or a combination LB/VF

technique. Each method has advantages and disadvantages depending on the application.

The fusion of lipid vesicles is routinely used in the formation of solid supported bilayers [49, 51, 52] primarily due to the ease of this approach. Small unilamellar vesicles (SUVs) or giant unilamellar vesicles (GUVs) can be used in this technique. SUVs can be prepared using a variety of methods from multilamellar vesicle extrusion [43, 53] to sonication and ultracentrifugation techniques [43, 54] and GUVS can be prepared by sucrose hydration [55, 56], electroformation [55, 57], and even the fusion of large unilamellar vesicles. However they are prepared, vesicles are added to a solid support where they adsorb and rupture into a lipid bilayer. Despite the simplicity of this approach, the straightforward addition of membrane proteins into lipid vesicles adds much versatility to this method [43]. However, the underlying mechanisms of vesicle fusion are not completely understood and the process is affected by many factors including vesicle composition, size, surface charge and roughness, pH, and ionic strength [58]. For these reasons, solid supported bilayers prepared using this method often contain more defects.

Historically, the LB/LS technique was the first method used to prepare supported bilayers [25, 45] and is still routinely used to create well defined bilayers with minimal defects. In this method, which was described in detail in Chapter 2.2.1, a lipid monolayer is first deposited onto a solid substrate using the LB technique

with the use of a Langmuir trough. This is done by a submerging the solid support, spreading (and compressing) a lipid monolayer at the air-water interface, and slowly withdrawing the substrate through the air-water interface while maintaining constant surface pressure (see Chapter 2.2.1). This constructs the first inner monolayer. The lipid bilayer is completed with the addition of a second monolayer (the outer leaflet of the bilayer), which is prepared in a similar fashion. In this LS method, following spreading and compression, the outer leaflet is added by pushing the solid-supported monolayer horizontally through the air-water interface. The compression process of this fabrication method produces high quality bilayers and is advantageous in that the inner and outer leaflets of the bilayer are prepared in different steps. This allows for the preparation of more complex, asymmetric, solid-supported bilayers**.** The disadvantage of this method is that is that the reconstitution of membrane proteins can be difficult.

The combination of these techniques, LB/VF [24] proves useful for applications involving reconstituted membrane proteins. Here, the fusion of SUVs atop a predeposited monolayer (formed by LB techniques) is used to create a solid supported bilayer. Like LB/LS techniques, this method is highly efficient for the formation of asymmetric membranes and, like VF techniques, membrane proteins are easily incorporated. While VF techniques suffer from increased bilayer defects, LB formation of the inner leaflet provides a quality base that is likely to reduce the probability of defects.

Regardless of fabrication method, the goal of solid supported bilayers is to capture the rich biological functionality that emerges when lipids and membrane proteins are permitted to move freely, and in all of the fabrication methods described above, bilayer fluidity is preserved [48]. This is a result of electrostatic, van der Waals, and hydration forces trapping the bilayer in a plane separated from the support by a 1-2nm thick layer of water [43]. This thin lubrication layer prevents the solid from interfering with the lateral fluidity of phospholipids. Moreover, the planar geometry of solid supported bilayers makes the fluidity easy to characterize using techniques such as fluorescence recovery after photobleaching and single particle tracking.

2.2.2. Polymer-Supported Phospholipid Bilayer

The fabrication of a biomembrane mimicking model system requires the preservation of both lipid and protein fluidity as many biological processes are regulated by peripheral and integral protein interactions [59]. While the solid-supported bilayers discussed in Chapter 2.2.1. maintain the diffusivity of lipids and peripherally attached protein components [25, 45, 60], these systems typically display limited to immobile integral membrane mobility [43]. This is a result of the trapped water layer between the bilayer and solid support, which was described in Chapter 2.2.1. This thin 1-2nm layer of water provides a sufficient lubrication layer capable of supporting lipid fluidity. However, this gap is not large enough to accommodate the extracellular domains of many integral

membrane proteins. The close proximity of these membranes to their underlying solid-support represents a fundamental drawback in these membrane systems as the frictional coupling experienced by membrane proteins can dramatically hinder lateral mobility and non-specific van der Waals interactions (effective over distances up to approximately 3nm) can immobilize and potentially denature these proteins [59].

Efforts to decouple supported membranes from their underlying solids and minimize unwanted and non-physiological protein-solid support interactions have led to the design of polymer-supported phospholipid bilayers [45]. Here, polymer supports have included such techniques as the formation of polymer cushions composed of polyacrylamide [61]**,** polyethylenimine [62]**,** or other hydrophilic polymers; the use of lipid-based spacer and tethers including silanized polyethyleleglycol-lipids [27], or lipopolymers [26, 63, 64]. However, regardless of the approach, the basic principle remains the same: reduction of frictional coupling by increasing membrane-substrate gap distance. Moreover, polymer-supported lipid bilayers maintain their 2D, planar structure. In addition, aside from decoupling the artificial membrane, such polymer supports add to membrane complexity and in some applications make them more biologically relevant as a well designed polymer cushion may behave much like the cytoskeleton [43].

The polymer-supported phospholipid bilayers utilized within this thesis were fabricated with the use of lipopolymers. In these systems, lipopolymers, or lipids with macromolecule headgroups, act as physiosorbed substrate-membrane spacers that decouple the artificial membrane from its solid support. These lipopolymer-containing bilayers can be prepared using the fabrication techniques discussed in Chapter 2.2.1 and have the advantage of added tunability over other forms of polymer cushions. In these systems, the membrane-substrate distance and the viscosity of the polymer layer, properties that impact the lateral diffusivity of membrane proteins and lipid assemblies, can be regulated through spacer length and lateral spacer density [59]. Moreover, the concentration of polymer tethers has been used to induce obstructed diffusion and further regulate the mobility of membrane components [63, 64]; this application is discussed in Chapter 4.1.1.

2.2.3. Multibilayer Systems

An alternative strategy to increase membrane-substrate gap distance is the formation of multibilayer stacks. Like their polymer-supported counterparts, the assembly of a double bilayer system can be used to increase membrane-substrate distance and in theory reduce the frictional coupling experienced by membrane constituents in close proximity to their solid-support. Multibilayer systems can be prepared through the successive transfer of monolayers [65] using the dipping methods described in Chapter 2.2.1, but are more often

fabricated by adding a second bilayer onto a solid-supported bilayer through the fusion of giant unilamellar vesicles (GUVs) [56, 66]. Here, GUVs are brought in contact with the underlying solid-supported bilayer via gravity. The addition of electrostatic lipids [56] or specific biotin/streptavidin functionalized lipid tethers [66] into the GUVs promotes adsorption and rupture into a fluid bilayer. While these double bilayer substrates were primarily developed for the study of membrane-membrane junctions and biological processes occurring in areas of close membrane proximity (e.g. replication of membranous organelles), the outermost membrane in multibilayer substrates have shown unique diffusion properties relative to the size of diffussants (e.g. individual lipids compared to lipid domains) [48]. Like the polymer-supported bilayers in Chapter 2.2.2, diffusion theory (discussed in Chapter 2.3) predicts that it should be possible to decouple and reduce frictional coupling through the formation of multibilayer systems used to increase membrane-substrate distance.

2.3. Diffusion Theory in 2D Model Membranes

2.3.1. Diffusion in Free Lipid Bilayers: Saffman-Delbrück Theory

Brownian diffusion within a lipid membrane is characterized by a translational (and rotational) diffusion coefficient. In the case of planar diffusion, as experienced by the lateral movement of lipids and proteins in a phospholipid

bilayer, the translational diffusion coefficient is related to the mean squared displacement (MSD) of a particle, Eq. 2.2, where *D* and *t* represent the diffusion

$$MSD = 4Dt \qquad \text{Eq 2.2.}$$

coefficient and time respectively and the factor of 4 relates to the dimensionality of movement (in the case of 1D movement, or rotational diffusion, this factor is replaced with a 2).

The diffusion of larger macromolecules (e.g. lipid clusters or proteins) in a sea of smaller molecules can be analyzed as cylinders, with an axis perpendicular to the planar membrane, moving under Brownian motion [67]. Under this assumption, and by accounting for a finite membrane size, the finite viscosity of the surrounding fluid, and irreversible thermodynamics, Saffman and Delbrück developed Eq. 2.3 to describe macromolecule diffusion in free lipid bilayers. Here, D_T and D_R represent translational and rotational diffusion respectively.

$$D_T = \frac{k_B T}{4\pi\mu h}\left(log\frac{\mu h}{\mu' a} - \gamma\right) \qquad D_R = \frac{k_B T}{4\pi\mu a^2 h} \qquad \text{Eq 2.3.}$$

In both equations, *k* is Boltzmann's constant, *T* is temperature, μ is the viscosity of the lipid membrane, μ' is the viscosity of the surrounding fluid (i.e. water), h is the thickness of the membrane, γ is Euler's constant, and a is the radius of the cylinder modeling the macromolecule.

2.3.2. Diffusion in Solid-Supported Membranes: Sackmann-Evans Theory

The Saffman-Delbrück model predicts the translation diffusion coefficient to have a logarithmic dependence on particle size. This is a biologically important consequence in that proteins (decoupled from the actin-cytoskeleton) can diffuse at rates comparable to that of lipids [68, 69]. However, while this unique property occurs in free lipid bilayers, the diffusion of larger molecules is hindered in solid-supported membranes; lipids within solid-supported membranes experience slowed diffusion rates and larger molecules show diffusion rates orders of magnitude lower than lipids [69]. This is a result of the viscous drag experienced by membranes in close contact to their rigid underlying solid support. Here, drag (also referred to as frictional coupling) results from the addition of two frictional forces, frictional shear stress resulting from the velocity field created by the diffusing molecule and the direct frictional force between a diffusion molecule and the solid [69, 70]. The viscous drag coefficient, λ, experienced by a bilayer near a rigid solid is described in Eq. 2.4 where ε is defined by Eq 2.5 [70, 71].

$$\lambda = 4\pi\eta_m z_m \left(\frac{\varepsilon^2}{2} + \frac{\varepsilon K_1(\varepsilon)}{K_0(\varepsilon)}\right) \qquad \text{Eq. 2.4.}$$

$$\varepsilon = a \left(\frac{b_s}{\eta_m z_m}\right)^{1/2} \approx a \left(\frac{\alpha\eta_w}{\eta_m z_m d}\right)^{1/2} \qquad \text{Eq. 2.5.}$$

In the equations above, $\eta_m$and η_w represent membrane viscosity and the viscosity of surrounding water respectively, z_m refers to the thickness of the membrane, K_0 and K_1 are modified Bessel functions of the second kind, a is the radius of a diffussant (considered as a lateral diffusion disk for larger molecules

and lipid clusters), b_s is the friction coefficient, α is a constant, and d is the distance between the lipid bilayer and underlying solid.

The Einstein relation, Eq. 2.6, states the lateral diffusion of a disk in a 2D fluid (i.e. lipid bilayer) is dependent on the viscous drag coefficient, λ, where *k* is the

$$D = \frac{kT}{\lambda} \qquad \text{Eq. 2.6.}$$

Boltzmann constant and *T* is temperature. Principles of the Sackmann-Evans theory, represented in the above equations, were used to develop the polymer-tethered and multi-bilayer systems discussed in Sections 2.2.2 and 2.2.3. These systems are used to alter bilayer/solid distance in an effort to decrease frictional coupling based on Eq 2.4 and 2.5. As seen in Eq 2.6, decreased frictional coupling enhances lateral diffusion of proteins. In the case of polymer-tethered and multi-bilayer solid-supported systems, bilayer/substrate distance is regulated in order to achieve diffusion rates characteristic of a more biologically relevant state, comparable to that in free lipid bilayers.

2.4. Cellular Mechanotransduction

2.4.1. Cellular Mechanosensitivity

Cells within tissue are continuously exposed to mechanical forces such as compression on bone, stretching of skin and muscle, and shear stress on blood vessel-forming cells. This has led to increasing recognition of such forces as stimuli responsible for reprogramming cells and triggering biochemical responses within cells capable of profoundly impacting cellular and tissue functions through a process known as mechanosensing [1, 72-75]. While many elements of the mechanotransduction system have been identified, it remains largely unknown how cellular components coordinate to produce an appropriate response to mechanical stimuli. Yet, mechanical properties such as cell matrix viscoelasticity and dimensionality have been shown to be critical factors affecting cellular mechano-response, an observation that has lead to a proposed correlation between matrix rigidity and those cellular processes associated with injury and disease [1-4, 6-10]. With the changes in tissue stiffness that occur in such pathogenic states as fibrosis and cancer, this is a valid assumption [5]. In fact, numerous studies suggest that the mechanical properties of a material to which cells adhere cannot only act in concert with, but even override soluble biochemical signals [5].

By anchoring and pulling on their surroundings, cells can probe the viscoelasticity of their environment, and have been shown to adapt to the stiffness of elastic substrates. Cells plated on traditional plastic or glass substrates often show features, such as cytoskeletal stress fibers, large clusters of adhesion receptors, and flattened cell morphologies, which are less predominant in the native tissue environment. Moreover, organs are composed of tissues with well-defined mechanical properties which have elastic moduli orders of magnitude softer than commonly used culturing substrates [5]. These shortcomings have led to the development of 2D polymeric films, of adjustable viscoelasticity [8, 9], and 3D collagen matrices [3, 11, 12], which better replicate the ECM environment of tissue cells and have been shown to form morphologies similar to host tissue conditions [3, 4, 9, 11, 12, 76-78]. Quantitative studies suggest that cells display their most physiologically relevant state when cultured on substrates of comparable stiffness to their native tissue environment [79].

Polyacrylamide (PAA) gels not only represent better ECM mimics than glass or plastic, but have provided a 2D surface that has afforded further insight into cellular response invoked by mechanical cues imparted by a substrate. These gels have tunable mechanical properties in that the viscoelasticity of the gel can be regulated by crosslinking density. Regulating the degree of crosslinking with PAA has been shown to induce changes in cell morphology and cytoskeletal organization [2, 8, 9, 14-17, 19]. The mechanical properties of 3D collagen matrices are tuned much the same way, where the degree of crosslinking

impacts substrate viscoelasticity (and pore size in the case of 3D gels). Cells placed in 3D matrices of varying stiffness have been shown to respond with dramatic changes in phenotype (e.g. the formation of dendritic fibroblasts) [3, 11, 12].

Aside from morphological changes, substrate viscoelasticity has been shown to influence cell proliferation [80-82], motility speed and directionality (e.g. durotaxis) [8, 83, 84], apoptosis [81], differentiation [14], and other dynamic properties as well, which are all interconnected by key cellular elements of mechanotransduction. Furthermore, it is important to note that a cell's response to mechanosensing can be strikingly different for varying cell types. For example, while fibroblast proliferation is suppressed by soft surfaces [80, 82], other cell lines have shown a complete insensitivity to stiffness [7, 85], and while fibroblast motility is accelerated on more rigid substrates, the opposite holds true for neuronal cells [2, 86-88]. Thus, while all cells probe their surroundings by applying force, this force must trigger a specific signaling pathway that orchestrates a particular cellular response. This process of converting a mechanical signal into a biological signal is known as mechanotransduction.

2.4.2. Elements of Mechanotransduction

It is now well established that the mechanical properties of a substrate greatly influence cell behavior. Yet, the exact molecular mechanisms that translate

mechanical stimuli into biological signals, through a process known as mechanotransduction, are still poorly understood. However, key elements of the mechanotransduction system have been identified and proposed signaling hypotheses are continually validated through ongoing research. The elements of the mechanotransduction system can be roughly divided amongst four groups: the cytoskeleton (e.g. actin), molecular motors (e.g. myosin), cellular membrane components (e.g. integrins), and macromolecules composing the ECM (e.g. adhesion proteins such as laminin) [5].

Much research suggests that signal transduction occurs in the peripheral regions of the cell, the location of focal adhesions [73]. Here, transmembrane integrins play a key role and act as tri-functional molecules capable of: binding ligands on other cells or on the ECM, connecting to the cytoskeleton, and regulating intracellular signaling pathways [89]. With these properties, integrins form a direct link from the ECM to the cytoskeleton as integrins are essentially glued to the actin cytoskeleton through a collection of intermediary proteins (e.g. vinculin, talin, paxillin, etc.). With an anchoring point, cells can gauge the mechanical properties of their environment through a process known as mechanosensing. This process primarily involves the interaction of actin and myosin, where myosin-mediated contraction is used to generate a pulling force, by the cell, and directed onto the substrate. The information acquired from this act is then transduced into a signal that elicits a specific cellular response.

It is thought that integrins and the collection of proteins responsible for linking them to the cytoskeleton function as the cell's mechanotransducers. The central idea is that integrins and proteins undergo various conformational changes and unfolding in response to force. These changes create phosphorylation sites and exposed cryptic binding sites for signaling molecules [73, 90]; this signal transduction method is depicted in Figure 2.4. Many ECM proteins (e.g. fibronectin) as well as proteins that link integrins to the cytoskeleton (e.g. talin) consist of tandem-repeat sequences [73]. Differences in stability between repeat units can dictate the unraveling sequence, thus displaying different peptide sequences depending on the amount of applied force [73, 91-93]. Moreover, the stability of a protein's tertiary structure results from hydrophobic forces, disulfide bridges, electrostatic forces, pH, and more. Such structural diversity adds variability to cells. Additionally, some protein complexes are known to exist as "catch bonds," and are stabilized through applied force. Such complexes can be used to regulate the amount of force applied. The plausibility of this type of signaling is evidenced through atomic force microscopy (AFM) studies showing that proteins such as talin and filamin can be stretched by physiologically relevant forces [94-96]. Moreover, different cell types transmit different amounts of force, neuronal cells at 1-60 pN compared to fibroblast cells which generate 7,000-100,000 pN [90]. This large difference should ultimately determine which signaling sites are exposed through protein unfolding. This also explains

differences in cellular response when comparing cell types. It should be noted that force activated ion channels may also play a role as mechanosensors [97, 98].

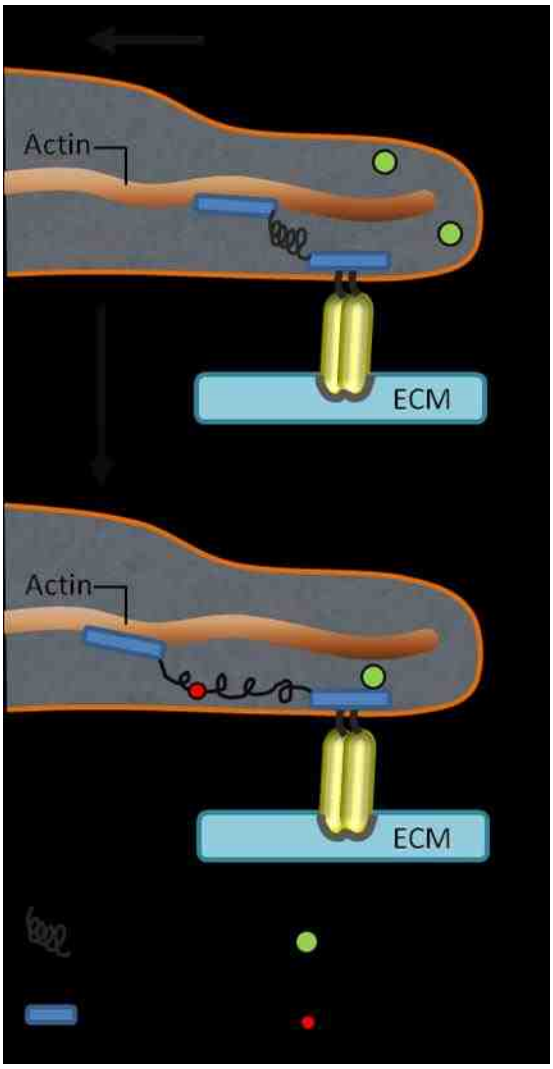

Figure 2.4. Signal transduction through protein unfolding and the exposure of phosphorylation and cryptic binding sites.

Mechanotransduction orchestrates more than localized responses such as protein recruitment at focal adhesion (FA) sites. As mentioned in Chapter 2.4.1, mechanotransduction can also result in processes like cellular differentiation, which is initialized in the nucleus of a cell, not peripheral regions. Could this simply be the result of soluble signals generated in these regions that then travel to the nucleus? This would not explain the speed of some long range cellular responses as physical models predict mechanical responses are 40 times faster than soluble signals [99]. Questions have led to the “hard-wired” cellular tensegrity model, where it has been proposed that mechanical linkages proceed farther into the cell than once thought and may actually directly link the nucleus to integrins residing in peripheral regions of the cell [5, 99]. This is depicted in Figure 2.5, which illustrates the recently identified LINC (linker of nucleoskeleton and cytoskeleton) complex, consisting of nesprins, sun, and lamin proteins [100].

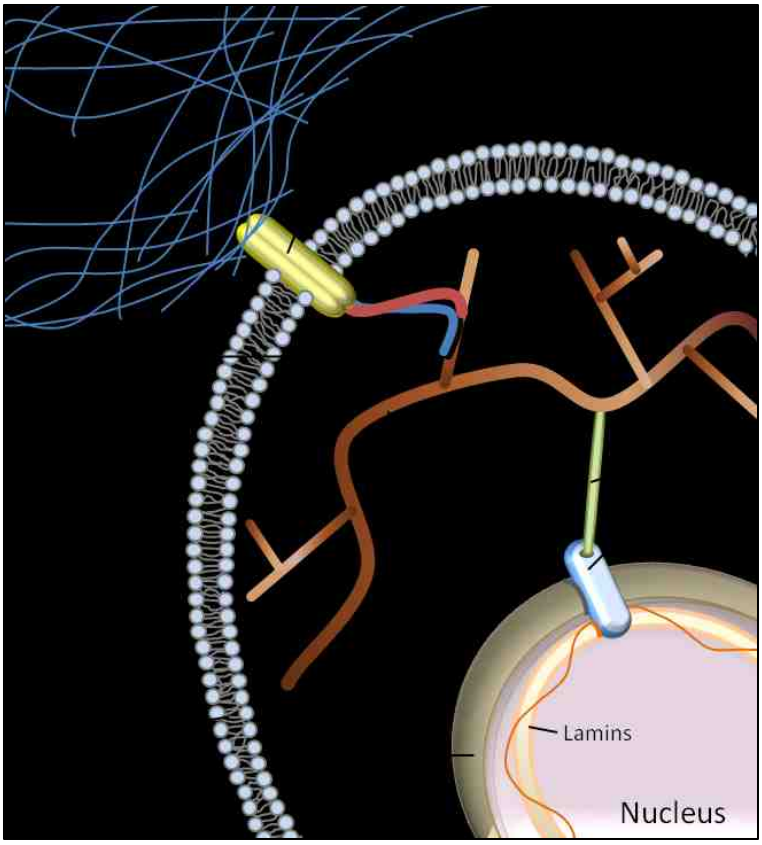

Figure 2.5. Force transmission between the ECM and the nucleus. Nesprins, sun, and lamin proteins form the LINC complex.

2.4.3. Cell Migration

Broadly speaking, the process of cell migration can be broken down into four key steps: (1) extension, (2) adhesion, (3) contraction, and (4) detachment, as illustrated in Figure 2.6. In step 1, an adhered cell creates protrusions, which extend in the direction of travel. These protrusions, collectively known as the "leading edge," are created by the cytoskeleton. In this case, the cytoskeletal component actin, found in highest concentration near the peripheral regions of the cell, is the primary contributor to this process; cellular extensions are formed

through actin polymerization. With the help of various actin binding proteins (e.g. thymosin, profilin, cofilin, and the Arp2/3 complex), and in the presence of ATP, the process of actin depolymerization/polymerization can be very rapid and is seen as a flow of actin in a process known as “treadmilling.” While actin is crucial to the extension process, other components of the cytoskeleton, primarily microtubules, are believed to play a role in adding directionality to movement. It is thought that microtubules may direct protrusions through the delivery of membrane vesicles to the leading edge, directly acting on the cell cortex, or through biochemical regulation [101].

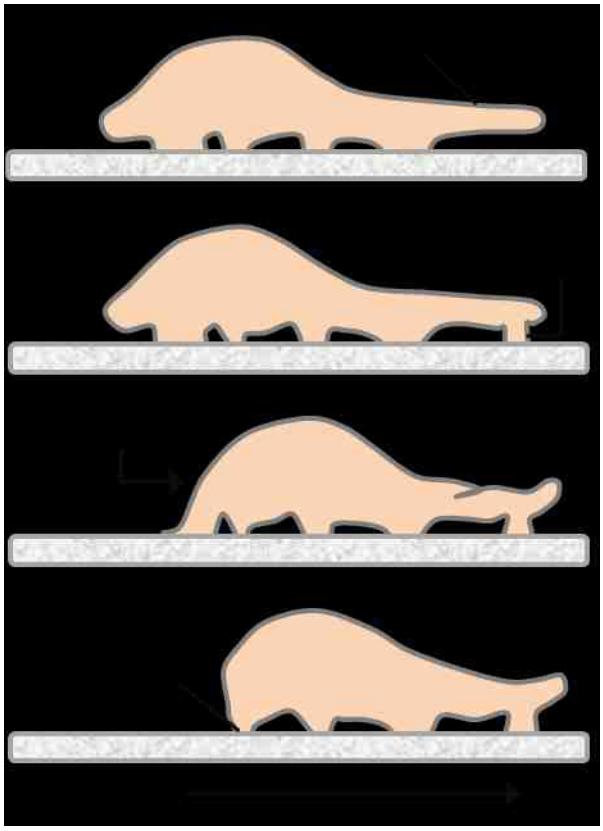

Figure 2.6. The four primary steps of cellular migration.

The protruding edge must adhere to the substrate in order to pull the cell forward. Attachment primarily consists of the integrin-mediated sites, as described in Chapter 2.4.2, where integrins couple ECM proteins to the cytoskeleton with the help of proteins such as paxillin, vinculin, and more. Proteins forming these FAs interact via weak, non-covalent bonds [73]. However, FAs do not exist as individual integrins, but rather integrin clusters that allow attachment sites to withstand pulling forces of high tensile strength. The size of an FA is dependent on the mechanical tension applied [101]. As discussed in chapter 2.4.2, force sensing and mechanotransduction can stimulate protein recruitment to strengthen FA sites.

Myosin II-based contraction of the actin cytoskeleton is used to generate the force necessary to pull the cell body forward while aiding in the disassembling of FA sites at the posterior of the cell [102]. However, the FA disassembly process is poorly understood. FAs are thought to exhibit a “clutch-like” mechanism that can be engaged and disengaged in response to force; observed FAs are mobile in stationary cells and immobile in migrating cells [101]. Proteolytic enzymes that hydrolyze ECM components may also play a role [101]. Often, as observed in time-lapse imaging, FA sites fail to disassemble in time and are simply ripped from the cell during contraction. Thus, the detachment process is a critical factor determining the migration velocities of cells. While somewhat counterintuitive, migration rates are slower on more rigid surfaces capable of higher traction

forces. This is a result of the larger, mature FAs formed on these substrates (a result of mechanosensing, mentioned above) slowing the detachment process.

CHAPTER 3: MATERIALS AND EXPERIMENTAL PROCEDURES

3.1 Materials

3.1.1. Phospholipid Membrane Materials

Lipids and lipopolymers including 1-palmitoyl-2-oleoyl-sn-glycero-3-phosphocholine (POPC), 1-stearoyl-2-oleoyl-sn-glycero-3-phosphocholine (SOPC), 1,2-Dipalmitoyl-sn-Glycero-3-Phosphothioethanol (Sodium Salt) (DPTE), 1,2-distearoyl-sn-glycero-3-phosphoethanolamine-N-[methoxy(polyethylene glycol)-2000] (ammonium salt) (PEG2000), 1,2-distearoyl-sn-glycero-3-phosphoethanolamine-N-[maleimide(polyethylene glycol)-2000] (ammonium salt) (PEG2000-Mal), and 1,2-dioleoyl-sn-glycero-3-[(N-(5-amino-1-carboxypentyl)iminodiacetic acid)succinyl] (nickel salt) (DGS-NTA(Ni)) were purchased from Avanti Polar Lipids (Alabaster, AL) and used without further modification. The lipopolymer 1,2-Distearoyl-sn-Gycero-3-Phosphoethanolamine-N-polymethyloxazoline(50) ($PMOX_{50}$) was synthesized in the lab of Professor Ranier Jordan (Technical University of Dresden). All fluorescent dye-labeled lipids used for tracking and Epi microscopy were

purchased from Invitrogen (Carlsbad, CA) and include: *N*-(6-tetramethylrhodaminethiocarbamoyl)-1,2-dihexadecanoyl-sn-glycero-3-phosphoethanolamine, triethylammonium salt (TRITC-DHPE), *N*-(7-nitrobenz-2-oxa-1,3-diazol-4-yl)-1,2-dihexadecanoyl-sn-glycero-3-phosphoethanolamine, triethylammonium salt (NBD-PE), and Texas Red® 1,2-dihexadecanoyl-sn-glycero-3-phosphoethanolamine, triethylammonium salt (TR- DHPE). Glass coverslips (24x40mm, No.1) used to support bilayer substrates were obtained from VWR Scientific Products (West Chester, PA). All cleaning and buffer solutions were prepared using solvents and chemicals purchased through Sigma-Aldrich (Milwaukee, WI). Ultrapure water (Milli-Q) used in the preparation of lipid bilayers was provided via a Millipore Water Purification System (Milford, MA).

3.1.2. Quantum Dot Materials

Cadmium acetate, selenium pellets, zinc nitrate hexahydrate, potassium ethylxanthate, Trioctylphosphine (TOP), Hexadecylamine (HDA), and HPLC grade solvents were purchased from Sigma-Aldrich. The phosphorus compounds Trioctylphosphine Oxide (TOPO), and Tributylphosphine (TBP) were purchased from Strem Chemicals (Newburyport, MA). All lipids and lipopolymers used for quantum dot encapsulation and functionalization were obtained from Avanti Polar Lipids and include: PEG2000, PEG2000-Mal, and 1,2-dipalmitoyl-sn-glycero-3-phosphocholine (DPPC). The primary amine linking- lipopolymer

1,2-distearoyl-sn-glycero-3-phosphoethanolamine-N-[NHS-Active Ester(polyethylene glycol)-2000] (ammonium salt) (PEG2000-NHS) was synthesized directly from PEG2000-Mal via hydrogenation catalyzed by palladium activated charcoal [103]. Laser quality Rhodamine 6G, used as an FCS control, was purchased through Exciton (Dayton, OH). All basic laboratory glassware and supplies were obtained from Fisher Scientific (Pittsburgh, PA).

3.1.3. Cell Culture Materials

All basic cell culturing chemicals were ordered from Invitrogen and include: low glucose Dulbecco's Modified Eagle Medium (DMEM) (phenol red and phenol red-free), RPMI-1649 medium, qualified fetal bovine serum (FBS), qualified horse serum (HS), penicillin-streptomycin antibiotic/antimycotic solution, 4-(2-hydroxyethyl)-1-piperazineethanesulfonic acid (HEPES), 0.25% trypsin, mouse laminin, cytochalasin D, trypan blue, and nerve growth factor (NGF). All culturing supplies (e.g. pipets, flasks, test tubes, etc.) were obtained from Fisher Scientific. Green fluorescent protein (GFP)-actin transfection vector were graciously provided by Simon Atkinson (IU School of Medicine). Focal adhesion transfection vectors (GFP-FAK) and stably transfected (GFP-actin) 3T3 cells were prepared by collaborators at the University of Erlangen, from the lab of Professor Ben Fabry. All neuron culturing and imaging were performed at the University of Leipzig in lab of Professor Josef Käs.

3.1.4. Polyacrylamide Gel Materials

All chemicals used in the preparation of PAA gels were purchased from Sigma-Aldrich and include: sodium hydroxide powder: (3-Aminopropyl)trimethoxy silane, 97%; ammonium persulfate (APS); glutaraldehyde, 25%; acrylamide/bis-acrlamide, 40% (PAA); electrophoresis-grade N,N,N,N'-tetramethylethylenediamine, >99.0% (TEMED); electrophoresis-grade ammonium persulfate, >98%; and 4-(2-hydroxyethyl)-1-piperazineethanesulfonic acid (HEPES). Dulbecco's PBS without Ca2+ and Mg2+, Fibronectin, and yellow-green 0.5µm carboxylate fluorospheres were obtained from Invitrogen. The crosslinkers used in these experiments, N-Sulfosuccinimidyl-6-(4'-azido-2'-nitrophenylamino) hexanoate(Sulfo-Sanpah) and N-[g-Maleimidobutyryloxy]succinimide ester (GMBS) were purchased through Pierce Biotechnology. Basic glassware and supplies including: 1x3in glass slides, 1x1cm gene frames, and 24x67 four-well multidishes were purchased from Fisher Scientific.

3.2 Experimental Procedures

3.2.1. Preparation of Single and Multibilayer Substrates

Polymer-tethered single bilayers (TYPE1), and the first layer of multi-bilayer (TYPE2) substrates, were assembled using a procedure based on previously

reported techniques [63, 64]. In this procedure, tethered-phospholipid bilayers are supported on glass microscopy coverslips prepared by baking at 515°C for 1h followed by sequential washing with 1% sodium dodecyl sulfate (SDS) in Milli-Q, NaOH-saturated methanol, and 0.1% HCl in Milli-Q cleaning solutions. Cleaning consisted of 30min bath sonication in each solution with Milli-Q washing between solutions. Slides were then stored in Milli-Q and used within one week. Initial monolayers were formed through the Langmuir-Blodgett technique, where a mixture of lipids (POPC) and polymer-tethered lipids ($PMOX_{50}$ in TYPE1 substrates and PEG2000 in TYPE2 substrates) was transferred onto a glass coverslip using a Teflon-coated Langmuir trough equipped with a dipper arm and film balance linker electronically to a compression arm. Here, the lipid mixture was spread at the air-water interface on the Langmuir trough and compressed to a film pressure of 30mN to form a lipid monolayer. After 20min equilibration, the dipper arm with attached glass coverslips was raised slowly. Feedback from the change in surface pressure sensed at the film balance induces the compression arm to move in response, thereby maintaining a constant surface pressure and thus coating the coverslip with a uniform monolayer mixture. Unused lipids were removed from the trough. The lipid mixture for the outer leaflet was then spread and compressed to 30mN and bilayers were completed using a Schaefer transfer technique, in which a depression slide is placed on the bottom of the Langmuir trough before the addition of lipids to the trough. After the addition of lipids and equilibration, the coverslip is firmly compressed onto the depression slide, at an angle, to prevent the formation of air bubbles in the resulting bilayer. This

method allowed for the preparation of asymmetric films necessary for TYPE1 single bilayers (and first layer of TYPE2 triple bilayer substrates). The completed substrates contained a polymer cushion, created by the physiosorbed lipopolymers in the inner leaflet, which uplift the bilayer and are thought to aid in minimizing cellular interactions with the underlying glass.

Multibilayer substrates were prepared atop these polymer-tethered bilayers. Here, additional planar lipid bilayers were added through the fusion of GUVs using a modified technique based on previously established procedures [56]. To enhance GUV fusion and multi-bilayer stack stability, adjacent bilayers were stabilized through flexible inter-bilayer linkages based on sulfhydral-maleimide coupling chemistry. With this iterative procedure, the lipid composition of stacked bilayers was alternated from POPC with 5mol% DPTE (sulfhydral-functionalized lipid) to POPC with 5mol% PEG2000-Mal (maleimide-functionalized lipopolymer). GUVs were formed by resuspending dried lipid stocks in a 0.1mM sucrose/1mM $CaCl_2$ solution, to a final concentration of 5-10mg/mL, and heating at 80°C for 2h. The GUV solution was then allowed to cool to room temperature and added to the bilayer system in a 0.1mM glucose /1mM $CaCl_2$ solution. The GUVs were brought into contact with underlying layers via a gravity gradient and were allowed to bind and unfold over a 2.5h period. Excess, unbound GUVs were then removed by rinsing with Milli-Q water.

For all single and multibilayer substrates utilized in cellular studies, the outermost layer was composed of a mixture of POPC with 5mol% DPTE and 0.3mol% TR-DHPE. The dye-labeled lipid, TR-DHPE, was used to ensure a homogenous film, through Epi microscopy, prior to plating cells on these substrates. The sulfhydral-functionalized lipid, DPTE, was used to facilitate a cell-substrate linkage. Bilayer substrates were affixed to the bottom of a petri dish drilled with a 1.5cm hole to allow for cell culturing on the incorporated bilayer substrate. This was done by coating the perimeter of the 1.5cm hole with a fine layer of vacuum grease (Dow Corning High Vacuum Grease, Fisher Scientific) and then compressing the coverslip onto the Petri dish under water. A large excess of a heterobifunctional linker (containing maleimide and active ester functionalities) was added to the exposed bilayer (within the 1.5cm hole in the Petri dish) and allowed to bind for 1h. Unbound linker was removed through rinsing with phosphate buffered saline (PBS) and an excess of the adhesion protein Laminin was then added. Primary amines on the surface of the protein bind the linker over a period of 1h and excess Laminin was then removed with PBS rinsing. At this point, substrates are ready for cell plating.

3.2.2. Single Molecule Fluorescence Microscopy

Wide-field, single molecule fluorescence microscopy (SMFM) was used to characterize lipid dynamics in multibilayer substrates and provide evidence that substrate fluidity can be tuned through bilayer stacking. The SMFM setup,

shown in Figure 3.1, consisted of an inverted microscopy (Zeiss Axiovert S100TV) equipped with a 100mW frequency doubled Nd:YAG laser (532nm) for fluorophore excitation. Laser light is passed through a computer-controlled shutter, a variable neutral density filter, expanding and collimating lenses, a diaphragm, and a quarter wave plate to provide a high-magnification objective (Zeiss, oil immersion, 100x NA=1.3) with circular polarized light to increase tracking accuracy. Fluorescence emission from the sample the passes through a dichroic mirror (chosen to collect TRITC emission (566nm)) and a Raman filter before hitting an intensified CCD camera (iPentaMAX 512EFT). For all tracking experiments, an exposure time of 10ms and a time lag of 40ms were used. Shutter control and image acquisition were performed using ISee Imaging software. To increase tracking accuracy, imaging was performed on an air table to minimize room vibrations. SMFM on single, double, triple, and quadruple bilayer systems was performed as previously described [63, 64]. All substrates used for SMFM studies were prepared with small, 10^{-8}mol%, quantities of TRITC-DHPE in their outermost bilayer.

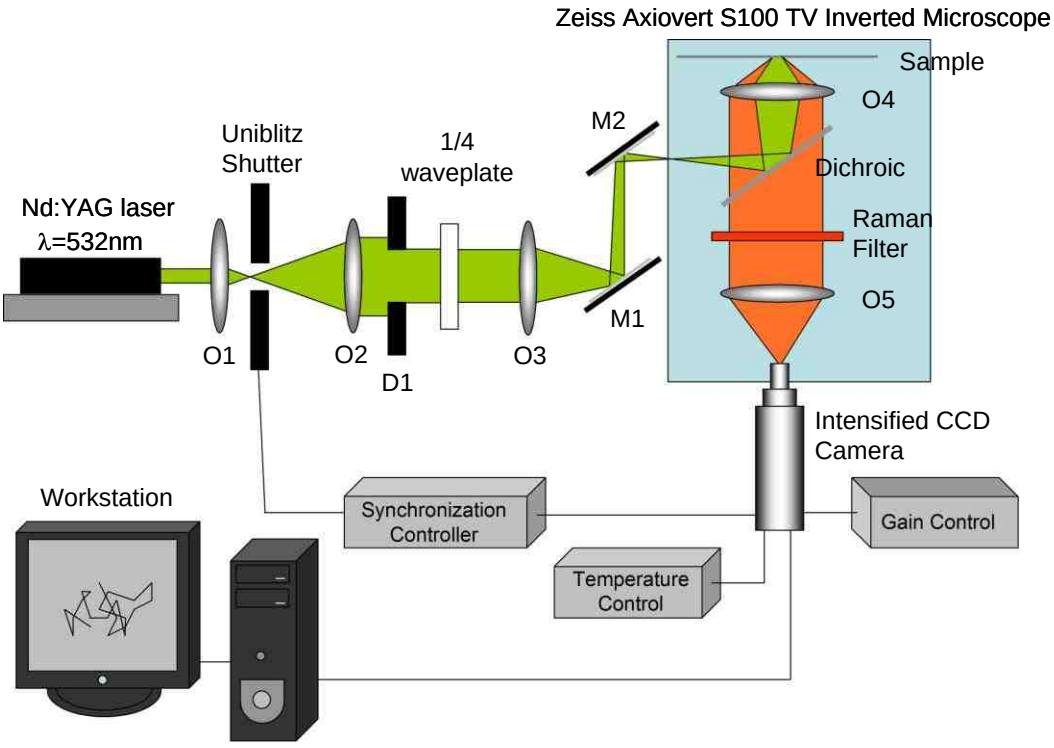

Figure 3.1. Wide-Field single molecule fluorescence microscope setup.

TIRF-based SMFM (SMFM-TF) was used in live cell experiments in collaboration with Ken Ritchie (Purdue University, West Lafayette) and consisted of a similar setup with a HeNe excitation laser (543nm), high magnification objective (Olympus, oil immersion, 100x, NA 1.4), and a cooled CCD camera (XR/Turbo-120z, Standford Photonics, Inc.). Here, the excitation beam was adjusted immediately outside ideal conditions for TIRF. This allowed for the deeper imaging needed to track fluorophores atop cells, but still resulted in the decreased background characteristic of TIRF-based techniques. The live cell experiments in which SMFM-TF was utilized are described in Chapter 3.2.7.

3.2.3. Single Molecule Tracking and Data Analysis

The analysis of SMFM data follows that previously reported [63, 64]. The imaging method described above was used to obtain a sequence of fluorescent images corresponding to the movement of individual dye-labeled lipids. The x and y coordinates of the fluorescent probes (identified through finding the adapted center of intensity of the Airy disks of the fluorophores) are determined for each snapshot in a collection of sequential images using ISee tracking software. Using these (x,y,t) coordinates, 2D trajectories can be generated and the squared displacement of the fluorescent probes with respect to time can be calculated using the equation below.

$$r_n^2(t_n) = [(x_n - x_0)^2 + (y_n - y_0)^2] \quad \text{Eq. 3.1}$$

The squared displacements collected between successive frames can then be averaged to obtain a mean squared displacement, $\langle r^2 \rangle$, for the given time lag, *t*, of 40ms. This displacement data can be used to compare the fluidity of different substrates as an increase in substrate fluidity is marked by larger displacements (i.e. faster diffusion). Moreover, lateral diffusion coefficients can be calculated from $\langle r^2 \rangle$ using equation 3.2.

$$\langle r \rangle^2 = 4Dt \quad \text{Eq. 3.2}$$

In addition, the information given from fluorophore displacements can also be used to plot cumulative distribution functions, or CDFs. A CDF represents a probability function displaying the likelihood of the observed displacements. These plots take into account each step a molecule makes, not just the average displacement, thus providing a more accurate account of a molecule's travel.

Moreover, fitting the CDF curve to a single exponential or double exponential function provides information on the type of movement present (e.g. Brownian, anomalous, or directed). For example, a CDF displaying Brownian diffusion is fitted with the single exponential function below.

$$P\left(r^2,\ t_{lag}\right) = 1 - exp\left(-\frac{r^2(t_{lag})}{\langle r^2(t_{lag})\rangle}\right) \qquad \text{Eq. 3.3}$$

Each sample was analyzed using a minimum of 150 tracks (or molecule displacements). Previous work in the lab indicates that a number greater than this ensures statistical accuracy, as previously verified on solid-supported fluid lipid bilayers (yielding one component fit).

3.2.4. Sonochemical Synthesis of Quantum Dots

Quantum dots served as the basis of the heterobifunctional linker used to bind cellular adhesion proteins, such as laminin, to the lipid bilayer-based substrates. QDs were a good candidate based on the existing nanoparticle functionalization expertise in our lab. Moreover, while the linker QDs used in cellular mechanoresponse experiments were not exploited for their photoluminscent properties, the ability remains. In future work, these linkers have the potential to be utilized as probes in dynamic studies as well. CdSe/ZnS quantum dots were synthesized using previously reported methods [104, 105]. Sonochemical synthesis procedures were developed in our lab as a safe, efficient, low temperature alternative to traditional thermal methods. CdSe core nanocrystals

were synthesized using $Cd(OAc)_2$ and crushed selenium (dissolved in TOP) with HDA and TOPO as coordinating solvents; the reaction scheme is depicted in Figure 3.2. Reagents were melted and placed in a sidearm test tube that could be supplied with argon during sonication. Ultrasonic power was applied through a rod sonifier (Branson Ultrasonics, Danbury, CT) to promote crystal growth. Core CdSe crystals were then shelled with zinc ethylxanthate for increased stability, longer storage, and decreased cytotoxicity.

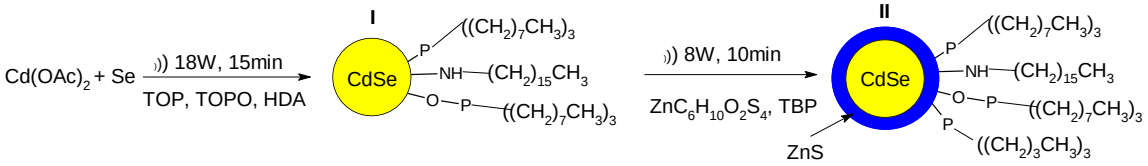

Figure 3.2. Reaction scheme for the sonochemical synthesis of CdSe/ZnS QDs.

3.2.5. Quantum Dot Functionalization

A biologically compatible linker should be water-soluble, non-toxic, resistant to aggregation, and display no non-specific adsorption. The linker should also be able to be linked to a protein and/or lipid of interest. Directly following their synthesis, QDs display none of these properties and, therefore, must be coated and functionalized. In all experiments, hydrophobic QDs were coated using a lipopolymer encapsulation technique previously reported [106, 107]. Lipid encapsulated QDs are an excellent candidate for linkers in biological systems due to their inertness and increased stability over more traditional coating

methods (e.g. hydrophilic thiol acids), a result of strong hydrophobic and electrostatic interactions. Here, QDs are encapsulated with a mixture of lipids (DPPC), lipopolymers (PEG2000), and functionalized lipopolymers (PEG2000-Mal and PEG2000-NHS) in a ratio of (38:60:1:1). This method allows QDs to maintain their hydrophobic coordinating solvent, and it is believed the acyl chains of the lipids organize around this solvent. With the hydrophilic ends of the lipid components facing outwards, the end result, shown in Figure 3.3, is a water soluble QD. However, this lipid composition was chosen to fulfill more obligations than simply altering solubility properties. The long polyethylene glycol (PEG) chains of the lipopolymers function as entropic springs to minimize aggregation, while the lipids pack into any exposed hydrophobic regions (resulting from the steric hindrance of bulky lipopolymers) to form a complete coating. Linker functionality was provided with a small 1mol% amount of both PEG2000-Mal and PEG2000-NHS lipopolymers that readily bind sulfhydrals and primary amines respectfully. Proper linker function was validated through SMFM imaging on QD-labeled sulfhydral lipids and reconstituted membrane proteins (Millipore, Billercia, MA) in phospholipid bilayers. Aggregation resistance and biological inertness were tested using FCS and live cell SMFM as discussed below.

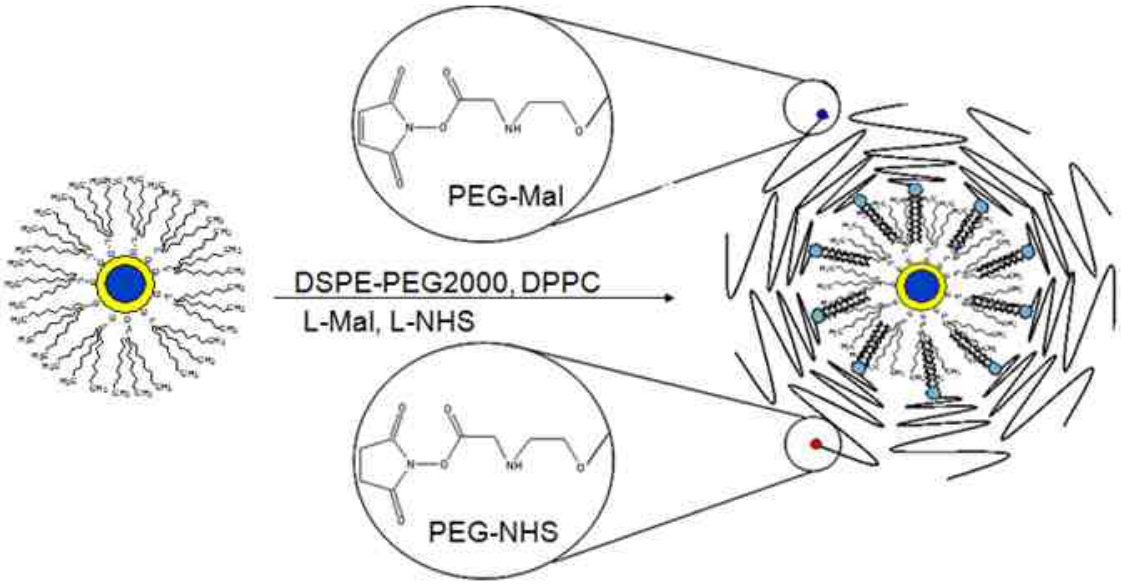

Figure 3.3. Lipopolymer encapsulation of QDs to form water soluble, heterobifunctional linkers.

3.2.6. Fluorescence Correlation Spectroscopy

Using a Zeiss Confocor2 Fluorescence Correlation Spectrometer attached to a Zeiss Axiovert 200m inverted microscope, FCS studies on functionalized QDs were used to determine stock concentrations as well as ensure aggregate-free, stable cell-substrate linkers. This technique is capable of monitoring changes in fluorescent intensities within a small confocal volume. A fluorescent probe, in bulk solution, diffusing through this confocal volume is excited, resulting in a change in fluorescence intensity. Fluorescent fluctuations are then used to generate an autocorrelation curve, Eq. 3.4, of the Gaussian intensity distribution, *G(t),* which reveals the number of particles in the confocal volume, *N*, as well as a characteristic diffusion time, τ_D (where τ represents correlation time and *s* is the

$$G(t) = 1 + \frac{1}{N}\left(\frac{1}{1+\left(\frac{\tau}{\tau_D}\right)}\right)\left(\frac{1}{\sqrt{1+\frac{1}{s^2}\left(\frac{\tau}{\tau_D}\right)}}\right) \quad \text{Eq. 3.4}$$

structure parameter). If the radius of the confocal spot is known (this can be experimentally determined using a fluorophore with an established diffusion coefficient [108]), the confocal excitation volume can be calculated under the approximation that the confocal spot is a sphere. With this information, solution concentrations are determined based on the number of particles residing in the confocal volume of the bulk solution. Moreover, the diffusion time calculated by the autocorrelation function provides insight concerning the degree of aggregation present in a sample. Larger particles (i.e. aggregates) will interact more with their surrounding fluid, resulting in slower diffusion times. In fact, a hydrodynamic radius of the particles can be calculated from the Stokes-Einstein relationship, Eq. 3.5, where *r* is the hydrodynamic radius, τ_D is the diffusion time,

$$r = \frac{2\tau_D \cdot k \cdot T}{3\pi \cdot \eta \cdot \omega^2} \quad \text{Eq. 3.5}$$

k is the Boltzmann constant, T in temperature, η in the solution viscosity, and ω is the radius of the confocal excitation volume.

3.2.7. Single Molecule Fluorescence Microscopy of QD-Labeled Lipids in Live Cell Membranes

Live cell imaging was employed to test the biological inertness of the QD-based cell-substrate linkers. Here, small unilamellar vesicles (SUVs) composed of a 3:1 SOPC:DOPE lipid mixture, previously shown to be fusogenic with the plasma membrane of cells [109, 110], were prepared using a published sonication procedure [111]. In addition, a small quantity, 10^{-3}%, of thiolated lipids (DPTE) were added as a docking point for maleimide functionalized, lipopolymer-coated QDs. QDs were added to an excess of SUVs to eliminate the possibility of free QDs interacting with any sulfhydral-containing biomolecules present in the cell membrane. The QD-labeled SUVs were allowed to fuse with cells for 15-20min before unbound SUVs were rinsed away with PBS. The fusion scheme is depicted in Figure 3.4.

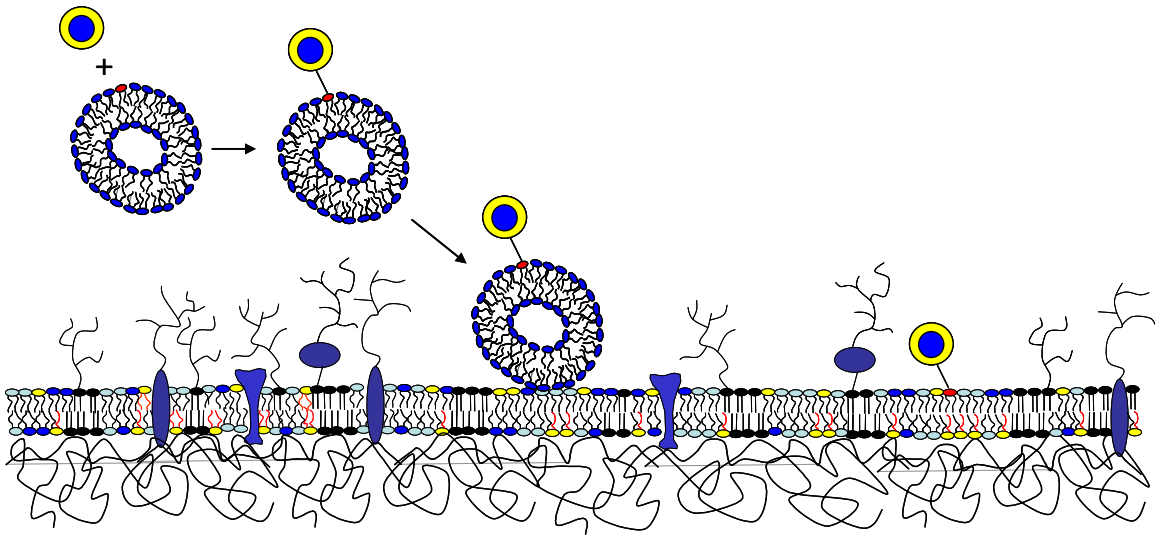

Figure 3.4. Fusion of QD-labeled SUVs with a cellular plasma membrane [107].

Live cell imaging and tracking were performed in the lab of collaborator Kenneth Ritchie (Purdue University) using an SMFM-TF setup similar to that depicted in Figure 3.1, but equipped with an incubation unit, a high-speed camera, and total internal reflection fluorescence (TIRF) to aid in cell imaging on the outermost plasma membrane of confluent cells by reducing background autofluorescene. Comparison of QD tracks with that of traditional dyes was used to reveal the amount of interaction with surrounding biological components. Additionally, cellular studies confirm that QDs show no notable cytotoxicity.

3.2.8. Cell Culture

Mouse NIH 3T3 fibroblasts, used on TYPE 2 substrates, were cultured in Dulbecco's Modified Eagle Medium (DMEM) supplemented with 10% fetal bovine serum and 1% penicillin-streptomycin antibiotic-antimycotic solution. Cells were stored at 37°C and 5% CO_2 and were passaged on a 2-3 day basis; cells were passaged no more than 12 times. Fibroblasts are strongly adherent so trypsin was used to cleave cells from culturing flasks. Before plating, cells were rinsed with PBS and trypsinized with 0.25% trypsin in DMEM. Cells were then supplied with fresh, warm media to deactivate trypsin and were subsequently centrifuged. The trypsin-containing media was removed and cells were resuspended in fresh media. Cells were counted using a hemocytometer and 1500 cells were plated on all substrates. This low number of cells allowed for single cell imaging over a period of 48h.

PC12 Neurons, used on TYPE 1 substrates, were cultured in the same fashion with a few notable exceptions. Neurons were supplied with medium prepared with RPMI-1640 supplemented with 10% horse serum, 5% fetal bovine serum, 1% penicillin-streptomycin antibiotic/antimycotic, and 1% 1M hepes (yielding a 10mM concentration). Like fibroblasts, neurons were stored at 37°C and 5% CO_2 and were passaged on a 2-3 day basis, and no more than 12 times. Neurons, however, are weakly adherent cells, thus eliminating the need for trypsin in cell passaging and plating. Instead, cells were dislodged from culture flasks by simply rinsing with fresh medium. Following cell plating onto, cells were supplied with the growth factor NGF (25ng/mL) to induce neurite outgrowth.

3.2.9. Cellular Transfection

Cellular transfection with GFP-Actin was used to observe the cytoskeletal reorganization of cells in response to changes in substrate viscosity. While traditional cell staining methods (e.g. phalloidin staining) are efficient, easy, and fast, the lipid bilayer-based substrate design prohibited their use as these stains are typically introduced into a cell with a detergent solution (e.g. triton x-100), which perforates the cell membrane; the use of such a detergent causes similar disruption to the lipid bilayer substrates. Instead, fibroblasts were transfected with GFP-Actin vectors one day prior to plating using Effectene (Qiagen), following the transfection protocol provided by the supplier. In short, a DNA-containing transfection solution (0.6µg of DNA, 4.8µL enhancer, 9µL effectene

reagent, and 286µL EC buffer) was added to a cell suspension of 15,000 cells in 250µL of growth media. The cell solution was added to an individual well of a 24well plate and incubated over night. Cells were plating the following day after rinsing with PBS and fresh media; plating density onto experimental substrates was approx. 850 cells/cm^2. The use of transient transfection techniques also enabled live cell imaging.

3.2.10. Live Cell Imaging

In order to perform live cell imaging, a stage setup capable of mimicking an incubator was obtained from collaborators at the University of Leipzig, and is described below. Cell imaging was performed in polystyrene Petri dishes containing 1.5cm holes at their bottom. Multibilayer substrates were affixed to Petri dishes underwater using vacuum grease; experiments on laminin-coated glass were performed in the same manner. During imaging, cells were kept at 37°C using a custom built Petri dish holder with a heat output controlled by a voltage regulator. Samples were provided with 5% CO_2 (balanced with air) using Teflon-machined Petri dish lids containing two gas ports (an inlet and outlet) and a glass top to allow for DIC and phase contrast imaging. Humidity was maintained by bubbling 5% CO_2 supply through a water trap prior to sample inlet. In addition, a water trap placed after the outlet reduced the evaporative loss of cell medium during long term studies. All live-cell DIC imaging was performed with a Zeiss Axiovert 200m equipped with a Zeiss AxioCam mRn. Live-cell

phase contrast and Epi microscopy were completed on a Leica DMI4000B inverted microscope.

3.2.11. Analysis of Neurite Outgrowth

Neurite outgrowth velocities were calculated from phase-contrast snapshots taken at different time intervals following cell plating. A custom-written Matlab program was used to trace and measure the length of neurites. Branched neurites were segmented into straight lines, which were then summed together for a total length. A screen shot from this tracing procedure is shown below, Figure 3.5. Neurite length was then divided by the time lag (from plating to snapshot acquisition) to determine outgrowth velocities.

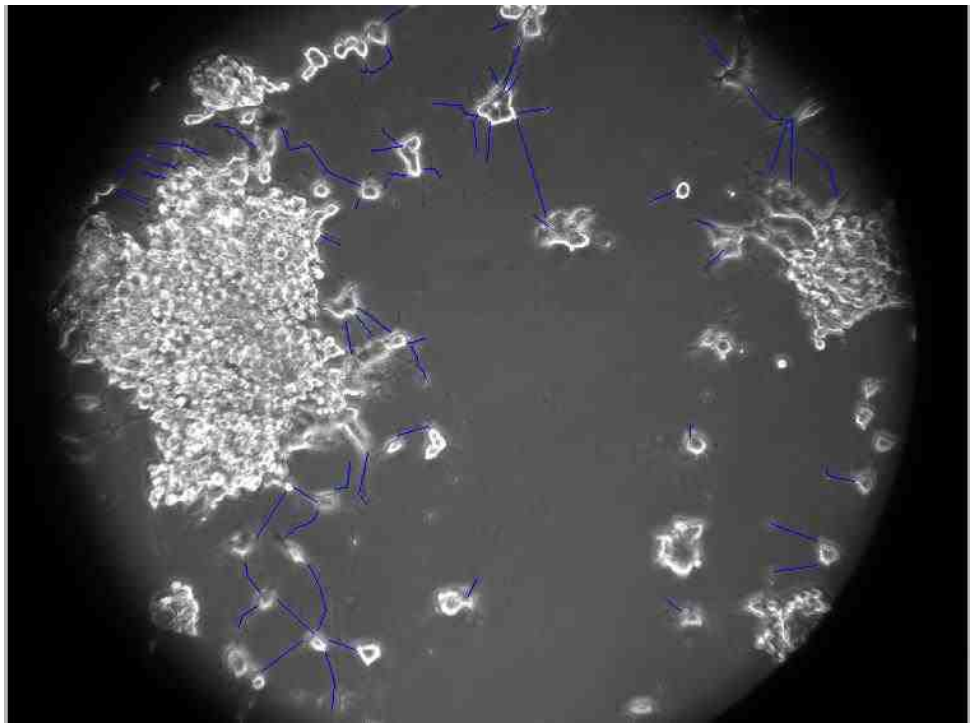

Figure 3.5. Matlab-based analysis of neurite outgrowth.

3.2.12. Analysis of Cellular Migration Speeds and Area Fluctuations

Fibroblast mobility was captured with time lapse imaging via a Zeiss Axiovert 200M equipped with Axiocam mRm camera and Axiovision software to control image acquisition. For cellular migration studies, several spots within a sample were identified and set to acquire DIC images with a 5min time lag. The end result was a multi-file tiff in the form of a movie. Using the Axiovision Tracking Package, cell nucleus movements were traced from frame to frame. Similar to the SMFM data analysis method described above, x and y coordinates of a cell nucleus were recorded for each sequential snap shot to provide 2D trajectories. Based on the constant time lag of 5min, an average migration speed was calculated for each cell. Based on the cell trajectories, torosity, or the directionality of movement, was also determined. Area fluctuations during cellular migration were also analyzed to provide insight into the type of migration observed (e.g. mesenchymal, amoeboid, etc.), but to capture more dynamic movements, the time lag was shortened to 2min. Changes in cell area were determined from a set of sequential snapshots. Here, cell area measurements were performed by hand using Adobe Photoshop and a tablet PC to outline cells. This imaging program provided the number of pixels residing in an outlined-shape, and with the pixel size (based on the object used for imaging) cell areas in μm^2 can be calculated. Relative area fluctuations were then determined by comparing the percent change in area of a cell from frame to frame.

3.2.13. Preparation of Polyacrylamide Gels

Polyacrylamide gels were prepared based on a published procedure [37]. Similar fluorophore embedded gels have previously been applied to studies on adherent fibroblasts [36, 38-40]. Here, 1x3in glass slides cleaned and silanized by submerging in 0.1M NaOH and 2% (3-Aminopropyl)trimethoxysilane stock solutions. The slides were then washed with deionized water and treated with 2.5% glutaraldehyde for 30min at room temperature before rinsing again with deionized water. Clean, dry, slides were then equipped with gene frames that served as reservoirs for the addition of the unpolymerized gel. PAA gels with embedded fluorescent beads were added by creating a mixture of 422μL of Milli-Q water, 76μL of PAA, and 2μL of green-yellow fluorospheres (Invitrogen). This mixture was vortexed, briefly sonicated, and cooled over ice before the addition of 2.5μL of APS (100mg/mL stock in Milli-Q) and 1μL TEMED. The mixture was again vortexed and 28μL was pipette inside each gene frame. Slides containing the unpolymerized gels were capped (using supplied gene frame tops) and placed upside down in a cooled centrifuge (4°C) where they were spun at 1500rpm for 20min. This temperature slowed the polymerization process while centrifugation brought the fluorescent beads to the surface of the gel. Gene frame covers were then removed and PAA gels were stored in PBS.

Prior to the addition of cells, the gel surface was activated with Sulfo-Sanpah (0.5mg/mL in 50mM HEPES), a photoreactive linker (Pierce Biotechnology), under UV radiation. Gels were rinsed with PBS and coated with fibronectin

(incubating the gel at 37°C overnight). Gels were then rinsed and 1500 3T3 fibroblasts were plated on each sample.

Force traction measurements on lipid bilayer-based cell substrates were performed adding the heterobifunctional linker GMBS (Pierce Biotechnology) to the fibronectin functionalized gels above. This was used to create a linkage between the protein and the sulfhydral functionalized lipid DPTE. GMBS was added in excess and allowed to bind over 1h. Unbound linker was removed with PBS rinsing. Lipid bilayer substrates were then built atop PAA gels as described in Chapter 3.2.1. Here, GUVs containing 5mol% PEG2000-Mal were used for the first lipid bilayer. Following completion of a single or multibilayer stack, substrates were prepped for cells as described in Chapter 3.2.1.

3.2.14. Traction Force Microscopy

Force traction microscopy was used to confirm the anticipated decrease in cellular traction forces resulting from the mobile linkers on phospholipid bilayer substrates. Here the fluorescent beads embedded in PAA gels described above were imaged, using wide-field Epi microscopy, 20h and 40h following cell plating. DIC images, and corresponding Epi images, were acquired for representative cells in a sample. Cells were then treated with a small amount of cytochalasin D (20µL in 200µL or trypsin) to halt cytoskeletal movements and release cells from the substrate. With cells released, fluorescent beads are displaced back to their

native location and Epi images are acquired a second time. Using custom Matlab software, the 2D displacements of the beads were tracked based on a published computational approach [30]. With the displacements and known elasticity of the underlying PAA, this program calculated the forces generated by the cell. Note, the elasticity of the PAA has been previously determined through AFM (by collaborators at the University of Erlangen), for the ratio of crosslinker used in the gel preparation.

CHAPTER 4. RESULTS AND DISCUSSION

4.1. Design and Fabrication of Biomembrane-Mimicking Cell Substrates

4.1.1. TYPE 1: Single, Polymer-Tethered Bilayers of Tunable Viscosity

Previous work from Deverall, et al. [63, 64] has revealed that lipid lateral mobility within a physiosorbed polymer-tethered phospholipid bilayer can be regulated through lipopolymer tethering concentration in the inner leaflet. Importantly, regulating the tethering concentration for 5-40mol% lipopolymer was shown to decrease lateral diffusivity in both leaflets of the lipid bilayer [63]. It has been suggested that the reduced diffusion in the outer leaflet is a result of lipopolymers acting as diffusion obstacles (pinning sites) and inducing roughening of the membrane, as illustrated in Figure 4.1 [63]. It has been hypothesized that the energy increase around such pinning sites affects diffusion in both leaflets due to the significant morphological coupling between them [63]. In essence, lipopolymers are thought to cause deviations from planar geometry and create regions of high membrane tension where diffusion is hindered [63].

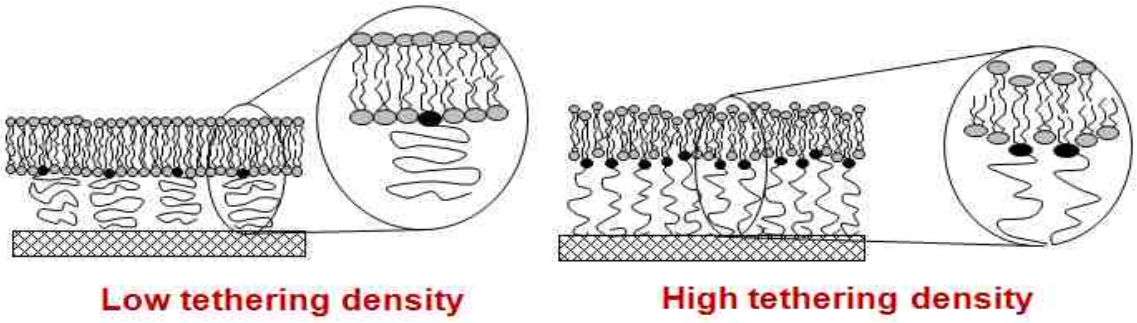

Figure 4.1. Polymer-tethering induced obstructed diffusion in TYPE 1 substrates [63].

Published SMFM-WF data of dye-labeled lipids in both the inner and outer leaflets of these polymer-tethered lipid bilayers confirm the idea of transbilayer coupling of obstructed lipid diffusion, as shown in Figure 4.1. In Figure 4.2 changes in lateral diffusion are represented by changes in $<r^2>$, mean squared displacement (MSD), where smaller displacements over a given, constant time lag indicate slowed diffusion. Moreover, these results indicated that bilayer fluidity in the outer leaflet can be tuned from fluid (5mol% tethering concentration) to nearly immobile (30% tethering concentration). It should be noted that these data were obtained using the lipopolymer N-dioctadecylamine polyethloxazoline. The TYPE 1 bilayers fabricated within this thesis contained the lipopolymer 1,2-O-dioctadecyl-sn-glycero-3-[poly(2-methyl-2-oxazoline)50] (PMOX50), but similar behavior is expected and has been shown with other lipopolymers within our research lab.

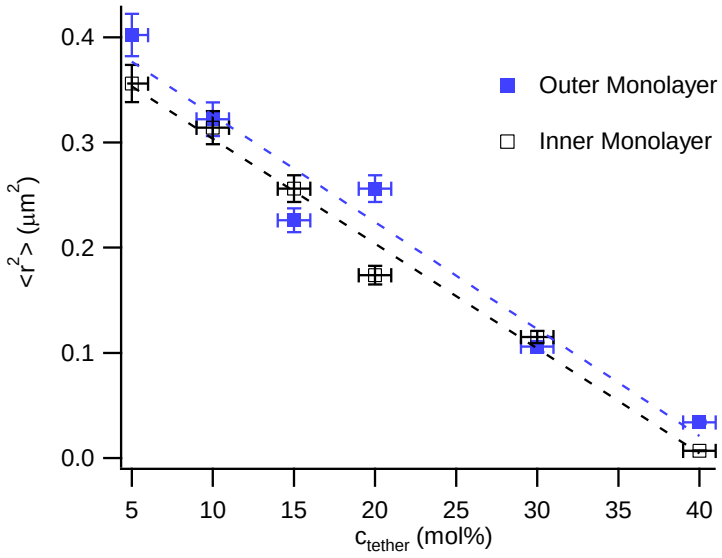

Figure 4.2. Mean squared displacement, $\langle r^2 \rangle$, data of TRITC-DHPE lipids illustrates the impact of tethering concentration on the lateral mobility of lipids within TYPE 1 substrates (time lag: 40ms, T=21°C) [63].

In terms of cell substrate design these single, polymer-tethered bilayers (denoted as TYPE1 substrates) provide a means of regulating cell-substrate linker mobility (thus, mimicking changes in substrate viscosity) through tethering concentration. Figure 4.3, illustrates the basic schematic of how lipid bilayer systems were used as biomembrane-mimicking cell substrates.

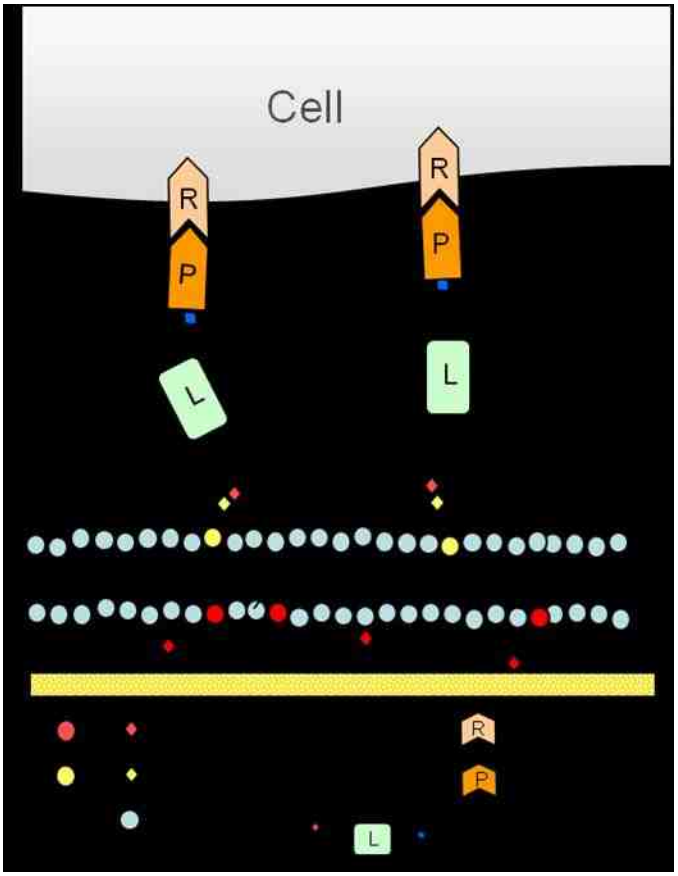

Figure 4.3. Schematic of TYPE 1 cell substrates.

Here lipid bilayers were fabricated from POPC with adjustable amounts of the lipopolymer $PMOX_{50}$ in the inner leaflet and 5mol% DPTE in the outer leaflet. DPTE, a sulfhydral functionalized lipid provided the basis of the mobile cell substrate linkers. Figure 4.3 indicates the use of two linkers L1 and L2. These linkers will be discussed in detail in Chapter 4.2.1, and include a commercially available linker (L1) and one consisting of a functionalized quantum dot (L2). These are heterobifunctional linkers capable of crosslinking the sulfhydral of DPTE to any primary amine expressed by a protein. In this case, protein P, in

Figure 4.3, is Laminin, an ECM adhesion protein commonly used in fibroblast and neuron cell studies. Thus, TYPE1 substrates consist of mobilized, laminin-functionalized cell linkers whose diffusion properties are easily tuned through polymer concentration.

4.1.2. TYPE 2: Multibilayer Stacks of Tunable Viscosity

Multi-bilayer stacks (denoted as TYPE2 substrates) were designed as an alternative, more robust approach for regulating cell linker mobility through bilayer viscosity. Unlike single solid-supported lipid bilayers previously employed as cell substrates [52, 112], TYPE 2 substrate viscosity is adjusted by altering the number of bilayers in the multi-bilayer stack. This parameter affects the distance between a bilayer and the rigid underlying surface, in turn, impacting the degree of frictional coupling (or viscous drag).

It is well recognized that the viscous force, F, experienced by a moving object (e.g., a cell) in the vicinity of a solid substrate, can be expressed as

$$F \propto \frac{Av\eta}{d} \qquad \text{Eq 4.1.}$$

where A is the area of the object, v is its velocity, η is the viscosity of the liquid, and d represents the distance between moving object and solid substrate [101]. Similarly, theoretical and experimental studies have shown that lipid/protein lateral diffusion in a solid-supported lipid bilayer depends on the degree of

frictional coupling between bilayer and underlying solid, a parameter regulated by the distance between bilayer and solid [70, 71, 113], as was described in Chapter 2.3.2.

Based on these established principles, TYPE 2 systems were designed as biomembrane-mimicking cell substrates comprised of a stack of multiple, polymer-tethered lipid bilayers that combine the important features of tunable substrate viscosity and laterally mobile linker molecules. In these systems, the number of bilayers in the multi-bilayer stack regulates the distance between adsorbed cells and solid substrate. Substrate viscosity, and consequently the lateral diffusion of cell linkers (affecting viscous drag force and cellular traction), is tuned through the formation of bilayer stacks, where additional bilayers result in a decrease in frictional coupling between the top, outermost bilayer and the solid substrate, as shown in Figure 4.4.

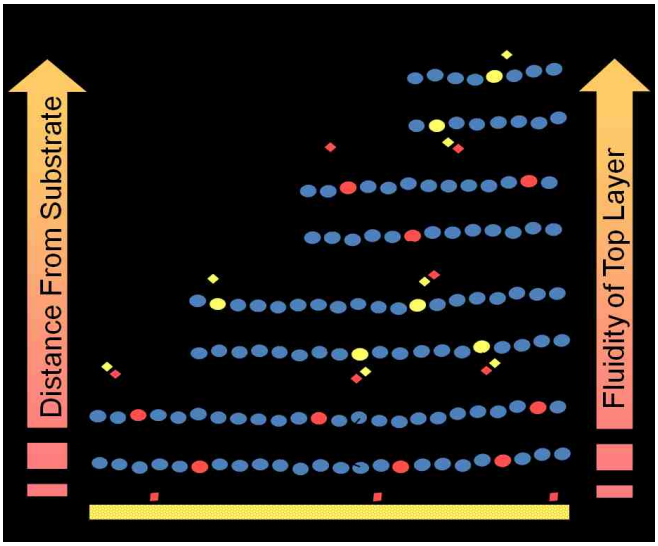

Figure 4.4. Regulating TYPE 2 substrate fluidity by controlling the distance between bilayer and underlying solid support.

Stacks of polymer-interconnected bilayers were fabricated from individual bilayers formed from giant unilamellar vesicles (GUVs) using a procedure adapted from literature [56]. The formation of planar bilayers was induced by gravity. GUVs formed by hydrating lipids in a sucrose buffer were placed in an equimolar solution of glucose buffer. As the GUVs sink to the substrate below, their intrinsic instability causes them to rupture and roll out to form a bilayer. This process is illustrated in Figure 4.5 (A).

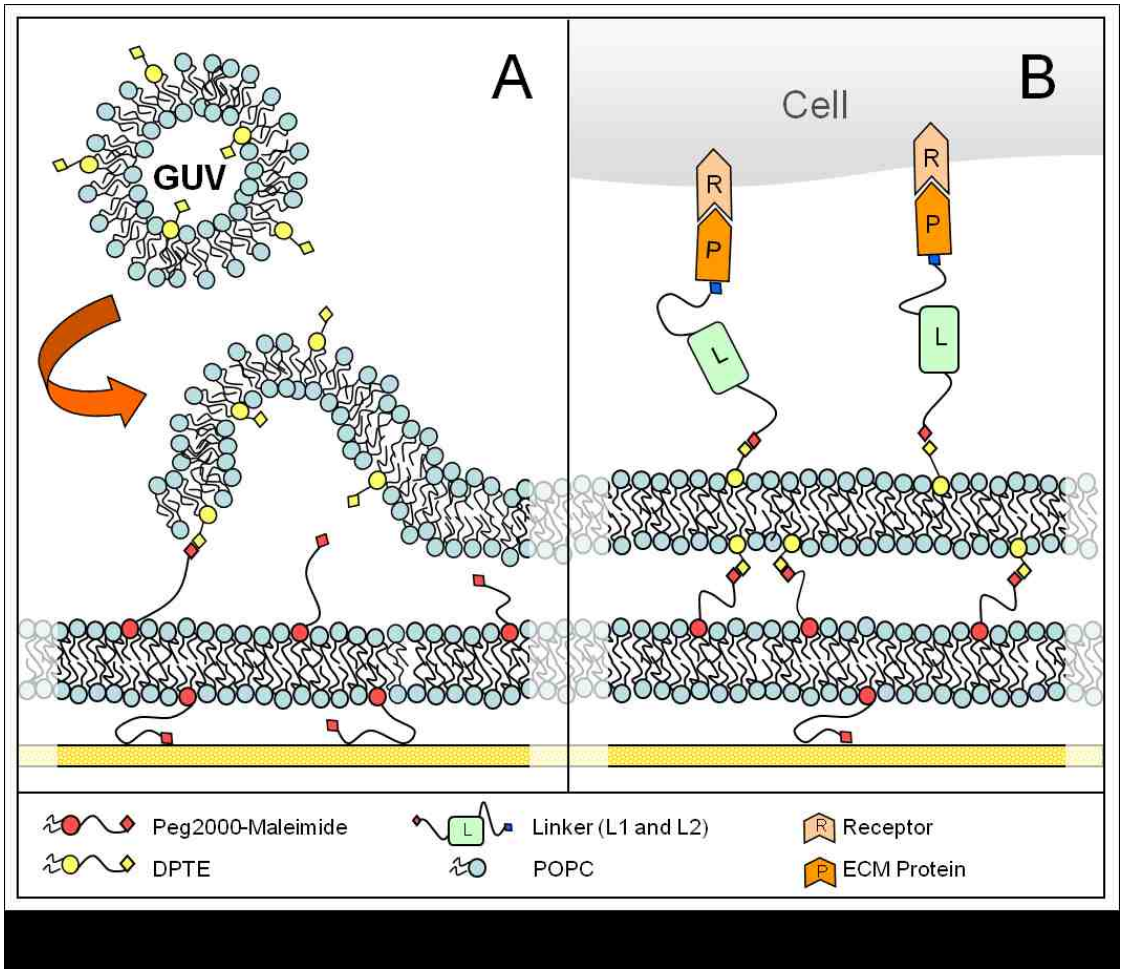

Figure 4.5. Schematic of TYPE 2 cell substrates. TYPE 2 bilayer stacking through GUV fusion (A) and cell/substrate linker design (B).

An important design aspect of these stacked bilayers is the addition of interbilayer connections that covalently link neighboring layers. This linkage was accomplished by routine sulfhydral-maleimide coupling chemistry using the thiolated lipid DPTE and maleimide-functionalized lipopolymer PEG2000-Mal. Using this inter-bilayer linker concept, subsequent planar bilayers were formed by adding GUVs containing complementary linker molecules. This is depicted in Figure 4.5, where a second bilayer, containing 5mol% PEG2000-Mal, is added to an initial bilayer containing 5mol% DPTE. The covalent, polymeric tethering between adjacent bilayers was developed to provide a more robust multi-bilayer system capable of withstanding cellular pulling forces.

Using this iterative procedure, TYPE 2 systems containing up to six stacked bilayers have been fabricated. In each case, the linker composition of the layers was adjusted to insure DPTE was present on the outermost bilayer. As indicated in Figure 4.5 (B), the same cell-substrate linker chemistry used in TYPE 1 substrates was also used in TYPE 2 systems. For the purposes of comparing cell behavior on substrates of different thicknesses, a single bilayer with PEG2000 lipopolymer on the inner leaflet and DPTE on the outer leaflet prepared by LB/LS were often utilized, labeled “TYPE 2, single”. This substrate showed intermediate characteristics relative to substrates plated on multibilayer TYPE 2 systems and laminin coated glass as discussed below.

4.2. Characteristics of TYPE 2 Multibilayer Substrates

4.2.1. Substrate Homogeneity

The homogeneity of TYPE 2 substrates was confirmed through Epi fluorescence microscopy. Here, the outermost layer of single, double, and quadruple bilayers were prepared with 0.5mol% NBD-PE to allow for fluorescence imaging. Bilayer systems appeared defect free (e.g. void of large holes, etc.) and contained only small amounts of excess, unfused, bound GUVs on the surface, as shown in Figure 4.6. Moreover, fluorescence recovery after photobleaching (FRAP) studies indicated increased lateral diffusion in the top bilayer with respect to increased bilayer stacking. Initial bleach spots formed after exposing samples to a 100watt mercury lamp with an appropriate filter set for 1min are shown in Figure 4.6. The progressively less defined bleach spots shown with increased stacking provide qualitative evidence of increased fluidity, as samples with higher lateral diffusion rates are capable of exchanging unbleached dye labeled lipids at a faster rate. The increased diffusion also supports a relatively defect free system, as defects will hinder lateral diffusion. Additionally, it should be noted that NBD-PE was chosen for FRAP experiments due to its photolability, which makes photobleaching easy; less toxic TR-DHPE, was used in cell experiments as a means of verifying homogeneity prior to cell plating. Furthermore, daily imaging verified that the bilayer stacks are stable for several days, even in the presence of cells.

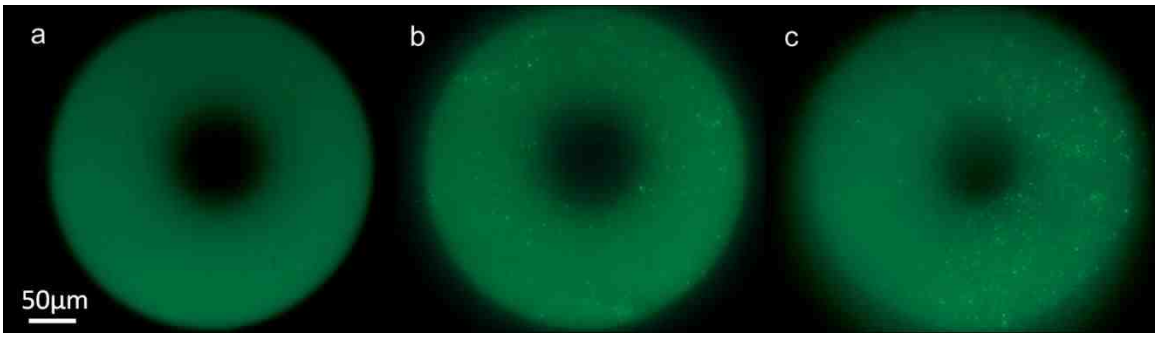

Figure 4.6. FRAP images of single (a), double (b), and quadruple (c) bilayers. Images represent initial bleach spots following a lamp exposure of 1min and show an increase in fluidity with number of stacked films, as indicated with bleached regions of progressively smaller diameters.

4.2.2. Lateral Diffusion Properties

To provide quantitative characterization of bilayer fluidity, SMFM experiments were conducted on dye-labeled TRITC-DHPE lipids in a single bilayer (for this experiment only, the single was constructed not through LB/LS but by GUV fusion onto a fresh glass substrate) and in the top bilayer of double, triple, and quadruple bilayer systems. The outermost layers of TYPE 2 systems were prepared with GUVs containing 10^{-8}mol% of these fluorophore-tagged lipids. As discussed in Chapter 4.1.2, TYPE 2 systems were comprised of polymer-interconnected bilayers where each bilayer contained 5mol% thiolated-lipids or lipopolymers designed to form a covalent linkage with neighboring layers. This percentage was chosen based on previous diffusion studies on polymer-tether bilayers. This percentage created stable linkages (Figure 4.4) and a suitable cell linker density, while providing accurate SMFM tracking analysis. Too low polymer concentrations can result in out-of-plane bilayer undulations that can

compromise the 2D tracking analysis [56]. Moreover, as discussed in Chapter 2.2.1, the concentration of polymer tethers within a bilayer has been shown to impact lateral diffusion by inducing obstacles, where increasing concentration results in lower diffusion coefficients [63, 64]. However, it has been shown that a tethering concentration of 5mol% has no notable impact on lateral diffusion [64, 114].

SMFM was performed as previously described on polymer-tethered bilayers [63, 64, 107], and lipid lateral mobility was measured in terms of the mean-square-displacement (MSD) at a constant time lag of 40ms. MSD was calculated as a function of time lag, t_{lag} [63, 64, 115, 116], as described in Chapter 3.2.3. Each sample was analyzed using 150 time steps of the same t_{lag} to ensure statistical accuracy. The results show that lateral diffusion is indeed regulated by the number of bilayers in a stack, Figure 4.7. MSD valves for single, double, triple, and quadruple bilayer systems were found to be 0.138, 0.196, 0.265, and 0.324μm^2 respectively. With MSD representing the average displacement of a fluorophore within a given time interval, larger displacements directly correlate to increased diffusion coefficients.

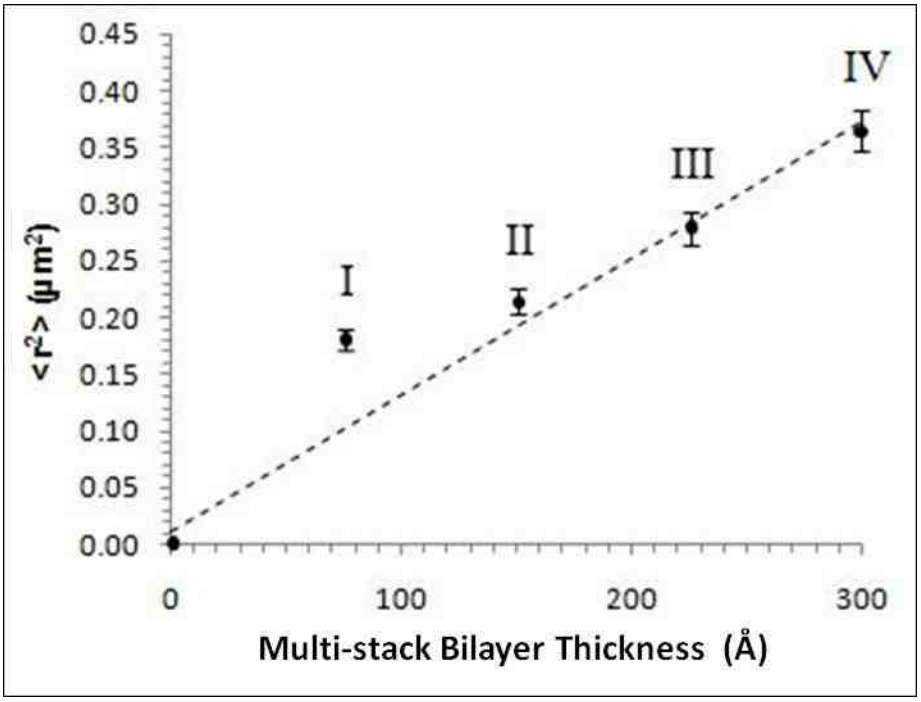

Figure 4.7. Mean squared displacement, $\langle r^2 \rangle$, data of TRITC-DHPE lipids in single (I), double (II), triple (III), and quadruple (IV) bilayer systems confirm increasing bilayer fluidity with increased bilayer stacking (time lag: 50ms, T=21°C). Each data point represents the average of a minimum of 150 tracks.

Analysis of the lipid lateral diffusion in multi-bilayer systems has been performed previously on double layer stacks composed of biotin/strepavidin-based interbilayer connections [66]. While the MSD reported here is comparable to that published, it differs in terms of the overall diffusion change from single to double bilayer (which is more in the TYPE 2 systems fabricated herein). As suggested within this published work, this effect is likely due to molecular crowding induced by the more bulky interbilayer connections [66].

The corresponding thickness values for each bilayer system in Figure 4.7 were calculated based on a lipid bilayer thickness of 41Å [117] and a polymer layer thickness of 34Å. Polymer layer thickness can be approximated by the Flory radius of the polymer chains using scaling arguments of polymer physics [118, 119]. The validity of this approach has been experimentally tested on similar polymer systems previously using fluorescence interference contrast microscopy [120].

The data shown in Figure 4.7 confirm that TYPE 2 substrate fluidity, and thus cell linker mobility, can be regulated through bilayer-substrate thickness (affecting the degree of frictional coupling). Additionally, multi-bilayer systems are capable of creating markedly higher bilayer fluidities than can be achieved in single, solid-supported bilayers. It should also be noted that bilayer stacking resulted in a near linear increase in fluidity from 2-4 bilayers and that the trend line passes through zero, which would represent a completely immobile surface. As shown in Figure 4.7, the linear trend line displays an excellent fit when single bilayer systems are omitted. While data from a single bilayer is shown for comparison, it represents a different system, free of interbilayer connections and any induced polymer effects, and as expected, has differing diffusion properties. Moreover, preliminary AFM studies indicate that multibilayer substrates show increased bilayer undulations. This factor, which results in deviations from planarity, will likely affect diffusion.

While the translational diffusion of dye-labeled lipid constituents in TYPE 2 substrates provides an efficient means of characterizing a change in substrate fluidity, it is unlikely that cells will grab and displace only individual lipids. Instead, it is expected that cells may regulate viscous drag force through the formation of FAs. In the case of lipid bilayer-based substrates, FAs would consist of clusters of cell-substrate linkers. Linker clustering would result in the diffusion of large assemblies of lipids. In theory the formation of FAs (i.e. lipid clusters) should lead to increased viscous drag and allow the cell to develop more traction on these fluid substrates. The diffusion of macromolecular structures was described in Chapter 2.3.2. As shown in equations 2.4 and 2.5, the viscous drag coefficient is directly affected by the radius of the diffussant, where increased size results in increased viscous drag.

In order to experimentally determine the impact of FA formation on viscous drag, diffusion tracking was performed with 1µm fluorescent beads on different TYPE 2 systems. A 1µm bead provides an excellent FA mimic as its size is comparable to a small FA (classical FAs are on the order of 2-5µm in diameter [121]. Here, a heterobifunctional linker containing maleimide and biotin functionalities (Maleimide-PEO_2-Biotin, Pierce Biotechnology) was added to TYPE 2 substrates containing 5mol% DPTE in their outermost layer. NeutrAvidin-coated fluorospheres (Invitrogen) were then added and allowed to bind; excess beads were removed with rinsing. Due to the size of the fluorospheres, bead tracking was performed on an Epi microscope using a 2min time lag. Diffusion

coefficients were calculated for the fluorescent beads and are plotted along with those obtained from lipid tracking in Figure 4.8.

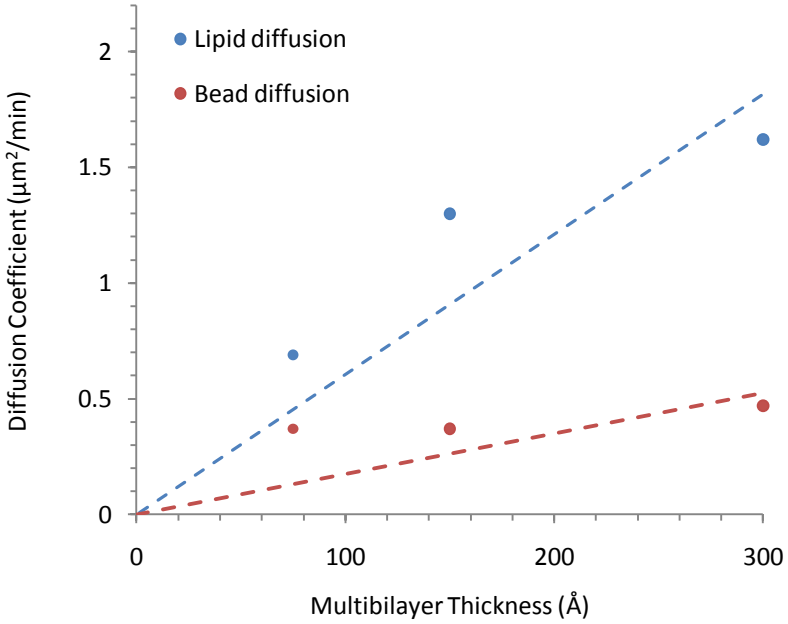

Figure 4.8. Impact of diffussant size on the diffusion coefficient in TYPE 2 substrates. Bead tracking was performed on an Epi microscope (time lag: 2min, T = 21°C). Each point represents the average of no less than 150 tracks (error bars of 5% are not displayed in figure, as they were masked by markers in some cases). Trendlines are simply used to guide the eye.

As shown in Figure 4.8, diffussant size greatly affects lateral mobility. The translational diffusion coefficients of lipids on TYPE 2 double and quadruple bilayers were 1.33 and 1.62μm^2/min respectively. In comparison, beads on TYPE 2 double and quadruple bilayers showed notably slower diffusion coefficients of 0.37 and 0.47μm^2/min. This reveals that cells may be able to modulate viscous drag through the regulation of FA size. Note, as mentioned

above, and as shown in Figure 4.8 the diffusion data for the single layer systems do not completely correlate with that for the multilayer systems. This is likely explained by potential presence of bilayer undulations in multibilayer substrates, which may affect the detected lateral mobility of diffusing fluorophores. The undulations are thought to be the result of water trapped between lipid bilayers [56] and have been observed through AFM on TYPE 2 substrates (data not shown). In the case of bead tracking, diffusion coefficients on single and double bilayers were identical. Groves, et al. studied the diffusion of lipid domains (another form of lipid clusters) in multibilayer systems and found the same result [56]. However, like lipid diffusion, bead diffusion on TYPE 2 substrates was shown to increase with stacking.

Additionally, the diffusion of lipid clusters (i.e. bead diffusion) can be modeled using the Sackmann-Evans theory for protein diffusion. From the obtained diffusion coefficients, the degree of frictional coupling can be calculated using the Stoke's-Einstein relation, Eq 2.6. Here, the frictional coupling, also referred to as the viscous drag coefficient, is affected by several factors including the frictional shear stress created by diffusion particles, polymer-induced effects, and the direct frictional coupling experienced by the bilayer in close proximity to its solid support, see Chapter 2.2.3. The viscous drag coefficients (calculated from the diffusion coefficients of beads) of TYPE 2 double and quadruple bilayers were calculated as 1.1×10^{-8} and 8.6×10^{-9}kg/s respectively based on Eq 2.6. With these drag coefficients the contribution of frictional coupling can be extracted and

approximated as a frictional coefficient using Eq 2.4 and Eq 2.5. Note, the calculated value represents an approximation because while the diffusion coefficients were acquired for 1µm beads, the actual radius of the diffusing lipid cluster is unknown. This is a factor of NeutrAvidin packing on the bead (i.e. linker density), and the actual available area for binding (a factor of the bead curvature). Estimates of the frictional coefficient on TYPE 2 double and quadruple bilayers were calculated assuming a diffussant radius between 0.5µm (the size of the whole bead) and 0.25µm (assuming that bead curvature only makes half the bead's surface area available for binding). This means the frictional coefficient is between $3.3x10^3$ and $1.3x10^4$kg/s on a double bilayer, and between $2.18x10^3$ and $8.17x10^3$kg/s for the quadruple system.

4.2.3. Substrate Integrity

In order for TYPE 1 and TYPE 2 systems to be useful for cell studies involving substrate viscosity, and its role in the mechanotransduction process, these bilayer systems must be able to withstand pulling forces administered by adherent cells. Moreover, direct interactions with the underlying substrate must be eliminated to confirm that observed cellular mechanoresponse is truly a result of substrate viscosity.

The morphology of fibroblasts cultured on glass is well documented. When grown on these rigid substrates, fibroblasts take on large, stretched, polygonic

shapes with prominent stress fibers; phenotypes atypical of cells in tissue. This characteristic phenotype can be used to confirm any potential interaction with the underlying solid substrate in TYPE 1 and TYPE 2 systems. Previously reported studies of cells plated atop lipid bilayers have concluded unwanted interaction with the underlying glass substrate based on the observation of similar polygonic cell shapes [122]. A fluid substrate designed to limit traction forces should, in theory, result in the inability maintain these stretched shapes containing large, mature stress fibers.

Plating GFP-actin transfected fibroblasts atop TYPE 1 substrates, in the absence of cell-substrate linkers, confirms the surpression of cellular interaction with the underlying glass, Figure 4.9. These confocal images show cells failing to spread on these bilayer substrates. While the edges of the cells contained extensions that actively probed the environment for areas to grip and develop traction, the spherical shape and lack of actin stress fibers confirms that these extensions were not reaching the underlying glass and indicates little, if any, interaction with the underlying glass.

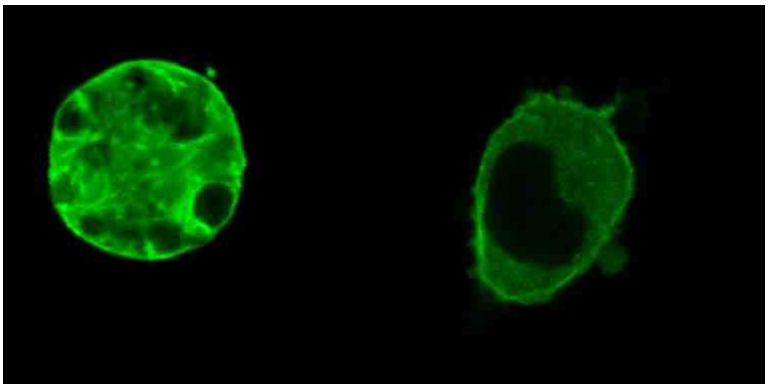

Figure 4.9. In the absence of cell-substrate linkers, plated fibroblasts on TYPE 1 substrates maintain a spherical morphology.

The addition of a polymer cushion beneath TYPE 1 (and TYPE 2) systems functions to uplift and disconnect the lipid bilayers from the underlying glass. Even in TYPE 1 single bilayers systems, this addition appears to eliminate interaction with underlying glass and shows a marked improvement over previous studies with lipid-bilayer based cell substrates. However, aside from the simple addition of lipopolymers, previous studies relied on vesicle fusion techniques to form bilayers. Using the LB/LS procedure described in Chapter 2.1.1, for fabricating TYPE 1 systems and the initial bilayer of TYPE 2 systems resulted in more homogeneous films with fewer defects.

In a similar experiment on TYPE 2 bilayers, cells were plated on a control substrate and a double bilayer containing cell-substrate linkers to ensure cell adhesion and spreading was a result of cells interacting with the fluid cell substrate linkers of the lipid bilayer and not with the underlying glass. The

control substrate consisted of essentially the “underside” of a double bilayer system, as shown in Figure 4.10. Here, cells were plated on a typical TYPE 2 substrate and a substrate displaying 5mol% PEG2000Mal on the surface. PEG-modified surfaces are well known for their ability to inhibit cell growth. Cells were allowed to grow for 24h before being analyzed in terms of adhesion (i.e. cell density and shape: spherical vs. nonspherical), spreading (i.e. cell area), and cytoskeletal organization (i.e. visible stress fibers vs. no visible stress fibers).

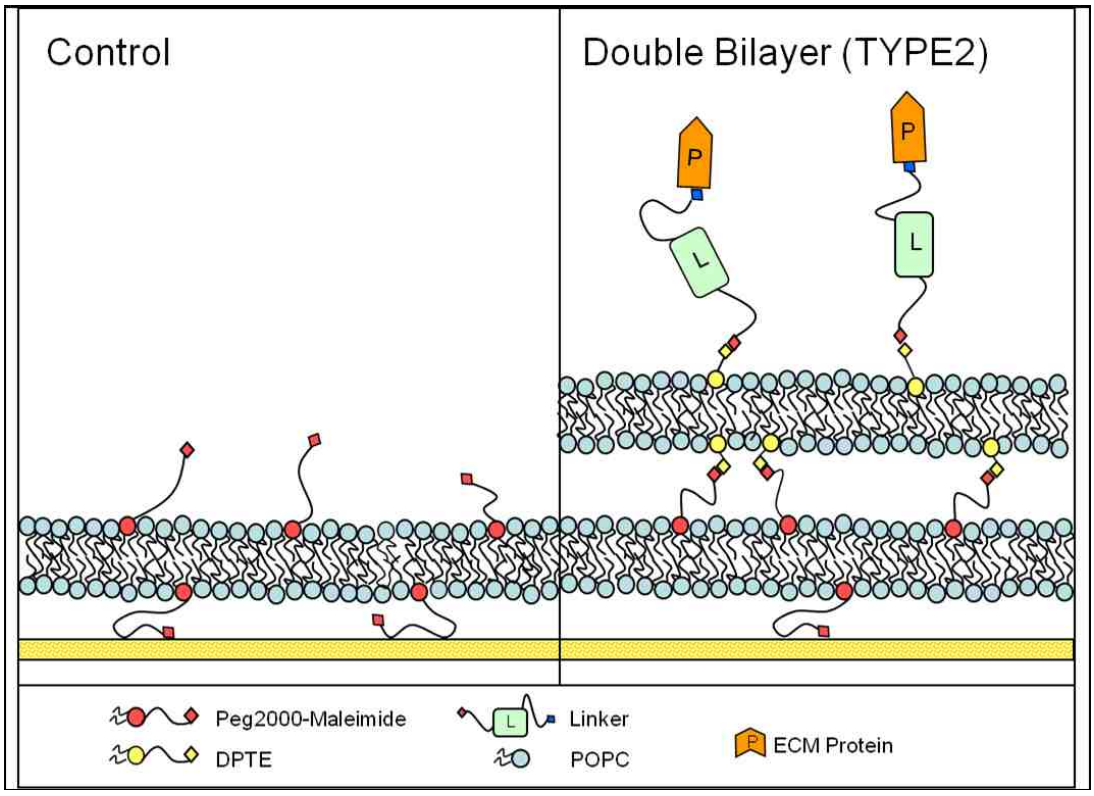

Figure 4.10. Schematic of control substrate designed to mimic the underside of a double bilayer system.

Cellular adhesion and cytoskeletal organization are shown in Table 4.1. Essentially all cells plated on the double bilayer system adhered and spread with only 0.9% maintaining a spherical (weakly adsorbed) shape. However, on the control system, 55% of cells failed to spread. Moreover, cell densities of 0.88cells/mm^2 on the TYPE 2 substrate and 0.46cell/mm^2 on the control suggested that only around 50% of the total plated cells even adhered to the control substrate. These data confirm that cell adhesion and spreading on TYPE 2 substrates are not a result of cell locating bilayer defects and interacting with the underlying glass.

Table 4.1. Evaluation of fibroblasts shape and cytoskeletal stress fiber formation 20h after plating on TYPE 2 double bilayer and control substrate (110 cells analyzed for each substrate).

Substrate	Spherical Cells	Stress Fiber Containing Cells	Cell Density
Control	55.0%	0%	0.46 cells/mm^2
Double Bilayer	0.9%	36%	0.88 cells/mm^2

Cellular spreading, 24h after plating on these substrates was also analyzed in terms of cell area, see Figure 4.11; data further validate that cell growth is not a result of bilayer defects.

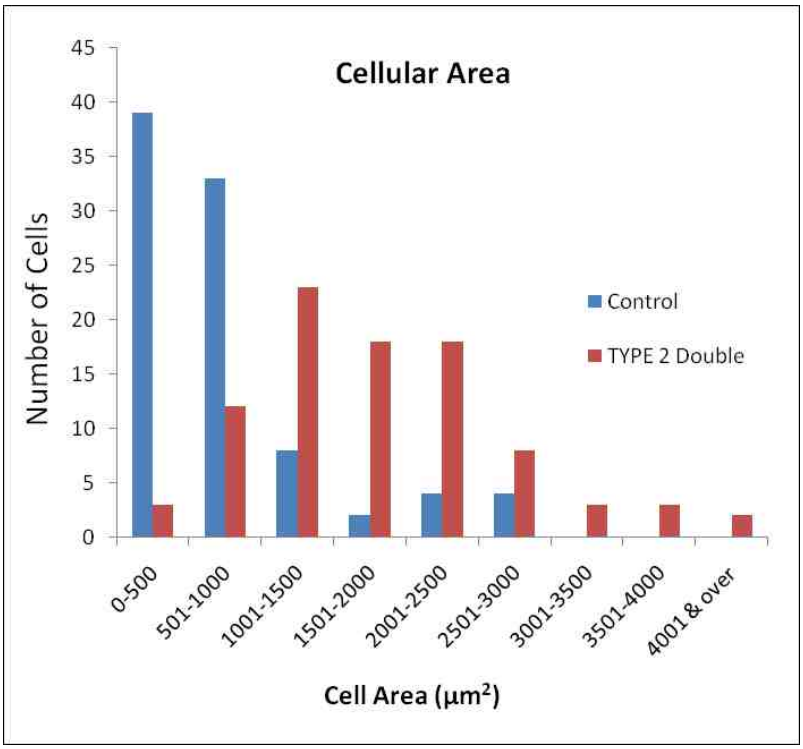

Figure 4.11. Cell area histogram of cells plated on control bilayer systems (see Figure 4.9) illustrates the lack of spreading on the control system compared to the TYPE 2 double bilayer (analysis performed 24h after plating).

Additionally, the stress fiber data contained within Table 4.1 suggested that even on fluid substrates with mobile cell linkers, cells can develop the necessary traction force to create stress fibers, even if the stress fibers are much smaller and more dynamic than those observed on rigid surfaces. This ability is likely due to the fact that, in a fluid system, cells can adhere and simply wait for additional cell linkers to diffuse by. Over time it is assumed that cells can gather clusters of cell linkers to form small FAs. The viscous drag experienced by a cell pulling on a cluster of linkers should be substantially larger than pulling a single cell linker and this may provide the cell with the ability to create thin, dynamic

stress fibers. Fluorescent bead tracking confirmed these results as shown in Chapter 4.2.2, where it was shown the diffusion coefficients of lipid clusters are notably reduced compared to individual lipids. The delayed spreading time observed on TYPE 1 and 2 substrates (typically on the order of 4h) suggests that this process may in fact be happening.

The control experiments above successfully addressed the possibility of defects present in TYPE 1 and 2 substrates on the basis of cell shape and cytoskeletal organization. However, what if cell adhesion and spreading induces defects that promote these processes? All cell work on TYPE 2 bilayers consisted of work with 3T3 fibroblasts. These cells were chosen for their robustness and the fact that they have been previously shown to display elasticity-dependent properties. However, the pulling force of fibroblasts is relatively strong, on the order of 7,000pN (leading edge) to 100,000pN (trailing edge).

Substrate integrity under adherent fibroblasts was validated through fluorescence microscopy. As stated previously, the outermost layers of all lipid bilayers, TYPE 2, were labeled with small quantities dye-labeled lipids (TR-DHPE). This enabled imaging prior to cell plating to confirm substrate homogeneity and imaging after plating to confirm substrate integrity. Fluorescence microscopy under plated cells was used to verify that adherent, migrating cells were not pulling the lipid bilayers apart and imparting defects. Intensity analysis of dye-labeled bilayers

under adherent cells shows no evidence of large scale cell-induced defects, Figure 4.12.

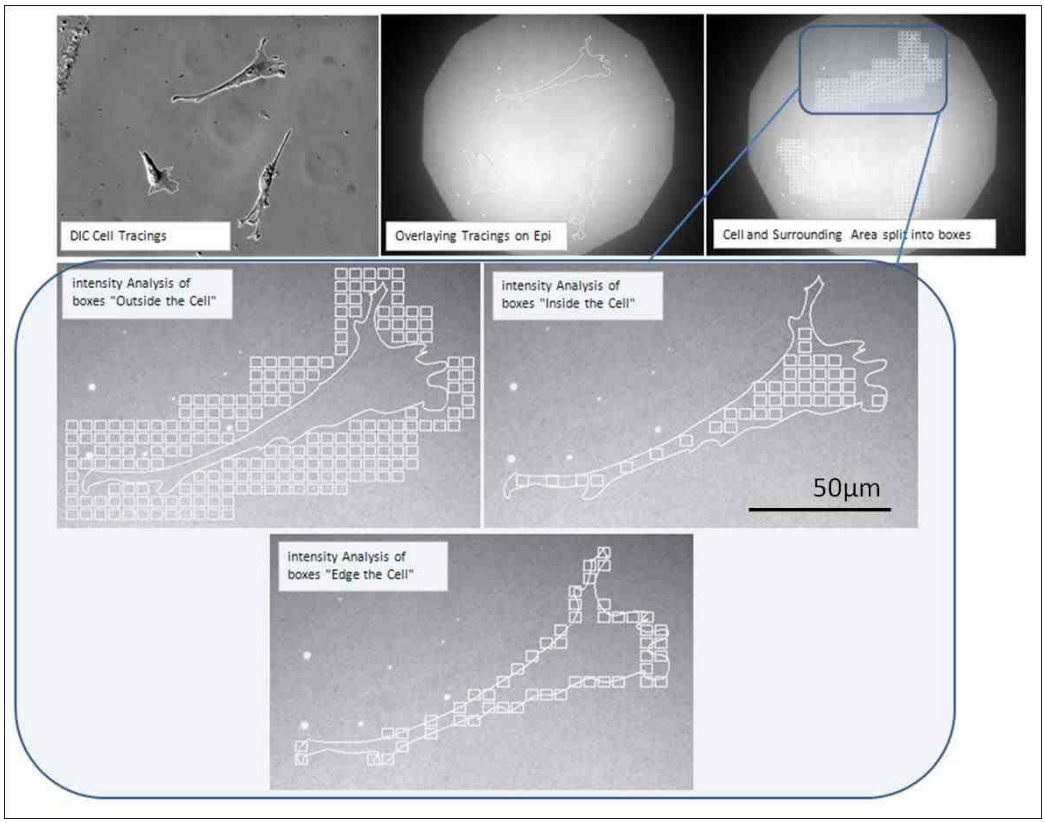

Figure 4.12. Fluorescence intensity analysis of TYPE 2 lipid bilayers under adherent cells. Average intensity values for DHPE-TR labeled bilayers were obtained outside, inside, and on the edge of adherent cells (analysis performed 20h after plating).

The presence of defects (e.g. holes) should result in a decrease in fluorescence intensity. Using imaging software, the average fluorescence intensity in areas inside the cell, outside the cells, and on the edge (shown by boxes in Figure 4.12.) were determined and are tabulated bellow. As shown in Table 4.2, little

variation in fluorescence intensity is shown. If cells were indeed penetrating the bilayer, this would be expected to occur near the edge regions. The fact that the intensity of the edges is in line with that inside the cell, and within the standard deviation of that outside the cell, shows that this is unlikely.

Table 4.2. Fluorescence intensities (Au) of TYPE 2 substrates in areas inside, outside, and on the edge of adherent cells. Fluorescent signal results from the addition of 5mol% TR-DHPE in substrates.

		Average Intensity	Std. Dev.
CELL 1	Outside the Cell	408.7	41
	Inside the Cell	394.4	19
	Edge of the Cell	390.2	32
CELL 2	Outside the Cell	468.0	21
	Inside the Cell	472.3	8
	Edge of the Cell	462.2	17
CELL 3	Outside the Cell	471.7	29
	Inside the Cell	474.9	11
	Edge of the Cell	473.9	19

The above controls were used to show the absence of visible defects. However, they do not account for the presence of smaller, sub-diffraction, inhomogeneities. While too small to capture through microscopy, the occurrence of any such areas would manifest themselves through changes in the lipid diffusion, and result in slower diffusion rates and/or larger immobile fractions. Small scale FRAP was

performed using a confocal microscope to address the possibility of increasingly small defects.

If cell penetration through the bilayer occurs, it is expected to be at the sites of FAs, areas where the cell is physically gripping the surface and developing traction force. Thus, cells were transiently transfected with GFP-FAK (focal adhesion kinase), plated on a TYPE 2 double layer containing 5mol% TR-DHPE (dye-labeled lipids), and allowed to adhere and spread overnight. The cells were imaged 20h after plating. The green fluorescence in Figure 4.13 (a) represents the labeled FAs. The image to the right, Figure 4.13 (b) shows an overlay of a DIC image and images collected through GFP and Texas Red filter sets. Confocal FRAP was performed on an area directly under an FA, marked as "*c*," and an area outside the cell, marked as "*d*." Figure 4.13 (c) and (d) show the initial bleach spot (left) and final recovery spot (right) after FRAP. Both areas of the bilayers displayed excellent recovery whether under and outside FAs. Quantitative FRAP data are plotted below, Figure 4.13 (e). The fluorescence recovery curves of both areas overlay nicely, corresponding to very similar rates of diffusion, and show roughly the same fluorescence plateau value, corresponding to very similar immobile fractions.

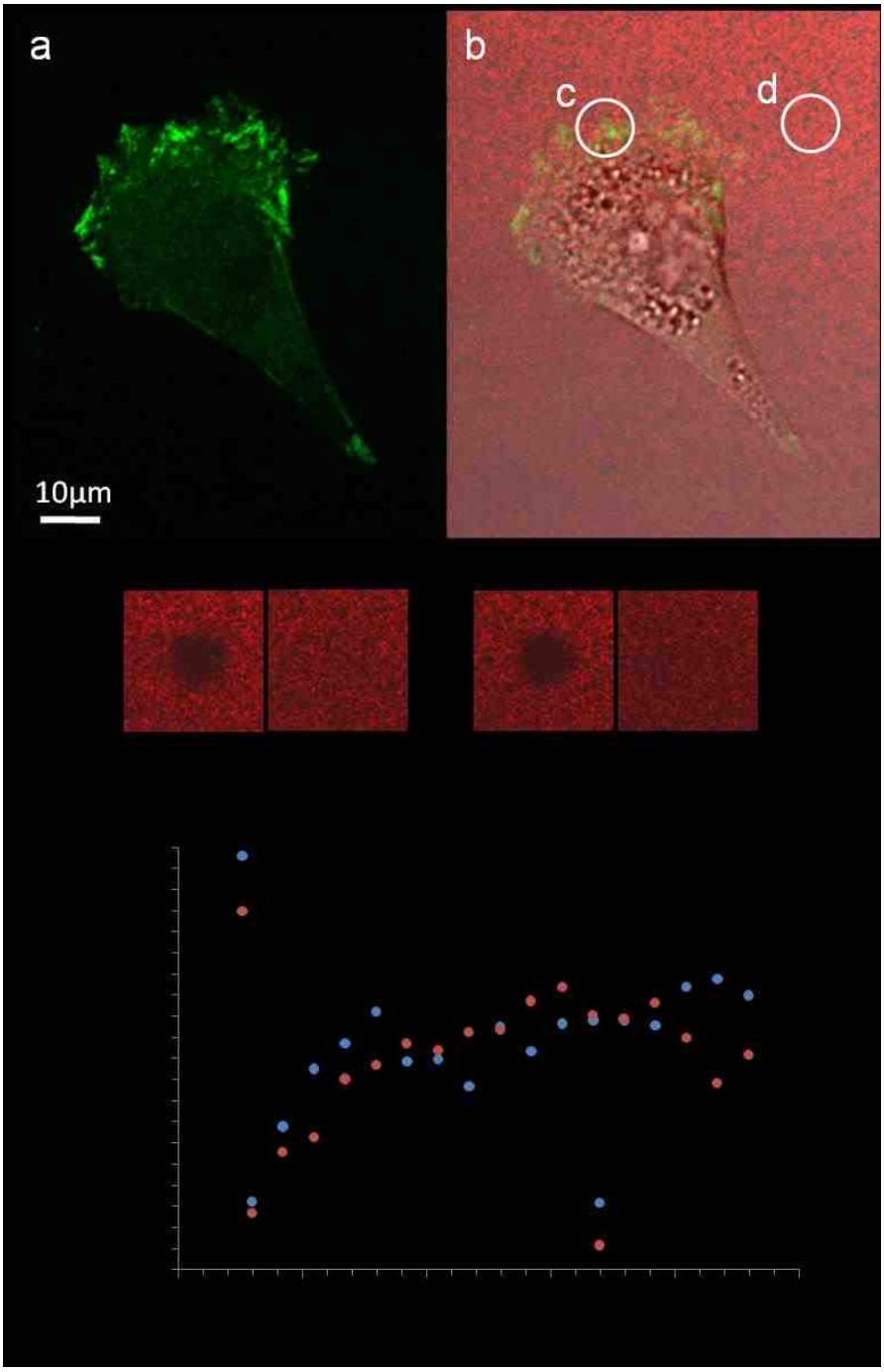

Figure 4.13. Confocal FRAP performed on dye-labeled (DHPE-TR) TYPE 2 bilayers underneath the FAs of adherent fibroblasts confirms substrate integrity. Confocal image of GFP-FAK transfected 3T3 fibroblasts is used to visualize FA distribution (A). Overlaid DIC, and fluorescent images (GFP and DHPE-TR) were used to chose an area underneath (C) and outside (D) FAs sites for confocal FRAP analysis. Obtain FRAP curves for spots (C) and (D) are comparable and show not net loss in fluidity (E).

This confirms that the presence of adherent cells does not affect the homogeneity of the bilayer and that the plated cells are truly resting on top of the substrate. Thus, any mechanoresponse shown on TYPE2 systems, must be a result of changes in substrate fluidity affecting cellular traction forces.

4.3. Design of Quantum-Dot Based Heterobifunctional Linkers

4.3.1. Linker Design

Heterobifunctional linkers were designed to efficiently link adhesion proteins to lipids present in TYPE 1 and TYPE 2 substrates. As illustrated in Figure 4.4., TYPE 2 bilayers were fabricated using an iterative approach that utilized the sulfhydral lipid DPTE in the outermost layer of these bilayer systems. Thus, maleimide/sulfhydral coupling chemistry was again utilized as part of the bifunctional linker. For the protein linking side, an NHS active ester was used to bind primary amines, which are widely present in proteins. Both maleimide/sulfhydral and ester/amine coupling chemistry is efficient, does not require a catalyst and can be performed in an aqueous environment at room temperature.

With prior knowledge of quantum dot (QD) synthesis and functionalization, QDs provided an excellent starting block for linkers. Moreover, utilizing QDs in the

linker design holds promise for dynamic imaging studies in the future. QDs were synthesized using a previously published sonochemical approach [105]. As discussed in Chapter 3.2.5, directly following their synthesis, CdSe/ZnS QDs are ill-suited for biological applications; they are not water soluble, prone to aggregation and non-specific adsorption, and display some cytotoxicity. However, QDs are efficiently coated through published lipopolymer encapsulation techniques [106, 107], see Chapter 3.2.5. Here, the amphiphilic nature of the lipopolymers is used to create a self-assembled lipid monolayer "shell" over hydrophobic QDs. Additionally, the PEG moieties of the lipopolymers function as entropic springs to hinder aggregation. Doping the lipopolymer mixture with small quantities of functionalized lipopolymers, in this case PEG2000-Mal and PEG2000-NHS, allowed the formation of QD-based linkers as illustrated in Figure 4.14.

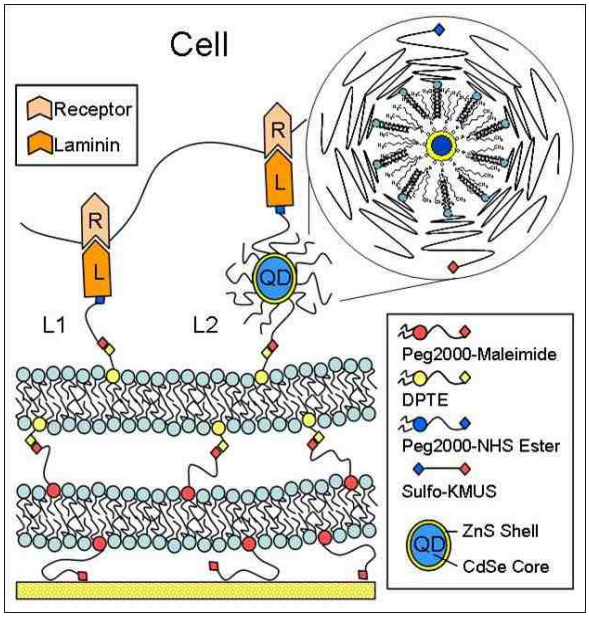

Figure 4.14. Design of cell-substrate linkers based on QDs encapsulated with functionalized lipopolymers.

The quality of the synthesized QD-based linkers was confirmed through FCS prior to use. FCS data reveal the size (hydrodynamic radius), aggregation state, and concentration of the linkers based on diffusion coefficients; see Chapter 3.2.6. Diffusion coefficients were compared to published data for lipopolymer encapsulated QDs [104] to ensure QD stocks were free of large aggregates, which would indicate impartial/failed encapsulation and hinder proper functioning. In practice, the characteristic diffusion time of monodisperse, lipopolymer encapsulated QDs is approximately 1400-1800µs (diffusion range is based on fluctuations in laser power from day-to-day).

Additionally, this encapsulation approach produced stable QD coatings owing to hydrophobic and electrostatic interactions of the lipopolymers with the coordinating solvent present on the surface of quantum dots. Shelf lives in the order of months have been observed, compared to weeks when using more traditional surface exchange coating procedures.

4.3.2. Linker Functionality in Live Cell Applications

Live-cell SMFM-TF on QD-labeled lipids in the plasma membrane provided further validation of proper linker functioning while simultaneously ensuring biocompatibility and overall bioinertness. Here, fusogenic SUVs were prepared, as described in Chapter 3.2.7, and labeled with maleimide functionalized lipopolymer encapsulated QDs. This linkage was facilitated by the thiol-

maleimide coupling chemistry described above; small quantities, 10^{-3}mol%, of DPTE were used in the preparation of SUVs. Labeling was verified through FCS, where differences in QD diffusion coefficients were observed upon binding as QD-labeled SUVs displayed an average diffusion time of 3257µs compared to 1533µs for unbound QDs. This change is a result of the increased size of the QD-labeled SUV, which slows diffusion.

Excess QDs, present in the fusogenic SUV solution, containing maleimide functional groups have the potential to nonspecifically interact with various cell membrane proteins (e.g. proteins with exposed cysteine residues). FCS was used to confirm the absence of unbound QDs prior to fusion. In a titration experiment, functionalized QDs were slowly added to the SUV stock. By monitoring changes in diffusion time the appropriate amount of QDs needed for labeling could be determined. When labeling is complete and further addition results in an excess of unbound QDs, the autocorrelation curve generated by FCS can no longer be described with a single component fit. Instead, the autocorrelation curve of labeled-SUVs in the presence of excess QDs is best described with a two component fit. In this case, the two component fit resulted in components with diffusion times of 3428.5µs and 1743.4µs, corresponding to QD-labeled SUVs and unbound QDs respectively.

A small amount of the QD-labeled SUV stock, free of excess QDs, was added to the culture media of adherent COS 7, HEK293, and 3T3 cells. Following fusion,

SMFM-TF was performed in collaboration with Ken Ritchie (Purdue University). Data were acquired at 30 frames per second (FPS). Histograms of the observed diffusion coefficients are presented in Figure 4.15. When compared to published diffusion coefficients for dye-labeled lipids, Table 4.3, the results obtained with QD-labeled lipids are very similar. The only divergence from published data was seen in the HEK293 cells. However, previous studies on HEK293 have indicated a rather large variation in diffusion coefficients for this cell line [123]. Figure 4.15, shows that, in fact, that HEK293 cells displayed the broadest diffusion coefficient distribution with QD-labeled lipids as well. The variation seen in this particular cell line likely results from their less flattened morphology; deviations from 2D impact the effectiveness of single molecule tracking.

Any unwanted interaction with membrane components, nonspecific adsorption, or toxicity effects would manifest themselves in the observed diffusion coefficients. The excellent agreement of QD diffusion data shown in Table 4.3 not only confirms proper linking, but also demonstrates the biocompatibility and inertness of lipopolymer encapsulated QDs.

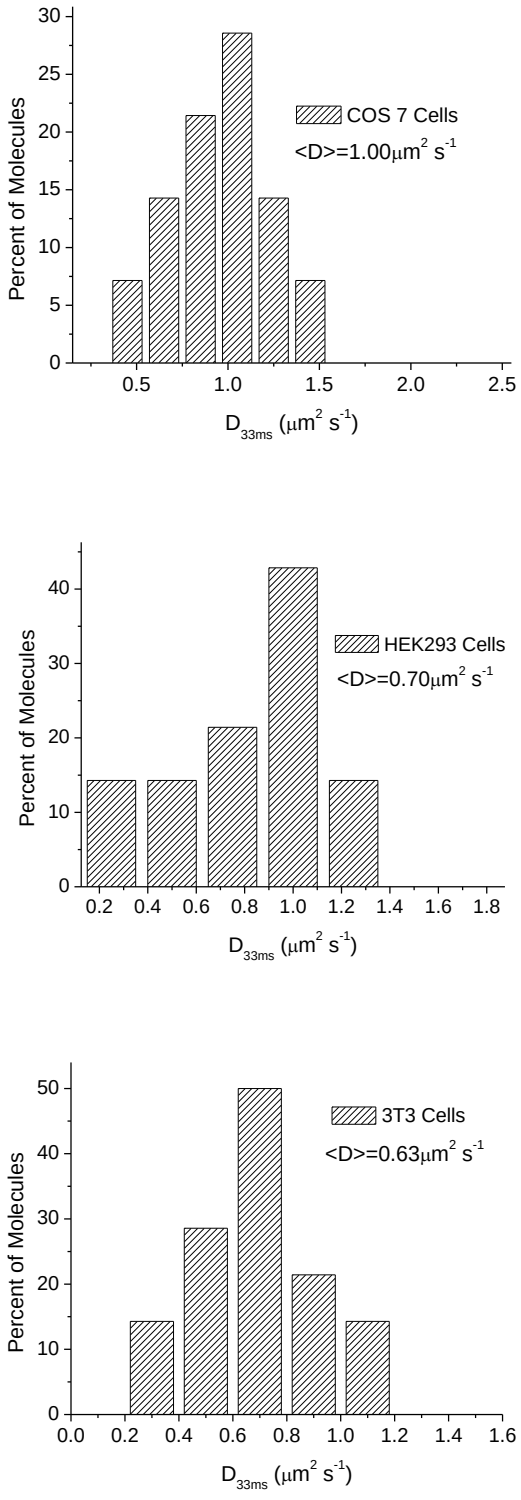

Figure 4.15. Diffusion coefficient histograms obtained from QD-labeled lipid tracking on live COS 7, HEK293, and 3T3 cells.

Table 4.3. QD-labeled lipid diffusion in cell plasma membranes compared to that previously obtained with dye-labeled lipids.

Probe	Cell Line	<D> $\mu m^2 s^{-1}$	Reference
Cy3-CtxB-GM1	COS-7	1.01	Kenworthy, et al. (2004) [124]
QD-DPPE	COS-7	1.07	This work
Cy3-DOPE	HEK293	0.41	Murase, et al. (2004) [123]
QD-DPPE	HEK293	0.70	This work [107]
$diIC_{18}Icc$	3T3	0.68	Metcalf et al. (1986) [125]
QD-DPPE	3T3	0.63	This work

The above SMFM-TF experiments demonstrate proper functioning of the maleimide component of lipopolymer QDs. Similar testing was performed to ensure proper active ester/amine binding. Here, QDs were coated with an identical lipopolymer composition except the PEG2000-Mal was replaced with PEG2000-NHS. This particular lipopolymer is not commercially available and was synthesized by removing the double bond on the maleimide functionality of PEG2000-Mal. This was performed in a straightforward hydrogenation reaction catalyzed by palladium activated charcoal. The formation of PEG2000-NHS was confirmed through NMR; indicated through the appearance of a peak at 2.7ppm.

Biocompatibility and functionality testing of PEG2000-NHS QDs were performed by a fellow lab member, Amanda Siegel. Newly prepared NHS functionalized QDs were bound to transferrin antibodies and applied to cells (adipocytes) expressing transferrin receptor in their plasma membrane. Live cell SMFM confirmed successful linking and allow for protein tracking within the plasma membrane. An example histogram of MSD values for the diffusion of QD-tagged transferring receptors diffusing in the plasma membrane of adipoctyes is shown in Figure 4.16.

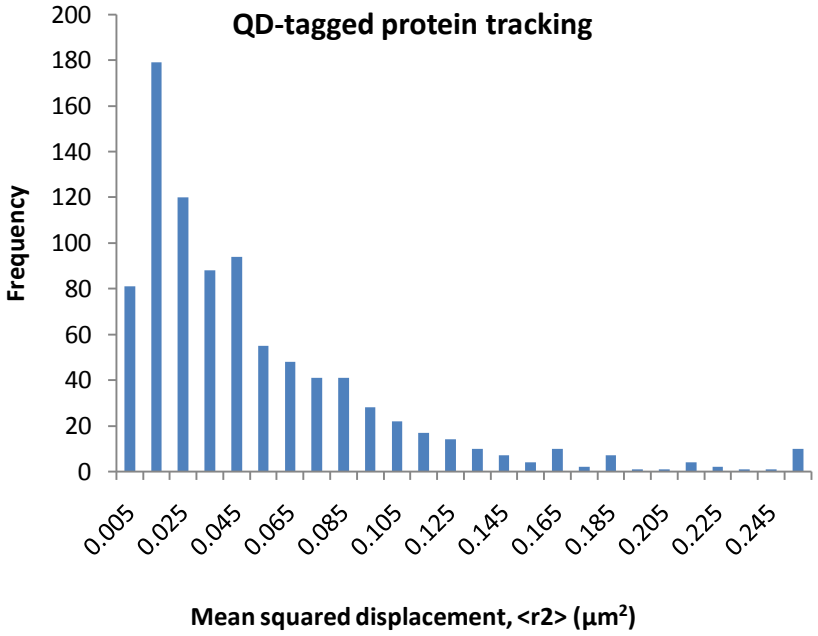

Figure 4.16. SMFM protein tracking using PEG2000-NHS-functionalized QDs confirms proper binding. Histogram displays $<r^2>$ values for QD-tagged transferrin receptors diffusing in the plasma membrane of adipocytes (time lag: 40ms, T = 21°C).

With both functional units of the cell linker tested for biocompatibility and proper linking, the QD-linkers depicted in Figure 4.14, containing quantities of PEG2000-Mal and PEG2000-NHS were used as cell/substrate linkers. Linker L1 (sulfo-KMUS), shown in Figure 4.13 was used as a control linker to ensure proper binding. This commercially available heterobifunctional linker contains sulfhydral and amine binding groups and was used as a comparison to lipopolymer coated QDs. The synthesized QD-based linkers were found to perform identically compared to the commercial linker.

4.4. Cellular Mechanoresponse on TYPE 1 Substrates of Tunable Viscosity

4.4.1. Neuron Outgrowth and Network Formation

In collaboration with Josef Käs, University of Leipzig, PC12 neurons were plated on TYPE 1 substrates. As described previously, substrate viscosity was tuned through tethering concentration, which impacted cell linker mobility. In this case, the mechanoresponse of neurons was characterized on TYPE 1 systems of 5% and 30% tethering concentrations. These percentages reflect the limits of fluidity regulation for these substrates, where 5% tethering concentration displays similar diffusion coefficients to a tether-free solid supported bilayer system and 30% represents a near immobilized diffusion; these results were reported previously and were shown in Figure 4.2.

Phase contrast microscopy was used to image the P12 neurons 20h after plating. The images acquired revealed that substrate viscosity had a profound impact on neurite outgrowth and network formation. Less viscous substrates showed accelerated growth; representative snapshots are shown in Figure 4.17.

Using Matlab, the length of individual neurite extensions were measured. Branching was accounted for by including the length of the branches in the total outgrowth for the neurite. Knowing the precise time of image acquisition allowed for the determination of neurite outgrowth velocities. As shown in Figure 4.18, increased outgrowth was observed on the more fluid system, 5mol% lipopolymer tethering concentration.

The increased growth and network formation seen on TYPE 1 substrates of higher fluidity correlates nicely with existing data of neuronal mechanoresponse to substrate elasticity. It has been shown previously [86, 87], that neurons prefer growth on softer substrates. This is largely explained by findings that reveal cells' preference for growth on substrates comparable to their native tissue environment [79]. In this case, for example, brain tissue is notably softer than connective tissue with an elastic modulus of 0.1-10 compared to 600-1,000nN/μm^2 [90]. Moreover, neuronal cells direct very small forces onto their substrates, orders of magnitude smaller compared with other cell lines [90]. This fact reveals that neuronal cells are not required to generate high traction forces for movements and growth. In fact, many believe neurite outgrowth is more a

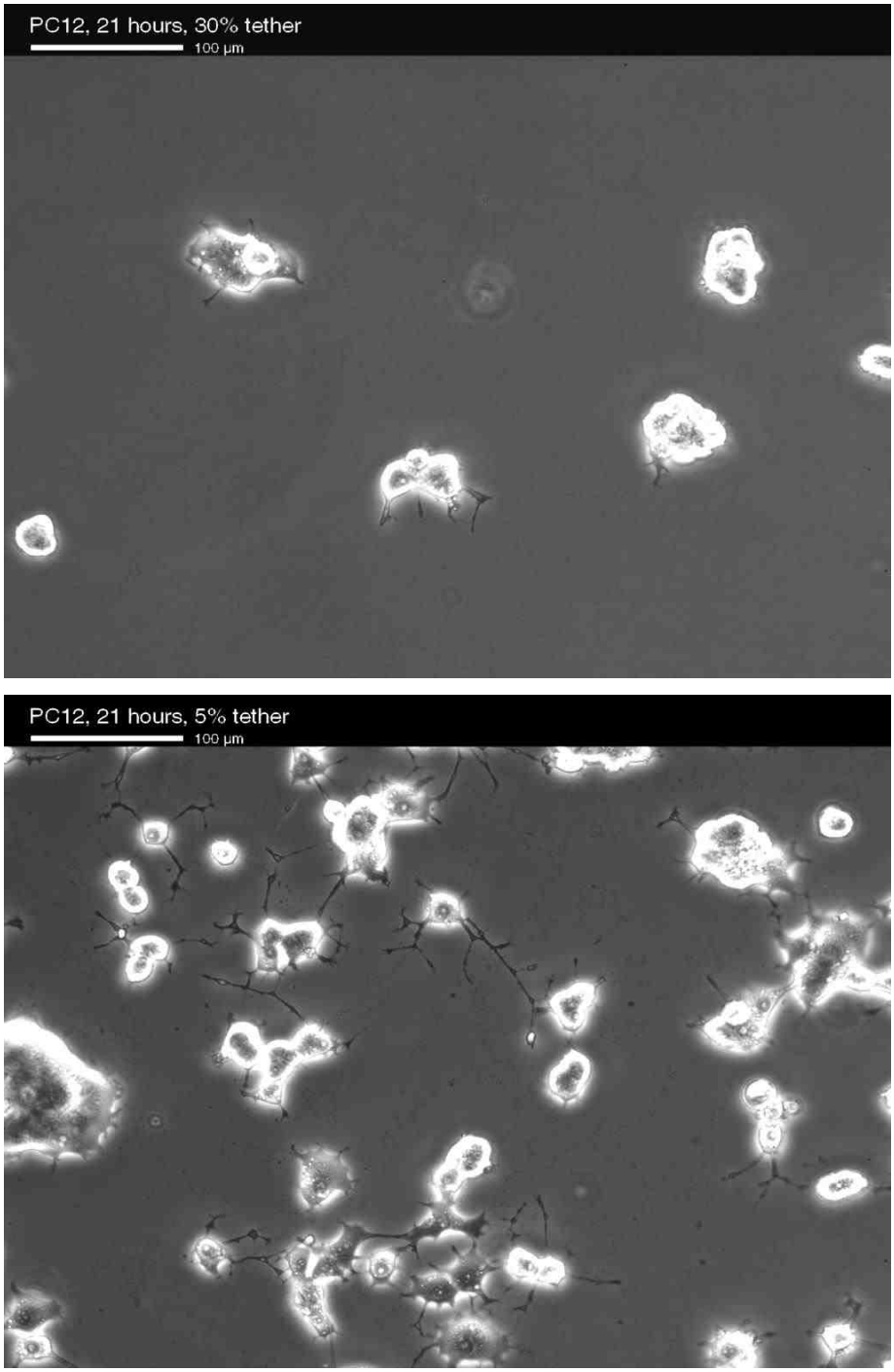

Figure 4.17. Neurite outgrowth and network formation is accelerated on more fluid, 5% tethering concentration (Bottom), compared to more viscous, 30% tethering concentration (Top) TYPE 1 substrates.

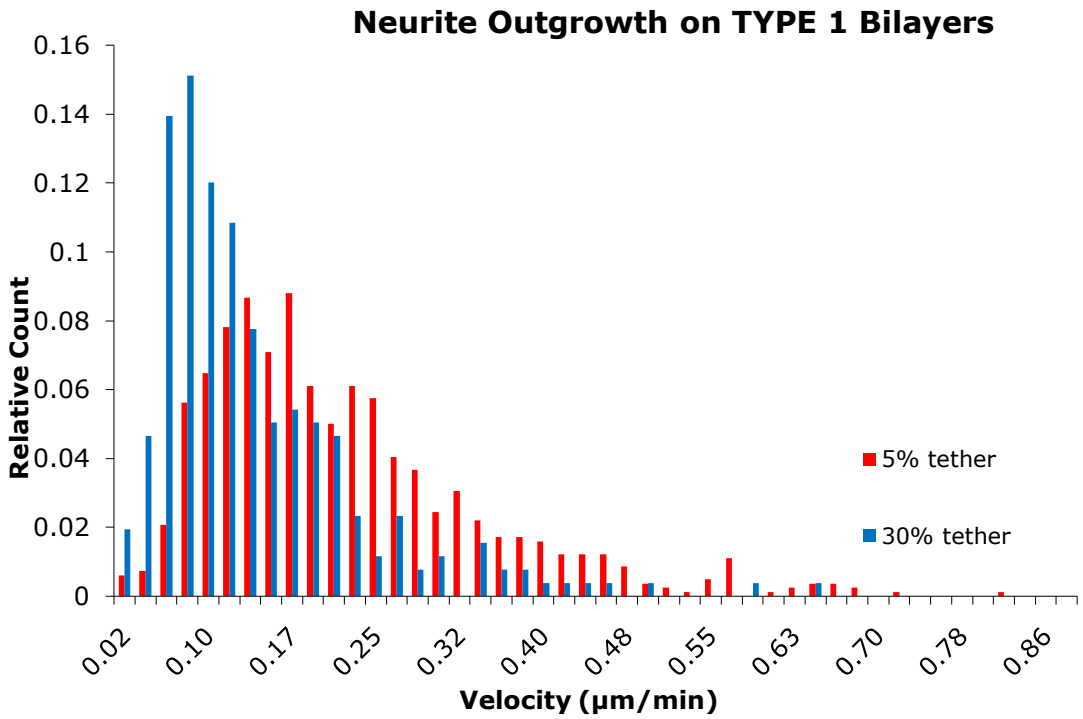

Figure 4.18. Neurite outgrowth velocity histograms on TYPE 1 substrates composed of 5% and 30% polymer-tether concentrations indicate increased growth on the more fluid substrate.

result of pushing than pulling [based on personal communications with Professor Josef Käs]. This explains the accelerated growth seen on more fluid TYPE 1 substrates.

Moreover, neuronal mechanosensing of substrates stiffness has been modeled using the “motor-clutch” force transmission system [126]. This model, which has been experimentally confirmed, predicts fast actin retrograde flow on stiff substrates and slow actin retrograde flow on soft substrates [126]. Additional research has shown that actin retrograde flow inversely impacts neuron growth

cone advancement [127, 128], explaining the previously observed increase in neurite outgrowth velocities on soft substrates [86, 87]. Similar mechanosensing may be utilized in the assessment of substrate viscosity as the mechanoresponse on TYPE 1 systems is similar to that on soft PAA gels.

The fact that neurons prefer more diffuse surfaces makes TYPE 1 substrates an excellent candidate for the study of mechanotransduction in neurons. While the addition of the polymer tether under TYPE 1 substrates appears to suppress cellular interaction with underlying glass (as suggested in Figure 4.9.), neurons' preferences for softer substrates eliminate the need for the more robust TYPE 2 multi-bilayer stacks. The inability of TYPE 1 substrates to illicit a response in fibroblasts led to the design and fabrication of TYPE 2, which are capable of more dramatic changes in substrate viscosity.

4.5. Cellular Mechanoresponse on TYPE 2 Substrates of Tunable Viscosity

4.5.1. Fibroblast Phenotypes

As discussed in Chapter 2.4, adherent cells continually probe their surroundings through actomyosin-mediated pulling forces. Mechanical cues are then transformed into biological signals that can lead to a variety of cellular responses, including changes in cellular phenotype. To explore the impact of linker mobility

(i.e. substrate viscosity) on cellular mechanotransduction and response, 3T3 fibroblasts were plated on TYPE 2 substrates containing 5mol% mobile Laminin-based cell linkers as illustrated in Figure 4.14. Cell adhesion and spreading on laminin-functionalized substrates is comparable to that on the more widely used fibronectin-based substrates [129]. While these robust cells, capable of generating large pulling forces, were ill-suited for experiments on TYPE 1 substrates, TYPE 2 systems presented stable (capable of withstanding cellular pulling forces) platforms where more dramatic changes in substrate viscosity could be achieved.

Cellular mechanoresponse in terms of phenotypical changes were observed through DIC and phase contrast images taken at 20h and 40h marks after plating. Immediately following plating, cells displayed delayed spreading and maintained their spherical shape for upwards of 4h. This is strikingly different compared to cells plated on laminin coated glass and culture dishes where spreading is typically observed within 30-60min. This behavior, described Chapter 4.1.3, is likely the result of adherent cells slowly collecting mobile cell linkers as they diffuse by in order to cluster cell-substrate linkers into FAs. In this case of mobile linkers, increasing the size of cell-substrate linker clusters should increase the viscous drag experienced during cellular contraction, giving cells the ability to modulate traction forces. This aspect was shown in Chapter 4.2.2 where 1μm beads were shown to diffuse at a much slower rate than individual lipids. FAs, while thought to be small and dynamic in these fluid substrates, are

potentially still needed to induce cell spreading. After 4h, fibroblasts showed pronounced spreading on TYPE 2 substrates.

Brightfield imaging of 3T3 fibroblasts on TYPE 2 substrates 20h and 40h after plating revealed drastic phenotype changes compared to that observed on traditional rigid culture dishes, and even that on softer PAA gels. Figure 4.19 depicts six representative cell shapes seen on TYPE 2 substrates.

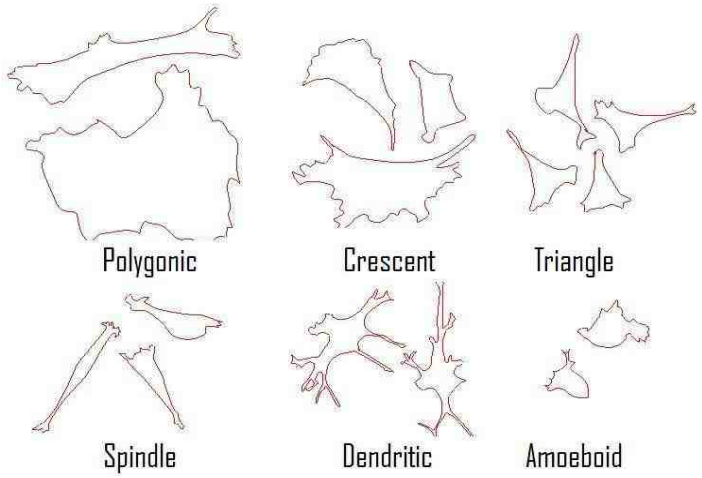

Figure 4.19. Characteristic fibroblast phenotypes on TYPE 2 substrates.

The relative abundance of the different shapes was correlated to substrate viscosity. The overlaid morphology histograms in Figure 4.20 show varying populations of these shapes with respect to glass (control), single, double, and quadruple TYPE 2 substrate (shape analysis preformed 40h following plating). These observed cell phenotypes are significant in that they show intriguing

parallels and remarkable differences compared to mechanoresponse previously observed traditional culturing surfaces (e.g. rigid plastic) and on 2D PAA gels of adjustable viscoelasticity. While larger polygonic and crescent shapes are typical on rigid surfaces and the smaller (i.e. triangle) shapes are representative for softer PAA substrates, the emergence of shapes with a tendency to form long cellular extensions is a deviation from that previously observed on PAA gels [8, 22]. Here, the presence of spindle and dendritic fibroblasts is fascinating as these phenotypes are characteristic for fibroblasts embedded in 3D collagen matrices [3, 77]. As shown in Figure 4.20, cells display increased populations of spindle and dendritic cells when plated on increasing fluid substrates where traction forces are further suppressed. In a general trend, fibroblasts take on progressively smaller, more spherical shapes displaying cellular extensions in response to decreased substrate viscosity. The predominant morphology of fibroblasts plated on glass is polygonic, on single bilayers it is crescent, and on TYPE 2 double and quadruple bilayers it is triangle and spindle respectively.

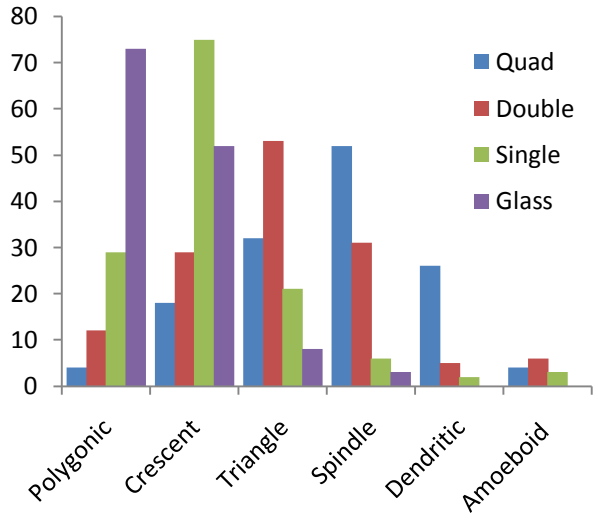

Figure 4.20. Overlaid cellular phenotype histograms for fibroblast plated on laminin-coated glass (control) and TYPE 2 single, double, and quadruple reveal the dependence of cell shape on substrate viscosity (150 cell were analyzed for each system 40h after plating).

Dendritic and spindle morphologies in fibroblasts show similar morphologies to neurons and are thought to represent the quiescent/resting state of these cells within a tissue [3]. As mentioned in Chapter 4.3.1, accelerated dendrite outgrowth has been previously reported for neurons plated on increasingly soft PAA gels. Comparable results have also been observed on neurons plated in 3D polymeric substances [130]. Similarly, using TYPE 2 substrates, fibroblasts have shown viscosity-dependent extension properties. The fraction of cells showing these processes increased with bilayer fluidity. While on single layer substrates only about 22% of the cells showed extensions of more than 5μm after 20h, this rate increased to approximately 39% on double and 57% on quadruple bilayer systems. On quadruple bilayers the extensions are more pronounced and can

span distances of up to 50μm. Moreover, the emergence of these shapes under conditions of high fluidity indicates that TYPE 2 systems may be capable of creating a 3D mimic using a 2D platform; this is a major advantage as characterization in 2D is far less complicated and problematic.

Additionally, analysis of cellular phenotype at both 20h and 40h after plating provided further evidence that the mechanoresponse observed was a direct effect of substrate viscosity and not any unwanted interaction with the underlying glass due to potential bilayer defects. Cell shape histograms at 20h and 40h, for cells plated on a quadruple TYPE 2 substrate, are shown in Figure 4.21. In the case of bilayer defects, it is expected that cells would take on larger, more polygonic shapes over time as a result of finding additional defects; interaction with the rigid underlying surface would provide immobile anchoring sites capable of creating larger traction forces. Instead, as indicated in Figure 4.21, cells actually progress to smaller, more spindle-like shapes over time; cell shape equilibrium was reached at approximately 40h. Not only does this indicate the absence of interaction with the underlying glass, it also suggests a potentially different form of movement and spreading that are discussed further in below. Moreover, with this data it can be confirmed that changes in fibroblast phenotype are a result of changes in substrate viscosity affecting cell-linker mobility. Less stretched shapes are expected under circumstances of lower traction. All traction forces present, be they small, are a result of the viscous drag force experienced as cells pull the mobile cell linkers.

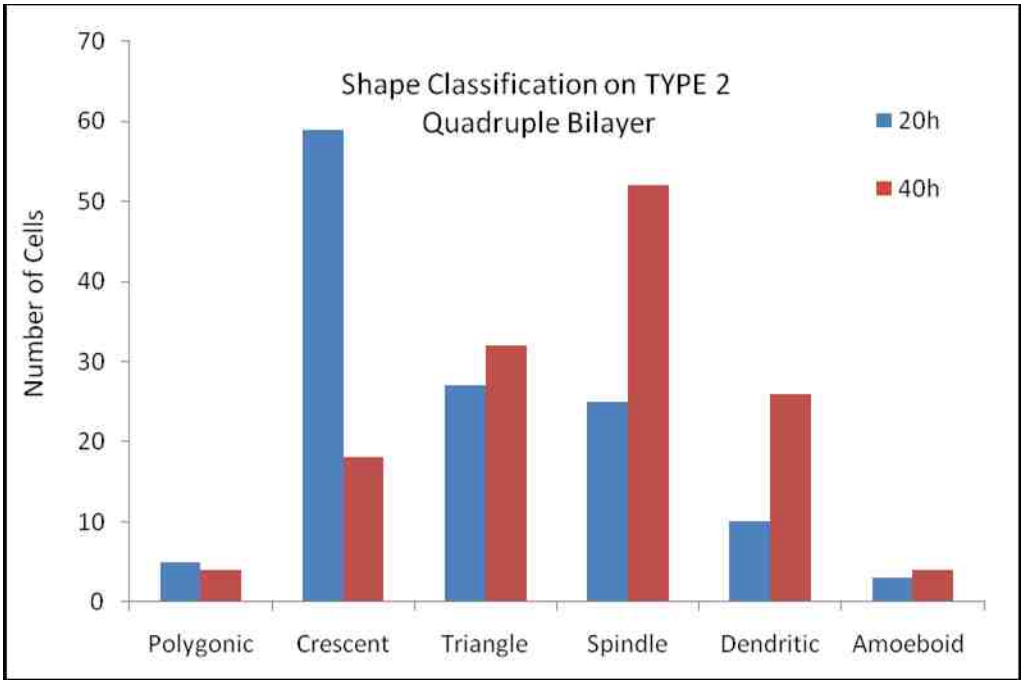

Figure 4.21. Cell shape classification 20h and 40h after plating shows the morphological progression of fibroblasts and supports the position that these systems show largely defect-free substrates (130 cells analyzed at each time point).

4.5.2. Fibroblast Actin Cytoskeleton

Cellular phenotypes correlate closely to the internal organization of the actin cytoskeleton. The stretched, polygonic shapes introduced in Chapter 4.4.1 are typical of fibroblasts cultured on tradition surfaces such as glass and plastic. These shapes result from the ability of the adherent cell to generate large traction forces and are characterized by cytoskeletal organizations containing large quantities of stress fibers. These actin bundles are required for cells to maintain these stretched shapes.

Cytoskeletal organization of 3T3 fibroblasts was visualized through transient transfection with GFP-actin. Here, transfected cells were plated on TYPE 2 substrates. Epi microscopy was performed 20 and 40h hours after plating and representative fluorescent and corresponding phase contrast images are displayed in Figure 4.22.

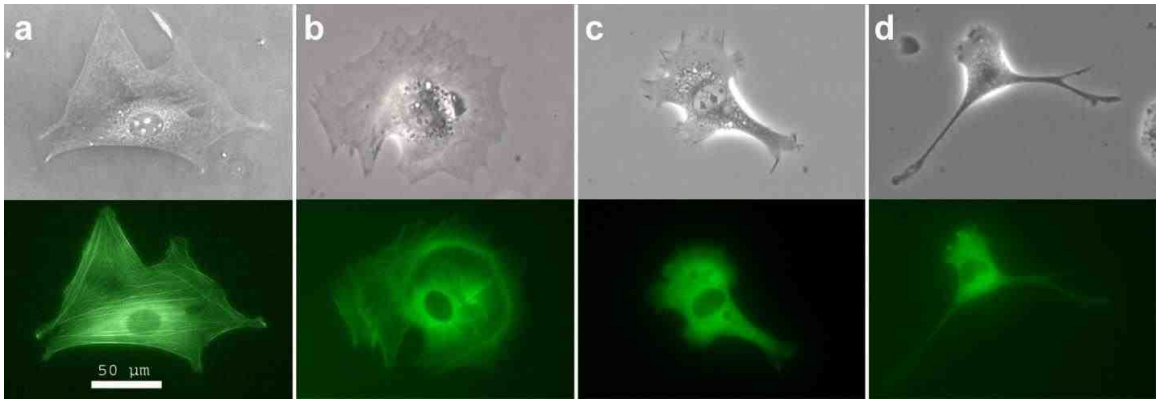

Figure 4.22. Micrographs of 3T3 fibroblasts cultured for 20 h on laminin-coated glass and TYPE 2 substrates. On laminin-coated glass (a), cells show numerous stress fibers spanning the whole cell. On single bilayers (b), stress fibers are reduced and replaced by cortical actin structures. On double (c) and quadruple (d) bilayers, cells polarize and begin forming long stretched processes.

Stress fiber structures of the actin cytoskeleton represent bundles of actin filaments. These structures can be divided into three groups based on subcellular location and interaction with FAs [131-133]; these divisions include ventral stress fibers (VSFs), transverse arcs (TAs), and dorsal stress fibers (DSFs). In brief, VSFs represent the traditionally observed stress fibers consisting of actin bundles, bound at both ends to FAs, and located in central

regions of the cell in a direction parallel to migration. Conversely, TAs represent curved actin bundles positioned closer to peripheral regions of the cells and oriented in a direction perpendicular to locomotion; these stress fibers are not directly attached to FAs. Lastly, DSFs are found in the peripheral regions of the cell where one end is attached to a FA and the other is directed toward the center of the cell.

These three types of stress fibers differ not only in location, but also in function. VSFs are bound to FAs at both ends, display a periodic α-actinin-myosin distribution, and are responsible for the majority of contractile force that a fibroblast applies to its substrate [132]. TAs, which also display α-actinin-myosin distributions, have the ability to contract as well [131]. However, with these structures not bound to FAs (in most cases), they cannot directly apply force to the substrate. Instead, force is directed through their interaction with DSFs, which are linked to FAs [131]. By definition, DSFs are not even stress fibers because myosin is rarely incorporated into these structures, therefore making them non-contractile; instead, these structures provide anchoring sites for TAs and are precursors of VSFs [131, 134].

As shown in the acquired images of GFP-actin transfected fibroblasts (Figure 4.22), GFP-actin 3T3 fibroblasts on laminin coated glass revealed numerous VSFs, as typically observed in fibroblasts on rigid substrates. On a single bilayer, a reduction in the amount of VSFs was observed while the overall shape

appeared similar to that on glass substrates. Cells cultured on TYPE 2 double bilayers began to show drastic changes in morphology and internal actin structures. Most importantly, the VSFs typically seen when plated on rigid substrates are not seen in TYPE 2 double and quadruple bilayers. Instead, a meshwork of cortical actin is observed, suggesting the presence of mechanically unloaded fibroblasts. This response is understandable on substrates were cellular traction is inhibited due to increased linker mobility. Here, the contractile force of VSFs cannot be generated.

While in many cases fibroblasts plated on TYPE 2 substrates show almost exclusively cortical actin, at times TAs and DSFs are still observed. This result is not unexpected in a fluid substrate as the formation of these structures is less tied to contractility. Instead, it is suggested that dorsal stress fibers are simply generated by the bundling of lamellipodium filaments and TAs primarily result from α-actinin-decorated actin filaments originating from the lamellipodial actin meshwork [131]. In fact, the presence of DSFs and not VSFs is quite telling because it indicates that while the precursors for VSF contractile assemblies are present, reduced cellular traction negates their need.

Moreover, the disappearance of VSFs is likely to impact aspects of cellular migration as all three types of stress fibers are typically observed in the mesenchymal migration of fibroblasts [127]. Cellular locomotion is traditionally described by alternating actin protrusion and contraction phases (as discussed in

Chapter 2.4.3) and the contractile nature of ventral stress fibers led to early speculation that these assemblies were responsible for cellular contraction [132, 135]. Yet, much research indicates that stress fibers may, at times, hinder migration as the formation of larger, more mature stress fibers are often observed within stationary cells [132, 136]. Therefore, the formation of VSFs is not required for locomotion. It is likely that these contractile fibers aid tail retraction and the disassembly of FAs at the posterior of the cell during migration, but stress fiber contractility in non-motile cells also strengthens FAs [132, 137] through the protein recruitment mechanisms discussed in Chapter 2.4.2. Other studies have confirmed that actomyosin can contribute to tail retraction without the involvement of VSFs [132, 138].

Actin dynamics of contractile structures provide insight into the roles of cell motility as VSFs fail to exhibit large-scale remodeling in a time frame applicable to cell locomotion [127]. As a result, VSFs are typically observed in less motile cells [127]. In contrast, TAs and DSFs are highly dynamic and function is unison to create a treadmilling contractile lamella [127]. In fact, in these structures, F-actin retrograde flow is slower, a feature which has been shown to inversely impact neuron growth cone advancement [127, 128]. This may aid in explaining the elevated appearance of neuronal-like cell extensions on TYPE 2 substrates of decreased viscosity in increased linker mobility.

Fluorescence images of the actin cytoskeleton indicate the ability of TYPE 2 substrates to reprogram cells into stress-free morphologies and reveal the importance of substrate viscosity in the mechanotransduction process. Representative images of the GFP-labeled actin cytoskeleton in the newly observed shapes in Figure 4.19: crescent, triangle, spindle, and dendritic and displayed in Figure 4.23.

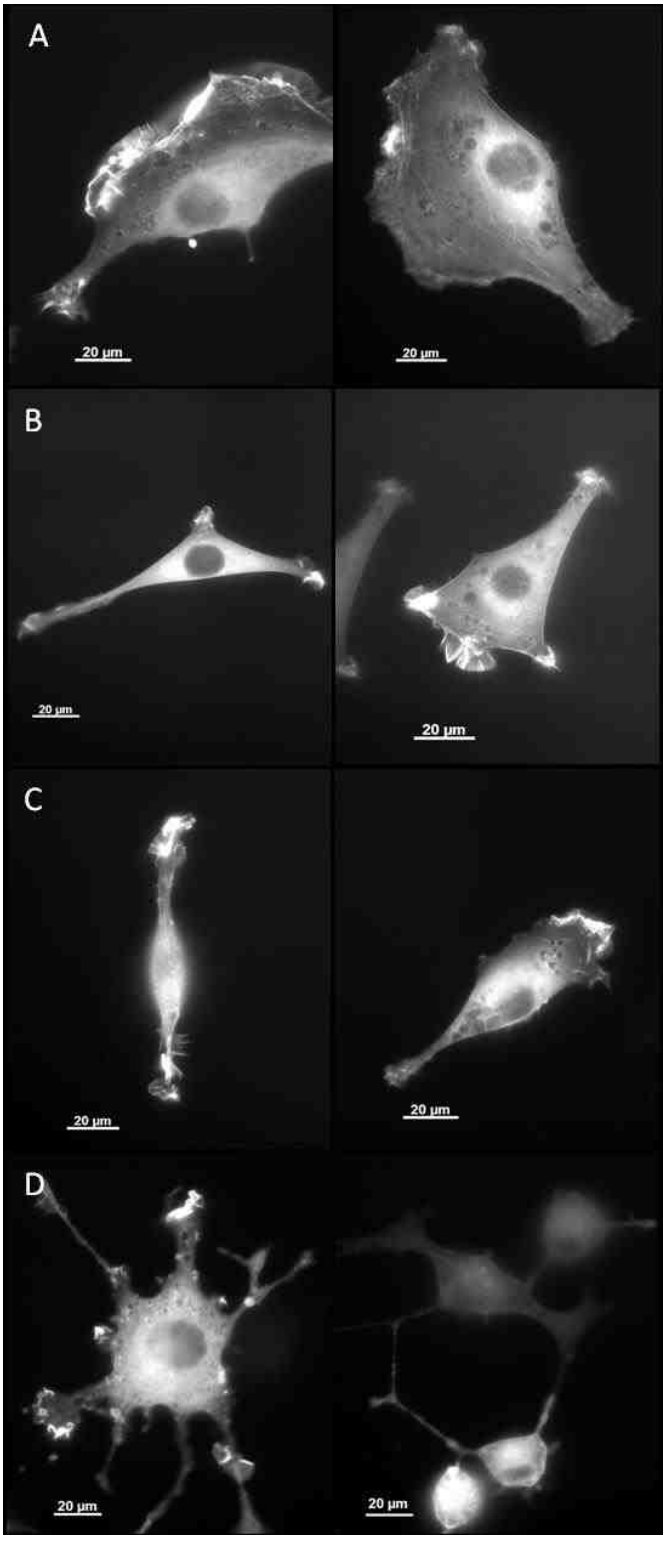

Figure 4.23. Representative images of the GFP-labeled actin cytoskeleton in crescent (A), triangle (B), spindle (C), and dendritic (D) shaped fibroblasts.

4.5.3. Fibroblast Movement: Migration and Area Fluctuations

Previous studies on PAA gels of varying viscoelasticity have shown increased migration speeds on substrates of decreased rigidity; this was discussed in Chapter 2.4.3. The observation is explained by the relatively inefficient and poorly understood process of FA disassembly during cell migration. In essence, on more rigid substrates cells are capable of generating larger pulling forces. As described in Chapter 2.4.2, these larger forces induce a cellular response through the process of mechanotransduction. In this case, stronger pulling forces lead to protein recruitment at FA sites in an effort to counter balance these forces and maintain homeostasis. Larger FAs take longer to disassemble, thus slowing cellular migration. Previous studies on substrates of varying elasticity have shown decreased focal adhesion size and density on softer substrates where cell develop less traction [139].

It was expected that migration speeds would increase with increased bilayer stacking in TYPE 2 substrates. Here, decreasing substrate viscosity, in turn increasing cell linker mobility, should lead to reduced cell traction forces. These lower forces should not require large FAs. Instead the presence of smaller, more dynamic FAs should result in increased migration speed. This trend was shown on TYPE 2 substrates. 3T3 fibroblasts were plated on glass (control), single, double, and quadruple TYPE 2 substrates. Cellular migration speeds were measure 20h after plating and consisted of average nucleus displacements over

a 5min time lag. The results are shown in Figure 4.24, where every data point represents a nuclear displacement over time. Quadruple displacement data are

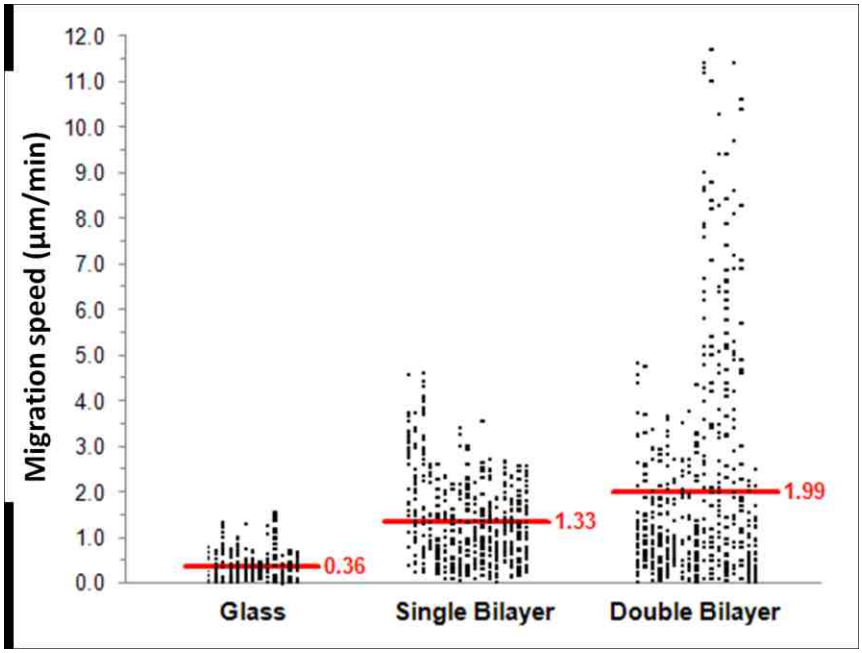

Figure 4.24. Nucleus tracking shows increased migration speeds of fibroblasts on TYPE 2 substrates. Each data point represents a nucleus displacement over a 5min time lag.

not shown due to the tendency of cells plated on quadruple bilayers to migrate out of the picture frame when performing long term studies using a 5min time lag. The above figure shows migrations speeds are dependent on substrate viscosity. As expected, increased stacking (i.e. increased linker mobility) resulted in heightened migration speeds. The red bars in Figure 4.24 indicate average nuclear displacements over the 5min time lag.

Additionally, by determining the migration speeds of the different phenotypes on TYPE 2 systems, using shorter time frames (2min) to be able to include data on quadruple bilayer systems, Figure 4.25 shows that migration speeds are not a consequence of cell shape. This important fact further confirms that the observed mechanoresponse is truly a result of substrate viscosity.

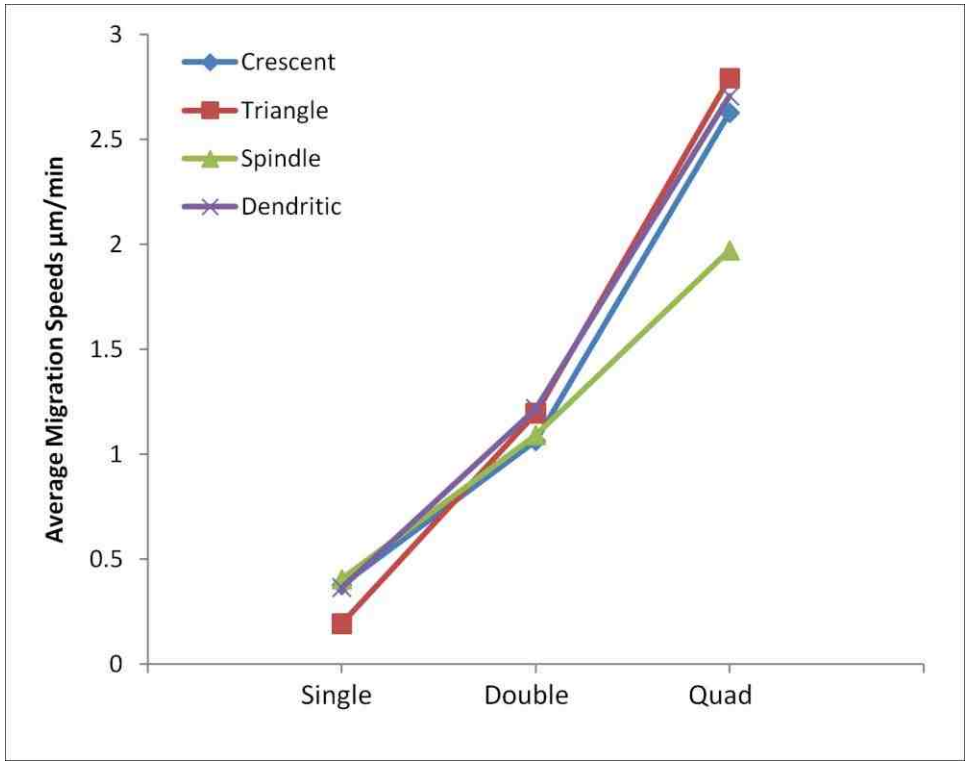

Figure 4.25. Fibroblast shape does not show a notable impact on migration speed indicating that changes in motility are the result of changes in substrate viscosity on TYPE 2 substrates (time lag: 2min, n=10 separate cells for each shape and substrate other than "dendritic," where n=3. Average standard deviations: Single=0.3µm/min, Double=0.2µm/min, Quad=0.4µm/min).

As mentioned in Chapter 4.4.1, fibroblasts on TYPE 2 substrates of high fluidity displayed interesting parallels to cells embedded in 3D matrices. Intriguingly,

these parallels do not stop at shape and it appears that cells may move in a similar way as well. Using the obtained migration data it was possible to determine the torosity, or directionality, of movement. From the coordinates of the nucleus displacements over three time points one can calculate a value for how "straight" a cell is moving, Figure 4.26. The formation of spindle-like cells in 3D matrices has been shown to increase directionally persistent migration [140]. Figure 4.26, shows that on TYPE 2 substrates, the spindle-shaped cells do show the highest degree of torosity, as indicated by a value closest to 1, which represents a straight line.

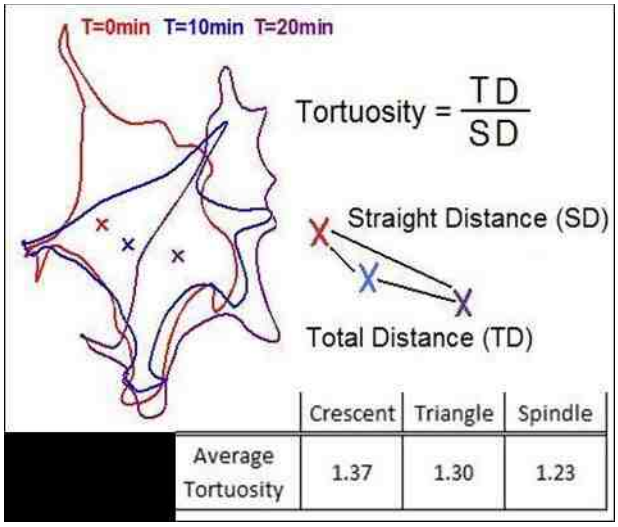

	Crescent	Triangle	Spindle
Average Tortuosity	1.37	1.30	1.23

Figure 4.26. Migration directionality, characterized by tortuosity values, is shown to be shape dependent (n=50 tracks per shape).

In Chapter 4.4.1 it was suggested that fibroblasts on TYPE 2 substrate may exhibit a different type of locomotion than traditional mesenchymal migration. In

the previous section this observation was made based on cell spreading and morphological changes over a 20h period. Studying fibroblast movement on these substrates has provided additional evidence that this may in fact be occurring. The size of FAs would not simply affect migration speed, as mentioned above, but would also affect a cell's ability to rapidly undergo shape changes; a process also requiring the rapid assembly and disassembly of FAs. It was observed that 3T3 fibroblasts moving on TYPE 2 substrates displayed dramatic shape changes within a short time scale. This observation was quantified by monitoring the percent change in cellular area, % ΔA, over a time lag of 2min. The results are shown in Figure 4.27 and indicate area fluctuations following plating on a TYPE 2 double bilayer system. The red bars in Figure 4.27 indicate the average % ΔA. Dramatic shape and area fluctuations are typically seen in amoeboid movement [141, 142]. Amoeboid migration is characterized not only by rapid shape changes, but also a lack of mature FAs and stress fibers [142-144]. Therefore, based on the observed cytoskeletal organization of fibroblasts on TYPE 2 substrates, this mode of migration is plausible. In contrast to mesenchymal migration, cell undergoing amoeboid migration interact weakly with their substrate (e.g. develop low traction forces) [144]. Two common subtypes of amoeboid migration consist of: (1) the rounded, blebby migration of cells (amoeboid-blebby) [144, 145], and (2) that occurring in slightly elongated cells generating actin-rich filopodia at the leading edge but displaying weak adhesive interaction with their substrate (amoeboid-pseudopodal) [144, 146]. In a third, less common mode, blebs are replaced with dendrites [144].

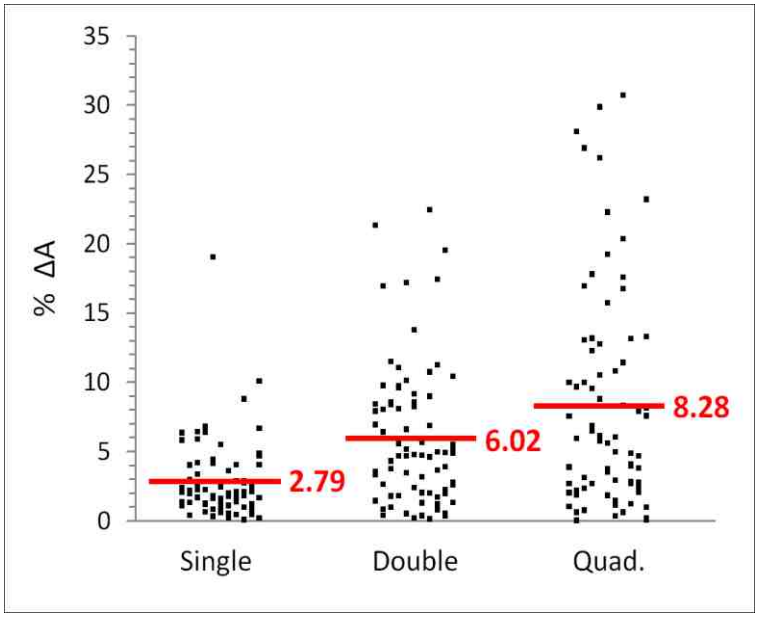

Figure 4.27. Histograms of the change in percent area with a 2min time lag. Increased area fluctuations observed in fibroblasts plated on TYPE 2 double bilayer substrates suggests the presence of a more amoeboid form of migration (time lag: 2min).

Interestingly, all of these phenotypes were found in TYPE 2 systems. Moreover, mesenchymal locomotion results in migrations speeds on the order of 0.1-1μm/min [147, 148] compared to amoeboid-blebby at 0.1μm/min [146] and amoeboid-pseudopodal at 10μm/min [141, 146]. Observed migrations speeds on the order of 2.7μm/min for fibroblasts on quadruple TYPE 2 substrates support a potential transition to more amoeboid movement. The collection of motility data presented here shows that regulating cellular traction forces through substrate viscosity affects not only migration speeds, but also may influence the type of migration present.

4.5.4. Fibroblast Force Transduction

Traction force microscopy (TFM) was used to verify that the fluid nature of TYPE 2 substrates does impact cellular traction forces (CTF). It was hypothesized that the mobile linkers in this system essentially create a “slippery” surface for cells. In other words, a surface where a cell can grip, but under increased pulling, linkages slip. The CTFs generated by 3T3 fibroblasts plated on TYPE 2 systems were measured through FTM. A cell’s inability to generate large traction forces would provide further explanation for the unique cellular morphology and motility observed on TYPE 2 substrates. As discussed in previous chapters, fibroblasts on TYPE 2 substrates display uncharacteristic neuronal-like phenotypes. Neurons have previous been shown to generate traction forces orders of magnitude less than that of fibroblasts (this is likely due to the diffuse nature of brain tissue compared to connective tissue) [90]. Moreover, cellular mobility is strongly influenced by the formation of large, mature focal adhesions, a process that is dependent on the mechanical properties of a substrate (as discussed in previous chapters).

Here, PAA gels with embedded fluorescent beads were used to determine the CTF of fibroblasts. TYPE 2 substrates were added atop PAA gels as shown in Figure 4.28, which provides a schematic for the three systems used in TFM experiments. Cells were plated on traditional “control” PAA gels (Figure 4.28. A) and gels containing TYPE 2 single and triple bilayers (Figure 4.28. B and C respectively). Fibroblasts were plated on these three substrates and allowed to

adhere and spread over 24h. At this point, Epi microscopy was used to image the fluorescent beads under adherent cells.

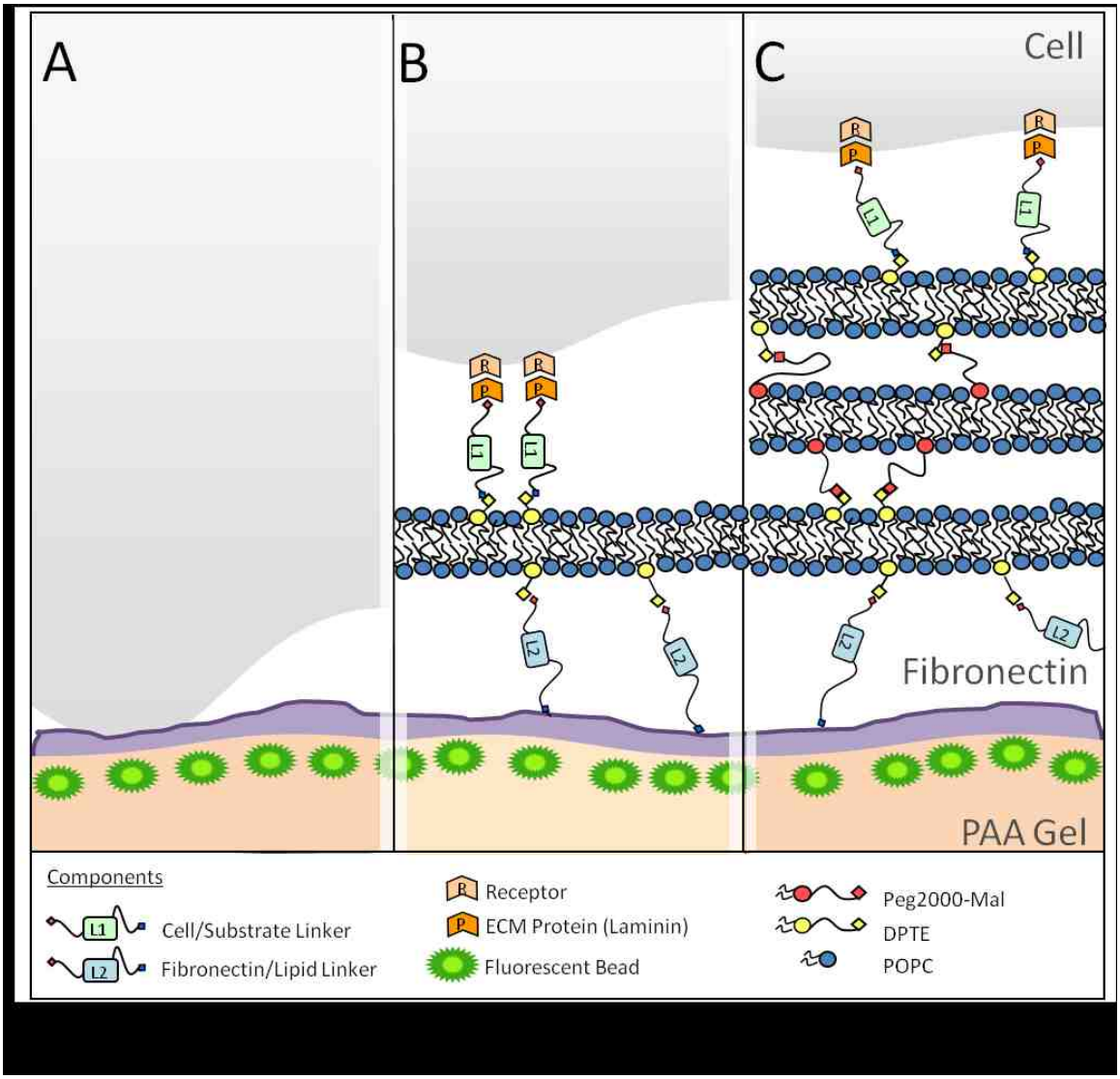

Figure 4.28. Schematic of PAA-based substrates used in TFM experiments. Fibroblasts were plated on standard (control) PAA gels (A) alongside single(B) and triple (C) bilayer-modified PAA gels.

These cells were then detached and the fluorescent beads were imaged again. The fluorescent snapshots provided “loaded” and “unloaded” images respectively. The “loaded” image was used to determine the placement of the fluorescent bead under the pulling forces of adherent cells while the “unloaded” image provided the placement of beads in the absence of cells. The elastic nature of PAA gels causes the beads to snap back to their original location following detachment.

Using custom written Matlab software, bead displacements between “loaded” and “unloaded” images were determined. With a known elastic modulus of the PAA gel (12825Pa) this software calculated the pulling force necessary to displace a bead a given distance. Using this information, for each bead present in the fluorescent snapshots, Matlab generates force traction maps (FTMs). Figure 4.29 shows representative FTMs for cells plated on a control PAA gel (A) and a triple bilayer (B). The fibroblast plated on the control gel, Figure 4.28 (A), displays a polygonic phenotype characteristic of fibroblasts plated on traditional cell substrates (e.g. plastic, glass, more rigid PAA gels). In contrast, the fibroblast on the TYPE 2 triple layer, Figure 4.28 (B), displayed the spindle-shape described in Chapter 4.4.1. As expected, and as indicated from the FTMs below, it is clear that cells plated on the TYPE 2 systems do exert less force onto their substrates.

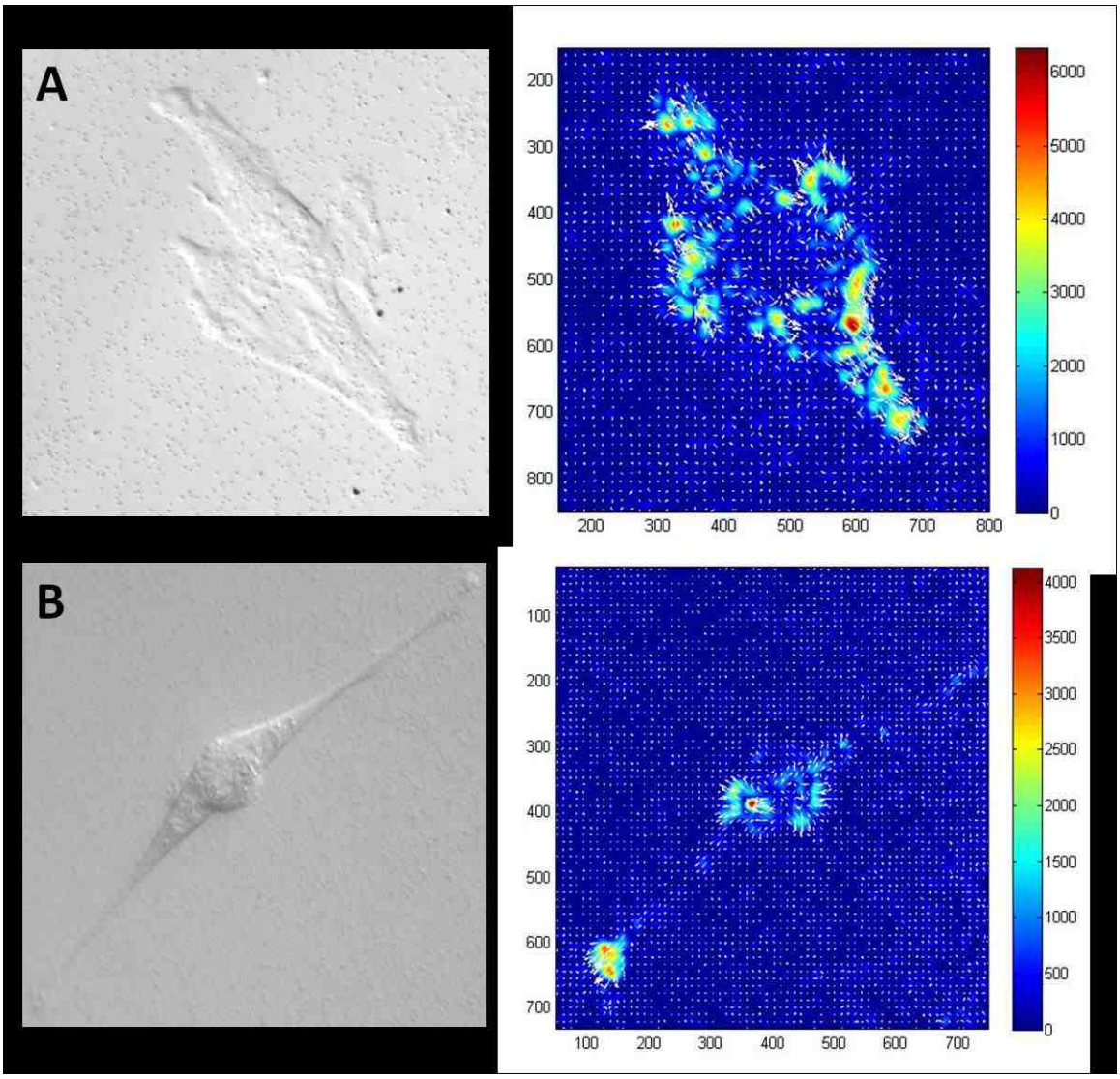

Figure 4.29. FTMs reveal the size and placement of CTFs generated by fibroblasts plated on control PAA gels (A) and triple bilayer-modified PAA gels (B).

The information contained in Figure 4.29, along with data sets from several other cells, was used to generate the graph in Figure 4.30, which illustrates a change in average CTF with decreased substrate viscosity (and increased cell linker

mobility). The CTF generated on the TYPE 2 triple bilayers are nearly half of that on the control, 2717Pa compared to 4733Pa.

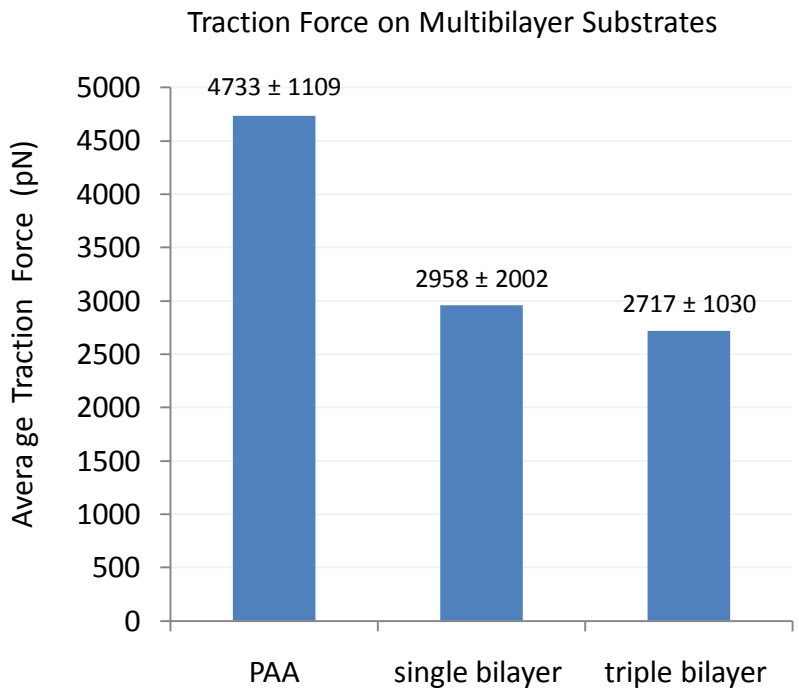

Figure 4.30. Comparison of the average CTF generated by fibroblasts plated on control and single and triple bilayer-modified PAA gels. Average CTFs are based on data sets containing 15 cells for each substrate.

The data obtained through TFM confirms that TYPE 2 substrates do act as lubrication layers and suggests that TYPE 2 bilayers do act as “slippery” substrates which hinder the formation of large traction forces. These results are expected based on the fact that these systems are comprised of mobile cell-substrate linkers and further confirms that the observed morphological and motility changes are truly a result of changes in substrate viscosity. Furthermore,

the emergence of more neuronal-like cell shapes, as described in Chapter 4.4.1, are explained by the inability of fibroblasts to develop traction. The mechanotransduction process has been discussed throughout this work and a decrease in the force generated by a cell (in response to substrate properties) should result in decreased protein recruitment to adhesion sites and formation of smaller, more dynamic FAs. This response, in turn, should lead to the less stretched, more spherical (less flattened) cell shapes present in TYPE 2 substrates because less force is needed to maintain these phenotypes. Moreover, the formation of smaller FAs simultaneously impacts both cellular migration velocities and area fluctuations, as discussed in Chapter 4.4.3. Thus, the determination of smaller CTFs on TYPE 2 substrates helps to further our understanding of the possible mechanotransduction pathways utilized in cellular viscosity sensing and provides supporting data to the proposed mechanisms used to explain the results seen, and discussed, in previous chapters.

CHAPTER 5. CONCLUSIONS

5.1. Conclusions

Phospholipid bilayer-based substrates were successfully designed and fabricated as biomembrane-mimicking cell substrates of adjustable viscosity where the synthesis of specific cell-substrate linkers were utilized to tune cell-linker mobility over a large range of viscosities. The use of these dynamic, yet robust substrates, capable of withstanding the pulling forces of adherent cells, has confirmed that cells do hold the machinery necessary for viscosity-sensing and have provided information on the mechanoresponse induced by changes in substrate viscosity. With this, the four objectives outlined in the introduction have been accomplished.

With lipid bilayers recognized as the principle mimetic for biological membranes their use as potential biomembrane-mimicking cell substrates was recognized years ago. However, various shortcomings in previous designs (arising from bilayer defects and unwanted cellular interaction with underlying supports) have limited their use as suitable substrates. Here, the use new design aspects and alternative fabrication techniques capable of creating high quality, stable,

homogeneous phospholipid bilayers has made their use as cell substrates a reality. With the design of two complementary systems, TYPE 1 and TYPE 2, substrate viscosity can be tuned over a large range. Regulating the polymer-tethering concentration in TYPE 1 substrates has been shown to induce more subtle changes while bilayer stacking in TYPE 2 substrates was capable of creating dramatic changes in substrate viscosity. The newly conceived TYPE 2 substrates feature an iterative design of polymer-interconnected bilayer stacking where substrate viscosity is regulated by bilayer-solid distance impacting the degree of frictional coupling. Importantly, the use of covalent linkages between successive bilayers has resulted in a stable, robust substrate.

The characterization of TYPE 2 substrates was performed through Epi microscopy and SMFM. Epi micrographs confirmed the fabrication of homogeneous multibilayer stacks while providing qualitative evidence of increased bilayer fluidity with stacking. This feature was quantitatively confirmed through single molecule tracking where the lateral diffusivity of both lipid and lipid clusters was shown to increase with respect to bilayer stacking. These results validated that lateral mobility in the outermost lipid bilayer can be tuned through bilayer-solid spacing using multibilayer systems.

A major obstacle in the use of solid-supported lipid bilayers as cell substrates has been ensuring that adherent cells do not interact with the underlying solid-support. In the past this unwanted interact has been observed and it appears

that this was largely the result of bilayer fabrication methods prone to defects and the design of supported bilayers with insufficient bilayer-solid spacing; as bilayer-solid proximity coupled with potential defects is likely to encourage this unwanted interaction. Cellular and substrate imaging on a variety of control experiments has confirmed bilayer integrity and that observed cellular mechanoresponse is truly induced by substrate viscosity and is not an artifact of bilayer defects. The analysis of shape and cytoskeletal organization on control substrates and in the absence of cell-substrate linkers has shown suppressed cellular interaction with the underlying bilayer support, even in single layer substrates. Moreover, Epi microscopy and confocal FRAP has verified that these substrates are capable of withstanding the pulling forces of adherent cells.

.

Heterobifunctional cell-substrate linkers were designed to conjugate cellular adhesion proteins (i.e. Laminin) to lipids within TYPE 1 and TYPE 2 substrates. These linkers were synthesized through the biofunctionalization of QDs. SMFM experiments on QD-tagged constituents of live cell plasma membranes indicate the proper functioning and biocompatibility of these linkers. Moreover, while not utilized within this research, the fluorescent properties of these linkers allow for dynamic studies in the future, which may provide further insight into the nature of cellular motility on these substrates.

With substrates and linkers in place, cellular mechanoresponse was observed on these low traction substrates of adjustable viscosity. Here, linker mobility was

shown to profoundly impact cellular phenotype, growth, and mobility. Neurons plated on TYPE 1 substrates showed accelerated dendrite growth and network formation on less viscous substrates; results that coincide with previous work on substrates of tunable viscosity where pronounced growth has been observed on softer substrates. On TYPE 2 substrates, fibroblasts underwent dramatic phenotype changes where the appearance of spindle and dendritic-like morphologies in response to reduced viscosity showed parallels to fibroblasts cultured in 3D matrices. In addition, fibroblasts displayed increased migration speeds and directionally persistent migration on substrates of decreasing viscosity. In fact, analysis of cell area fluctuations during motility indicates that fibroblasts may be exhibiting an amoeboid movement in response to these changes. These results have shown that neurons and fibroblasts have the ability to sense changes in substrate viscosity.

In conclusion, this research has provided new biomembrane-mimicking cell substrates capable of tuning cellular mechanoresponse through the regulation of substrate viscosity. These novel substrates have the potential to significantly increase our understanding of the mechanotransduction process by complementing existing elastic substrates and enabling researchers to truly address the cellular impact of substrate viscoelasticity. The value of such information is increasing recognized as research continues to show a correlation between disease and mechanical stimuli.

5.2. Outlook

The research contained within this thesis focused on cellular mechanoresponse induced by changes in substrates viscosity affecting cell-substrate linker mobility. Here, cell-substrate linkers contained laminin, an adhesion protein presented by the ECM. As described within this work, adherent cells attach to adhesion proteins and form FAs, which are considered to play a large role in the mechanotransduction process. However, FAs are not the only mechanotransducers used by cells.

Mechanically loaded tissues show extensive networks of adherent junctions, which provide a direct physical coupling between adjacent cells [76]. The role of adherent junctions in force sensing is increasingly recognized as an important process in mechanotransduction [89, 149-153]. Moreover, the diffusion mediated assembly and disassembly processes are not only important in the formation of FAs, but also in the formation of adherent junctions [7, 18-20, 22]. Thus, these cell-cell contacts should also be impacted by substrate viscosity (i.e. linker mobility). While a lack of appropriate cell substrates has hindered research involving the formation of AJs in response to mechanical stimuli such as viscosity [76], cadherin-mediated adherent junctions have been shown to play roles in mechanosensing and the regulation of cell attachment and migration, wound contraction, intracellular mechanotransduction, cellular differentiation, and more [76, 149, 154-162]. Much research supports a crosstalk between cadherins and the actin cytoskeleton [163-165]. Additionally, evidence suggests that FAs and

cadherin-mediated adherent junctions may cooperatively or antagonistically impact cellular mechanics [76].

The lipid-bilayer based cell substrates presented within this work provide an excellent plasma membrane mimic, and incorporating cadherin-based cell-substrate linkages could enable the study of artificial cell-cell adherent junctions and their formation in response to changes in substrate viscosity. Moreover, such substrates could be applied to the study of disease processes such as cancer progression. This process has been tied to mechano-response: cadherin-based adherent junctions are thought to play a primary role in this pathway as adhesion and progression of tumor cells is largely regulated by E-cadherin [166, 167], while metastatic cells develop most adhesion through N-cadherin [168-170]. In addition, substrate stiffness affecting matrix resistance to cell tension forces has been shown to impact cancer development [171]. Studies on N-cadherin and E-cadherin functionalized cell substrates of varying viscosity represent a means of controlling mechanoresponse both mechanically and biochemically, and may provide a better understanding of the critical mechanotransduction elements in cancer cell development.

N-cadherin-functionalized TYPE 1 and 2 substrates have been fabricated in our lab. A schematic of these substrates is illustrated in Figure 5.1. The outermost bilayer of these substrates contains a variable amount of the Ni-NTA functionalized lipid 1,2-di-(9Z-octadecenoyl)-sn-glycero-3-[(N-(5-amino-1-

carboxypentyl)iminodiacetic acid)succinyl] (nickel salt).This lipid will provide a suitable link for commercially available 6x histidine-tagged N-cadherin (the extracellular domain, residues 1-724). Currently, these substrates have been tested using NG108 neurons and myoblasts, both of which are known to express N-cadherin.

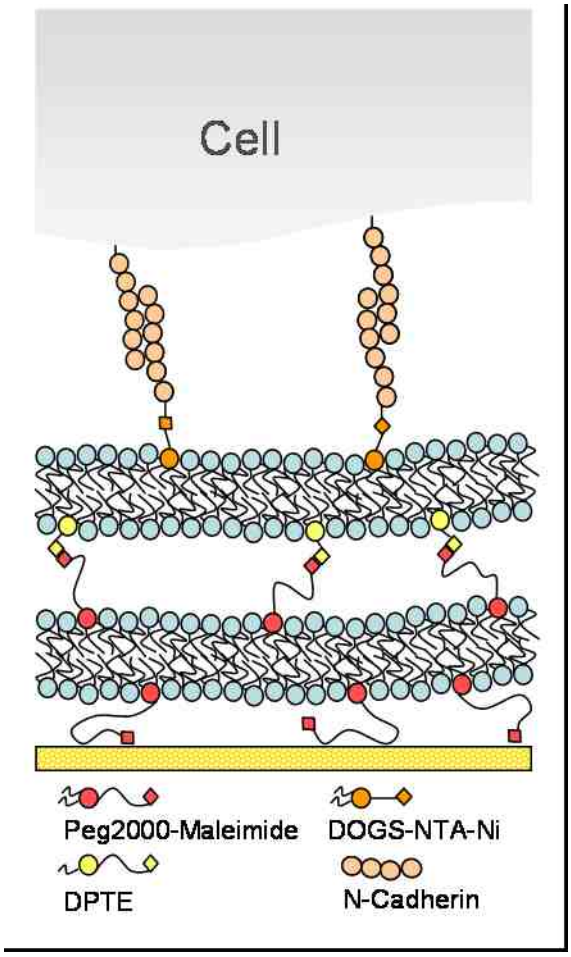

Figure 5.1. Schematic of TYPE 2 substrates featuring N-cadherin cell linkers.

LIST OF REFERENCES

LIST OF REFERENCES

1. Discher, D.E., P. Janmey, and Y.-l. Wang, *Tissue Cells Feel and Respond to the Stiffness of Their Substrate.* Science, 2005. **310**(5751): p. 1139-1143.

2. Georges, P.C., et al., *Matrices with Compliance Comparable to that of Brain Tissue Select Neuronal over Glial Growth in Mixed Cortical Cultures.* Biophysical Journal, 2006. **90**(8): p. 3012-3018.

3. Grinnell, F., *Fibroblast biology in three-dimensional collagen matrices.* Trends in Cell Biology, 2003. **13**(5): p. 264-269.

4. Hay, E.D., *Interaction of embryonic cell surface and cytoskeleton with extracellular matrix.* American Journal of Anatomy, 1982. **165**(1): p. 1-12.

5. Janmey, P.A., et al., *The hard life of soft cells.* Cell Motility and the Cytoskeleton, 2009. **66**(8): p. 597-605.

6. Matsumoto, T., et al., *Local elastic modulus of atherosclerotic lesions of rabbit thoracic aortas measured by pipette aspiration method.* Physiol Meas, 2002. **23**(4): p. 635-48.

7. Paszek, M.J., et al., *Tensional homeostasis and the malignant phenotype.* Cancer Cell, 2005. **8**(3): p. 241-254.

8. Pelham, R.J. and Y.-l. Wang, *Cell locomotion and focal adhesions are regulated by substrate flexibility.* Proceedings of the National Academy of Sciences of the United States of America, 1997. **94**(25): p. 13661-13665.

9. Pelham, R.J., Jr. and Y.-l. Wang, *High Resolution Detection of Mechanical Forces Exerted by Locomoting Fibroblasts on the Substrate.* Mol. Biol. Cell, 1999. **10**(4): p. 935-945.

10. Zaman, M.H., et al., *Migration of tumor cells in 3D matrices is governed by matrix stiffness along with cell-matrix adhesion and proteolysis.* Proceedings of the National Academy of Sciences, 2006. **103**(29): p. 10889-10894.

11. Alcaraz, J., C.M. Nelson, and M.J. Bissell, *Biomechanical Approaches for Studying Integration of Tissue Structure and Function in Mammary Epithelia.* Journal of Mammary Gland Biology and Neoplasia, 2004. **9**(4): p. 361-374.

12. Cukierman, E., R. Pankov, and K.M. Yamada, *Cell interactions with three-dimensional matrices.* Current Opinion in Cell Biology, 2002. **14**(5): p. 633-640.

13. Engler, A.J., et al., *Myotubes differentiate optimally on substrates with tissue-like stiffness.* The Journal of Cell Biology, 2004. **166**(6): p. 877-887.

14. Engler, A.J., et al., *Matrix elasticity directs stem cell lineage specification.* Cell, 2006. **126**(4): p. 677-89.

15. Georges, P.C. and P.A. Janmey, *Cell type-specific response to growth on soft materials.* J Appl Physiol, 2005. **98**(4): p. 1547-1553.

16. Rehfeldt, F., et al., *Cell responses to the mechanochemical microenvironment--Implications for regenerative medicine and drug delivery.* Advanced Drug Delivery Reviews, 2007. **59**(13): p. 1329-1339.

17. Yeung, T., et al., *Effects of substrate stiffness on cell morphology, cytoskeletal structure, and adhesion.* Cell Motility and the Cytoskeleton, 2005. **60**(1): p. 24-34.

18. Balaban, N.Q., et al., *Force and focal adhesion assembly: a close relationship studied using elastic micropatterned substrates.* Nat Cell Biol, 2001. **3**(5): p. 466-72.

19. Engler, A., et al., *Substrate compliance versus ligand density in cell on gel responses.* Biophys J, 2004. **86**(1 Pt 1): p. 617-28.

20. Riveline, D., et al., *Focal contacts as mechanosensors: externally applied local mechanical force induces growth of focal contacts by an mDia1-dependent and ROCK-independent mechanism.* J Cell Biol, 2001. **153**(6): p. 1175-86.

21. Shenoy, V.B. and L.B. Freund, *Growth and shape stability of a biological membrane adhesion complex in the diffusion-mediated regime.* Proc Natl Acad Sci U S A, 2005. **102**(9): p. 3213-8.

22. Solon, J., et al., *Fibroblast adaptation and stiffness matching to soft elastic substrates.* Biophys J, 2007. **93**(12): p. 4453-61.

23. Cremer, P.S. and S.G. Boxer, *Formation and Spreading of Lipid Bilayers on Planar Glass Supports.* The Journal of Physical Chemistry B, 1999. **103**(13): p. 2554-2559.

24. Kalb, E., S. Frey, and L.K. Tamm, *Formation of supported planar bilayers by fusion of vesicles to supported phospholipid monolayers.* Biochim Biophys Acta, 1992. **1103**(2): p. 307-16.

25. Tamm, L.K. and H.M. McConnell, *Supported phospholipid bilayers.* Biophys J, 1985. **47**(1): p. 105-13.

26. Naumann, C.A., et al., *The Polymer-Supported Phospholipid Bilayer: Tethering as a New Approach to Substrate−Membrane Stabilization.* Biomacromolecules, 2001. **3**(1): p. 27-35.

27. Wagner, M.L. and L.K. Tamm, *Tethered polymer-supported planar lipid bilayers for reconstitution of integral membrane proteins: silane-polyethyleneglycol-lipid as a cushion and covalent linker.* Biophys J, 2000. **79**(3): p. 1400-14.

28. Wang, H.-B., et al., *Focal adhesion kinase is involved in mechanosensing during fibroblast migration.* Proceedings of the National Academy of Sciences of the United States of America, 2001. **98**(20): p. 11295-11300.

29. Wang, J. and J.-S. Lin, *Cell traction force and measurement methods.* Biomechanics and Modeling in Mechanobiology, 2007. **6**(6): p. 361-371.

30. Yang, Z., et al., *Determining substrate displacement and cell traction fields--a new approach.* Journal of Theoretical Biology, 2006. **242**(3): p. 607-616.

31. Ehrlich, H.P., *The role of connective tissue matrix in wound healing.* Prog Clin Biol Res, 1988. **266**: p. 243-58.

32. Burton, K. and D.L. Taylor, *Traction forces of cytokinesis measured with optically modified elastic substrata.* Nature, 1997. **385**(6615): p. 450-454.

33. Galbraith, C.G. and M.P. Sheetz, *A micromachined device provides a new bend on fibroblast traction forces.* Proceedings of the National Academy of Sciences of the United States of America, 1997. **94**(17): p. 9114-9118.

34. Tan, J.L., et al., *Cells lying on a bed of microneedles: An approach to isolate mechanical force.* Proceedings of the National Academy of Sciences of the United States of America, 2003. **100**(4): p. 1484-1489.

35. Sabass, B., et al., *High resolution traction force microscopy based on experimental and computational advances.* Biophys J, 2008. **94**(1): p. 207-20.

36. Beningo, K.A., M. Dembo, and Y.-l. Wang, *Responses of fibroblasts to anchorage of dorsal extracellular matrix receptors.* Proceedings of the National Academy of Sciences of the United States of America, 2004. **101**(52): p. 18024-18029.

37. Beningo, K.A. and Y.-L. Wang, *Flexible substrata for the detection of cellular traction forces.* Trends in Cell Biology, 2002. **12**(2): p. 79-84.

38. Butler, J.P., et al., *Traction fields, moments, and strain energy that cells exert on their surroundings.* Am J Physiol Cell Physiol, 2002. **282**(3): p. C595-605.

39. Dembo, M. and Y.L. Wang, *Stresses at the cell-to-substrate interface during locomotion of fibroblasts.* Biophys J, 1999. **76**(4): p. 2307-16.

40. Rajagopalan, P., et al., *Direct comparison of the spread area, contractility, and migration of balb/c 3T3 fibroblasts adhered to fibronectin- and RGD-modified substrata.* Biophys J, 2004. **87**(4): p. 2818-27.

41. Wang, J.H. and B. Li, *Application of cell traction force microscopy for cell biology research.* Methods Mol Biol, 2009. **586**: p. 301-13.

42. Marganski, W.A., M. Dembo, and Y.L. Wang, *Measurements of cell-generated deformations on flexible substrata using correlation-based optical flow.* Methods Enzymol, 2003. **361**: p. 197-211.

43. Castellana, E.T. and P.S. Cremer, *Solid-Supported Lipid Bilayers: From Biophysical Studies to Sensor Design.* ChemInform, 2007. **38**(14): p. no-no.

44. Richter, R.P., R. Berat, and A.R. Brisson, *Formation of solid-supported lipid bilayers: an integrated view.* Langmuir, 2006. **22**(8): p. 3497-505.

45. Kiessling, V., et al., *Wiley Encyclopedia of Chemical Biology*. Supported lipid bilayers: development and applications in chemical biology. Vol. 4. 2008: Wiley.

46. Singer, S.J. and G.L. Nicolson, *The fluid mosaic model of the structure of cell membranes.* Science, 1972. **175**(23): p. 720-31.

47. Saxton, M.J. and K. Jacobson, *Single-particle tracking: applications to membrane dynamics.* Annu Rev Biophys Biomol Struct, 1997. **26**: p. 373-99.

48. Groves, J., *Supported Lipid Bilayers as Mimics for Cell Surfaces and as Tools in Biotechnology*, in *BioMEMS and Biomedical Nanotechnology*, M. Ferrari, T. Desai, and S. Bhatia, Editors. 2007, Springer US. p. 305-323.

49. Brian, A.A. and H.M. McConnell, *Allogeneic stimulation of cytotoxic T cells by supported planar membranes.* Proc Natl Acad Sci U S A, 1984. **81**(19): p. 6159-63.

50. Meier, W.P. and W. Knoll, eds. *Polymer Membranes/Biomembranes*. Vol. 224. 2010, Springer: New York.

51. Groves, J.T. and S.G. Boxer, *Micropattern formation in supported lipid membranes.* Acc Chem Res, 2002. **35**(3): p. 149-57.

52. Groves, J.T. and M.L. Dustin, *Supported planar bilayers in studies on immune cell adhesion and communication.* J Immunol Methods, 2003. **278**(1-2): p. 19-32.

53. Mayer, L.D., M.J. Hope, and P.R. Cullis, *Vesicles of variable sizes produced by a rapid extrusion procedure.* Biochimica et Biophysica Acta (BBA) - Biomembranes, 1986. **858**(1): p. 161-168.

54. Barenholz, Y., et al., *A simple method for the preparation of homogeneous phospholipid vesicles.* Biochemistry, 1977. **16**(12): p. 2806-10.

55. Akashi, K., et al., *Preparation of giant liposomes in physiological conditions and their characterization under an optical microscope.* Biophys J, 1996. **71**(6): p. 3242-50.

56. Kaizuka, Y. and J.T. Groves, *Structure and dynamics of supported intermembrane junctions.* Biophys J, 2004. **86**(2): p. 905-12.

57. Estes, D.J. and M. Mayer, *Giant liposomes in physiological buffer using electroformation in a flow chamber.* Biochim Biophys Acta, 2005. **1712**(2): p. 152-60.

58. Reimhult, E., F. Höök, and B. Kasemo, *Intact Vesicle Adsorption and Supported Biomembrane Formation from Vesicles in Solution: Influence of Surface Chemistry, Vesicle Size, Temperature, and Osmotic Pressure†.* Langmuir, 2002. **19**(5): p. 1681-1691.

59. Tanaka, M. and E. Sackmann, *Polymer-supported membranes as models of the cell surface.* Nature, 2005. **437**(7059): p. 656-663.

60. Tamm, L.K., *Lateral diffusion and fluorescence microscope studies on a monoclonal antibody specifically bound to supported phospholipid bilayers.* Biochemistry, 1988. **27**(5): p. 1450-7.

61. Kuhner, M., R. Tampe, and E. Sackmann, *Lipid mono- and bilayer supported on polymer films: composite polymer-lipid films on solid substrates.* Biophys J, 1994. **67**(1): p. 217-26.

62. Wong, J.Y., et al., *Polymer-cushioned bilayers. I. A structural study of various preparation methods using neutron reflectometry.* Biophys J, 1999. **77**(3): p. 1445-57.

63. Deverall, M.A., et al., *Transbilayer coupling of obstructed lipid diffusion in polymer-tethered phospholipid bilayers.* Soft Matter, 2008. **4**(9): p. 1899-1908.

64. Deverall, M.A., et al., *Membrane lateral mobility obstructed by polymer-tethered lipids studied at the single molecule level.* Biophys J, 2005. **88**(3): p. 1875-86.

65. Charitat, T., et al., *Adsorbed and free lipid bilayers at the solid-liquid interface.* European Physical Journal B, 1999. **8**: p. 583-593.

66. Murray, D.H., L.K. Tamm, and V. Kiessling, *Supported double membranes.* J Struct Biol, 2009. **168**(1): p. 183-9.

67. Saffman, P.G. and M. Delbruck, *Brownian motion in biological membranes.* Proc Natl Acad Sci U S A, 1975. **72**(8): p. 3111-3.

68. Eggl, P., et al., *Diffusion in quasi two-dimensional macromolecular solutions.* Macromolecules, 1990. **23**(14): p. 3472-3480.

69. Sackmann, E., *Supported membranes: scientific and practical applications.* Science, 1996. **271**(5245): p. 43-8.

70. Merkel, R., E. Sackmann, and E. Evans, *Molecular friction and epitactic coupling between monolayers in supported bilayers.* J. Phys. France, 1989. **50**(12): p. 1535-1555.

71. Evans, E. and E. Sackmann, *Translational and rotational drag coefficients for a disk moving in a liquid membrane associated with a rigid substrate.* Journal of Fluid Mechanics, 1988. **194**(1): p. 553-561.

72. Ingber, D.E., *Cellular mechanotransduction: putting all the pieces together again.* FASEB J., 2006. **20**(7): p. 811-827.

73. Vogel, V. and M. Sheetz, *Local force and geometry sensing regulate cell functions.* Nat Rev Mol Cell Biol, 2006. **7**(4): p. 265-275.

74. Bischofs, I.B. and U.S. Schwarz, *Cell organization in soft media due to active mechanosensing.* Proceedings of the National Academy of Sciences of the United States of America, 2003. **100**(16): p. 9274-9279.

75. Gieni, R.S. and M.J. Hendzel, *Mechanotransduction from the ECM to the genome: are the pieces now in place?* J Cell Biochem, 2008. **104**(6): p. 1964-87.

76. Janmey, P.A. and C.A. McCulloch, *Cell mechanics: integrating cell responses to mechanical stimuli.* Annu Rev Biomed Eng, 2007. **9**: p. 1-34.

77. Rhee, S. and F. Grinnell, *Fibroblast mechanics in 3D collagen matrices.* Advanced Drug Delivery Reviews, 2007. **59**(13): p. 1299-1305.

78. Wong, J.Y., J.B. Leach, and X.Q. Brown, *Balance of chemistry, topography, and mechanics at the cell-biomaterial interface: Issues and challenges for assessing the role of substrate mechanics on cell response.* Surface Science, 2004. **570**(1-2): p. 119-133.

79. Engler, A.J., et al., *Embryonic cardiomyocytes beat best on a matrix with heart-like elasticity: scar-like rigidity inhibits beating.* J Cell Sci, 2008. **121**(22): p. 3794-3802.

80. Hadjipanayi, E., V. Mudera, and R.A. Brown, *Close dependence of fibroblast proliferation on collagen scaffold matrix stiffness.* Journal of Tissue Engineering and Regenerative Medicine, 2009. **3**(2): p. 77-84.

81. Wang, H.-B., M. Dembo, and Y.-L. Wang, *Substrate flexibility regulates growth and apoptosis of normal but not transformed cells.* Am J Physiol Cell Physiol, 2000. **279**(5): p. C1345-1350.

82. Winer, J.P., et al., *Bone marrow-derived human mesenchymal stem cells become quiescent on soft substrates but remain responsive to chemical or mechanical stimuli.* Tissue Eng Part A, 2009. **15**(1): p. 147-54.

83. Gray, D.S., J. Tien, and C.S. Chen, *Repositioning of cells by mechanotaxis on surfaces with micropatterned Young's modulus.* Journal of Biomedical Materials Research Part A, 2003. **66A**(3): p. 605-614.

84. Lo, C.M., et al., *Cell movement is guided by the rigidity of the substrate.* Biophys J, 2000. **79**(1): p. 144-52.

85. Hsiong, S.X., et al., *Differentiation stage alters matrix control of stem cells.* Journal of Biomedical Materials Research Part A, 2008. **85A**(1): p. 145-156.

86. Flanagan, L.A., et al., *Neurite branching on deformable substrates.* Neuroreport, 2002. **13**(18): p. 2411-5.

87. Jiang, F., et al., *Neurite Outgrowth on a DNA Crosslinked Hydrogel with Tunable Stiffnesses.* Annals of Biomedical Engineering, 2008. **36**(9): p. 1565-1579.

88. Saha, K., et al., *Substrate modulus directs neural stem cell behavior.* Biophys J, 2008. **95**(9): p. 4426-38.

89. Schwartz, M.A. and D.W. DeSimone, *Cell adhesion receptors in mechanotransduction.* Current Opinion in Cell Biology, 2008. **20**(5): p. 551-556.

90. Moore, S.W., P. Roca-Cusachs, and M.P. Sheetz, *Stretchy proteins on stretchy substrates: the important elements of integrin-mediated rigidity sensing.* Dev Cell, 2010. **19**(2): p. 194-206.

91. Craig, D., et al., *Tuning the mechanical stability of fibronectin type III modules through sequence variations.* Structure, 2004. **12**(1): p. 21-30.

92. Craig, D., et al., *Comparison of the early stages of forced unfolding for fibronectin type III modules.* Proceedings of the National Academy of Sciences of the United States of America, 2001. **98**(10): p. 5590-5595.

93. Oberhauser, A.F., et al., *The Mechanical Hierarchies of Fibronectin Observed with Single-molecule AFM.* Journal of Molecular Biology, 2002. **319**(2): p. 433-447.

94. del Rio, A., et al., *Stretching Single Talin Rod Molecules Activates Vinculin Binding.* Science, 2009. **323**(5914): p. 638-641.

95. Gee, E.P.S., D.E. Ingber, and C.M. Stultz, *Fibronectin Unfolding Revisited: Modeling Cell Traction-Mediated Unfolding of the Tenth Type-III Repeat.* PLoS ONE, 2008. **3**(6): p. e2373.

96. Zhou, A.-X., J.H. Hartwig, and L.M. Akyürek, *Filamins in cell signaling, transcription and organ development.* Trends in Cell Biology, 2010. **20**(2): p. 113-123.

97. Geiger, B. and A. Bershadsky, *Exploring the Neighborhood: Adhesion-Coupled Cell Mechanosensors.* Cell, 2002. **110**(2): p. 139-142.

98. Sharif-Naeini, R., et al., *TRP channels and mechanosensory transduction: insights into the arterial myogenic response.* Pflugers Arch, 2008. **456**(3): p. 529-40.

99. Wang, N., J.D. Tytell, and D.E. Ingber, *Mechanotransduction at a distance: mechanically coupling the extracellular matrix with the nucleus.* Nat Rev Mol Cell Biol, 2009. **10**(1): p. 75-82.

100. Jaalouk, D.E. and J. Lammerding, *Mechanotransduction gone awry.* Nat Rev Mol Cell Biol, 2009. **10**(1): p. 63-73.

101. Bray, D., *Cell Movements: from molecules to motility*. 2 ed. 2001, New York: Garland Publishing.

102. Clark, K., et al., *Myosin II and mechanotransduction: a balancing act.* Trends in Cell Biology, 2007. **17**(4): p. 178-186.

103. Alker, D., L.M. Harwood, and C.E. Williams, *Carbamate derived stable precursors for generating chiral azomethine ylids under mild conditions.* Tetrahedron, 1997. **53**(37): p. 12671-12678.

104. Murcia, M.J., et al., *Fluorescence correlation spectroscopy of CdSe/ZnS quantum dot optical bioimaging probes with ultra-thin biocompatible coatings.* Opt Commun, 2008. **281**(7): p. 1771-1780.

105. Murcia, M.J., et al., *Facile Sonochemical Synthesis of Highly Luminescent ZnS−Shelled CdSe Quantum Dots.* Chemistry of Materials, 2006. **18**(9): p. 2219-2225.

106. Dubertret, B., et al., *In vivo imaging of quantum dots encapsulated in phospholipid micelles.* Science, 2002. **298**(5599): p. 1759-62.

107. Murcia, M.J., et al., *Design of quantum dot-conjugated lipids for long-term, high-speed tracking experiments on cell surfaces.* J Am Chem Soc, 2008. **130**(45): p. 15054-62.

108. Zhang, P., et al., *Sizes of water-soluble luminescent quantum dots measured by fluorescence correlation spectroscopy.* Analytica Chimica Acta, 2005. **546**(1): p. 46-51.

109. Farhood, H., N. Serbina, and L. Huang, *The role of dioleoyl phosphatidylethanolamine in cationic liposome mediated gene transfer.* Biochimica et Biophysica Acta (BBA) - Biomembranes, 1995. **1235**(2): p. 289-295.

110. Miller, C.R., et al., *Liposome−Cell Interactions in Vitro: Effect of Liposome Surface Charge on the Binding and Endocytosis of Conventional and Sterically Stabilized Liposomes†.* Biochemistry, 1998. **37**(37): p. 12875-12883.

111. Naumann, C., T. Brumm, and T.M. Bayerl, *Phase transition behavior of single phosphatidylcholine bilayers on a solid spherical support studied by DSC, NMR and FT-IR.* Biophys J, 1992. **63**(5): p. 1314-9.

112. Chan, P.Y., et al., *Influence of receptor lateral mobility on adhesion strengthening between membranes containing LFA-3 and CD2.* J Cell Biol, 1991. **115**(1): p. 245-55.

113. Purrucker, O., et al., *Control of Frictional Coupling of Transmembrane Cell Receptors in Model Cell Membranes with Linear Polymer Spacers.* Physical Review Letters, 2007. **98**(7): p. 078102.

114. Albertorio, F., et al., *Fluid and air-stable lipopolymer membranes for biosensor applications.* Langmuir, 2005. **21**(16): p. 7476-82.

115. Kusumi, A., Y. Sako, and M. Yamamoto, *Confined lateral diffusion of membrane receptors as studied by single particle tracking (nanovid microscopy). Effects of calcium-induced differentiation in cultured epithelial cells.* Biophys J, 1993. **65**(5): p. 2021-40.

116. Schmidt, T., et al., *Characterization of Photophysics and Mobility of Single Molecules in a Fluid Lipid Membrane.* The Journal of Physical Chemistry, 1995. **99**(49): p. 17662-17668.

117. Vacklin, H.P., F. Tiberg, and R.K. Thomas, *Formation of supported phospholipid bilayers via co-adsorption with beta-D-dodecyl maltoside.* Biochim Biophys Acta, 2005. **1668**(1): p. 17-24.

118. de Gennes, P.G., *Polymers at an interface; a simplified view.* Advances in Colloid and Interface Science, 1987. **27**(3-4): p. 189-209.

119. Garg, S., et al., *Domain registration in raft-mimicking lipid mixtures studied using polymer-tethered lipid bilayers.* Biophys J, 2007. **92**(4): p. 1263-70.

120. Kiessling, V. and L.K. Tamm, *Measuring distances in supported bilayers by fluorescence interference-contrast microscopy: polymer supports and SNARE proteins.* Biophys J, 2003. **84**(1): p. 408-18.

121. Goffin, J.M., et al., *Focal adhesion size controls tension-dependent recruitment of alpha-smooth muscle actin to stress fibers.* J Cell Biol, 2006. **172**(2): p. 259-68.

122. Groves, J.T., L.K. Mahal, and C.R. Bertozzi, *Control of Cell Adhesion and Growth with Micropatterned Supported Lipid Membranes.* Langmuir, 2001. **17**(17): p. 5129-5133.

123. Murase, K., et al., *Ultrafine membrane compartments for molecular diffusion as revealed by single molecule techniques.* Biophys J, 2004. **86**(6): p. 4075-93.

124. Kenworthy, A.K., et al., *Dynamics of putative raft-associated proteins at the cell surface.* J Cell Biol, 2004. **165**(5): p. 735-46.

125. Metcalf, T.N., J.L. Wang, and M. Schindler, *Lateral diffusion of phospholipids in the plasma membrane of soybean protoplasts: Evidence for membrane lipid domains.* Proc Natl Acad Sci U S A, 1986. **83**(1): p. 95-9.

126. Chan, C.E. and D.J. Odde, *Traction dynamics of filopodia on compliant substrates.* Science, 2008. **322**(5908): p. 1687-91.

127. Gardel, M.L., et al., *Mechanical integration of actin and adhesion dynamics in cell migration.* Annu Rev Cell Dev Biol, 2010. **26**: p. 315-33.

128. Lin, C.H. and P. Forscher, *Growth cone advance is inversely proportional to retrograde F-actin flow.* Neuron, 1995. **14**(4): p. 763-71.

129. Couchman, J.R., et al., *Adhesion, growth, and matrix production by fibroblasts on laminin substrates.* J Cell Biol, 1983. **96**(1): p. 177-83.

130. Sundararaghavan, H.G., et al., *Neurite growth in 3D collagen gels with gradients of mechanical properties.* Biotechnol Bioeng, 2009. **102**(2): p. 632-43.

131. Naumanen, P., P. Lappalainen, and P. Hotulainen, *Mechanisms of actin stress fibre assembly.* J Microsc, 2008. **231**(3): p. 446-54.

132. Pellegrin, S. and H. Mellor, *Actin stress fibres.* J Cell Sci, 2007. **120**(20): p. 3491-3499.

133. Small, J.V., et al., *Assembling an actin cytoskeleton for cell attachment and movement.* Biochim Biophys Acta, 1998. **1404**(3): p. 271-81.

134. Hotulainen, P. and P. Lappalainen, *Stress fibers are generated by two distinct actin assembly mechanisms in motile cells.* J Cell Biol, 2006. **173**(3): p. 383-94.

135. Kreis, T.E. and W. Birchmeier, *Stress fiber sarcomeres of fibroblasts are contractile.* Cell, 1980. **22**(2 Pt 2): p. 555-61.

136. Couchman, J.R. and D.A. Rees, *The behaviour of fibroblasts migrating from chick heart explants: changes in adhesion, locomotion and growth, and in the distribution of actomyosin and fibronectin.* J Cell Sci, 1979. **39**: p. 149-65.

137. Chrzanowska-Wodnicka, M. and K. Burridge, *Rho-stimulated contractility drives the formation of stress fibers and focal adhesions.* J Cell Biol, 1996. **133**(6): p. 1403-15.

138. Small, J.V. and G.P. Resch, *The comings and goings of actin: coupling protrusion and retraction in cell motility.* Curr Opin Cell Biol, 2005. **17**(5): p. 517-23.

139. Guo, W.H., et al., *Substrate rigidity regulates the formation and maintenance of tissues.* Biophys J, 2006. **90**(6): p. 2213-20.

140. Petrie, R.J., A.D. Doyle, and K.M. Yamada, *Random versus directionally persistent cell migration.* Nat Rev Mol Cell Biol, 2009. **10**(8): p. 538-549.

141. Lammermann, T., et al., *Rapid leukocyte migration by integrin-independent flowing and squeezing.* Nature, 2008. **453**(7191): p. 51-55.

142. Lämmermann, T. and M. Sixt, *Mechanical modes of `amoeboid' cell migration.* Current Opinion in Cell Biology, 2009. **21**(5): p. 636-644.

143. Friedl, P., S. Borgmann, and E.B. Brocker, *Amoeboid leukocyte crawling through extracellular matrix: lessons from the Dictyostelium paradigm of cell movement.* J Leukoc Biol, 2001. **70**(4): p. 491-509.

144. Friedl, P. and K. Wolf, *Plasticity of cell migration: a multiscale tuning model.* J Cell Biol, 2010. **188**(1): p. 11-9.

145. Fackler, O.T. and R. Grosse, *Cell motility through plasma membrane blebbing.* J Cell Biol, 2008. **181**(6): p. 879-84.

146. Yoshida, K. and T. Soldati, *Dissection of amoeboid movement into two mechanically distinct modes.* J Cell Sci, 2006. **119**(Pt 18): p. 3833-44.

147. Pankova, K., et al., *The molecular mechanisms of transition between mesenchymal and amoeboid invasiveness in tumor cells.* Cell Mol Life Sci, 2010. **67**(1): p. 63-71.

148. Wolf, K., et al., *Compensation mechanism in tumor cell migration: mesenchymal-amoeboid transition after blocking of pericellular proteolysis.* J Cell Biol, 2003. **160**(2): p. 267-77.

149. Ganz, A., et al., *Traction forces exerted through N-cadherin contacts.* Biol Cell, 2006. **98**(12): p. 721-30.

150. Ko, K.S., P.D. Arora, and C.A. McCulloch, *Cadherins mediate intercellular mechanical signaling in fibroblasts by activation of stretch-sensitive calcium-permeable channels.* J Biol Chem, 2001. **276**(38): p. 35967-77.

151. le Duc, Q., et al., *Vinculin potentiates E-cadherin mechanosensing and is recruited to actin-anchored sites within adherens junctions in a myosin II-dependent manner.* J Cell Biol, 2010. **189**(7): p. 1107-15.

152. Smutny, M. and A.S. Yap, *Neighborly relations: cadherins and mechanotransduction.* J Cell Biol, 2010. **189**(7): p. 1075-7.

153. Thiery, J.P., *Epithelial-mesenchymal transitions in development and pathologies.* Curr Opin Cell Biol, 2003. **15**(6): p. 740-6.

154. Bamji, S.X., *Cadherins: actin with the cytoskeleton to form synapses.* Neuron, 2005. **47**(2): p. 175-8.

155. Cheng, S.L., et al., *A dominant negative cadherin inhibits osteoblast differentiation.* J Bone Miner Res, 2000. **15**(12): p. 2362-70.

156. Goichberg, P. and B. Geiger, *Direct involvement of N-cadherin-mediated signaling in muscle differentiation.* Mol Biol Cell, 1998. **9**(11): p. 3119-31.

157. Gumbiner, B.M., *Regulation of cadherin-mediated adhesion in morphogenesis.* Nat Rev Mol Cell Biol, 2005. **6**(8): p. 622-34.

158. Hinz, B., et al., *Myofibroblast Development Is Characterized by Specific Cell-Cell Adherens Junctions.* Mol. Biol. Cell, 2004. **15**(9): p. 4310-4320.

159. Huttenlocher, A., et al., *Integrin and cadherin synergy regulates contact inhibition of migration and motile activity.* J Cell Biol, 1998. **141**(2): p. 515-26.

160. Okamura, K., et al., *Cadherin activity is required for activity-induced spine remodeling.* J Cell Biol, 2004. **167**(5): p. 961-72.

161. Pandolfi, F., et al., *Expression of cell adhesion molecules in human melanoma cell lines and their role in cytotoxicity mediated by tumor-infiltrating lymphocytes.* Cancer, 1992. **69**(5): p. 1165-73.

162. Redfield, A., M.T. Nieman, and K.A. Knudsen, *Cadherins promote skeletal muscle differentiation in three-dimensional cultures.* J Cell Biol, 1997. **138**(6): p. 1323-31.

163. Kovacs, E.M. and A.S. Yap, *Cell-cell contact: cooperating clusters of actin and cadherin.* Curr Biol, 2008. **18**(15): p. R667-R669.

164. Lambert, M., et al., *Nucleation and growth of cadherin adhesions.* Exp Cell Res, 2007. **313**(19): p. 4025-40.

165. Mege, R.M., J. Gavard, and M. Lambert, *Regulation of cell-cell junctions by the cytoskeleton.* Curr Opin Cell Biol, 2006. **18**(5): p. 541-8.

166. Alt-Holland, A., et al., *E-cadherin suppression directs cytoskeletal rearrangement and intraepithelial tumor cell migration in 3D human skin equivalents.* J Invest Dermatol, 2008. **128**(10): p. 2498-507.

167. Wong, A.S. and B.M. Gumbiner, *Adhesion-independent mechanism for suppression of tumor cell invasion by E-cadherin.* J Cell Biol, 2003. **161**(6): p. 1191-203.

168. Cowin, P., T.M. Rowlands, and S.J. Hatsell, *Cadherins and catenins in breast cancer.* Curr Opin Cell Biol, 2005. **17**(5): p. 499-508.

169. Hazan, R.B., et al., *Exogenous expression of N-cadherin in breast cancer cells induces cell migration, invasion, and metastasis.* J Cell Biol, 2000. **148**(4): p. 779-90.

170. Ramis-Conde, I., et al., *Multi-scale modelling of cancer cell intravasation: the role of cadherins in metastasis.* Phys Biol, 2009. **6**(1): p. 016008.

171. Huang, S. and D.E. Ingber, *Cell tension, matrix mechanics, and cancer development.* Cancer Cell, 2005. **8**(3): p. 175-6.

VITA

VITA

Daniel Eugene Minner

EDUCATION

Purdue University Indianapolis, IN (August 2005 – December 2010)
Ph.D. in Chemistry
Minor in Biomolecular Imaging

Purdue University Indianapolis, IN
B.S. in Chemistry, May 2005

POSITION

2005-2010 Graduate Student. Thesis advisor: Christoph A. Naumann
Department of Chemistry and Chemical Biology
Indiana University Purdue University at Indianapolis (IUPUI)
Indianapolis, IN 46202

HONORS AND AWARDS

2010 Travel Fellowship Award, IUPUI Graduate Student Office
2007, 2008 Travel/Research Fellowship, University of Leipzig
2007 1st Place Poster Award, Indiana Microscopy Society

TEACHING/MENTORING

Course Instructor (Department of Chemistry and Chemical Biology, IUPUI)
2010 Guest Lecturer in “Biomimetics” (CHEM 696)
2006-2009 Laboratory Instructor for “Experimental Chemistry II”

2005	Laboratory Instructor for "Principles of Chemical Instrumentation"

Student Mentoring

2010	Summer Project SEED co-mentor Kevin Song
2009-2010	School year co-mentor for David O'Brien
2008-2009	Project SEED, school year co-mentor for Guilherme Sprowl
2005-2009	Undergraduate mentor in Chemical Resource Center (IUPUI)

TECHNICAL EXPERTISE

Thesis Research "Design of fluid, biomembrane-mimicking lipid bilayer substrates capable of tuning cellular mechanoresponse through regulation of substrate viscosity" (August 2005 – December 2010)

- Biocompatible Nanoparticle preparation and bioconjugation/linker design
- Sonochemical synthesis and surface functionalization of CdSe/ZnS quantum dots
- Organic and inorganic synthesis
- Fluorescence and UV-VIS spectroscopy
- Fluorescence correlation spectroscopy
- Single molecule fluorescence imaging on membrane model systems
- Preparation of lipid bilayer model membrane systems using a variety of techniques
- EPI fluorescence microscopy
- Confocal Microscopy
- Phase-contrast and differential interference contrast (DIC) microscopy

Collaborative research with Josef Käs, University of Leipzig, Germany. "Cell adsorption and motility on biomembrane-mimicking substrates of adjustable fluidity" (2007-2010)

- Cell culture and live-cell imaging
- Cellular transfection

Collaborative research with Wolfgang Goldman, University of Erlangen, Germany. "Cellular force transduction on biomembrane-mimicking lipid bilayer substrates" (2010)

- Polyacrylamide substrate preparation
- Force traction microscopy and analysis

Collaborative research with Ken Ritchie, Purdue University, West Lafayette, IN. "Design of quantum dot-conjugated lipids and proteins for high-speed single molecule tracking on cell surfaces (August 2006-2008)

- Incorporation of QD-labeled phospholipids into live cell membranes for diffusion analysis

Collaborative research with Weiming Yu, Northwestern University, Evanston. "Quantum dots as size ruler in the study of Proteinuria and kidney failure" (August 2005-2009)

- Preparation of "ultra-thin" coated quantum dots as biological rulers

PUBLICATIONS

Daniel E. Minner, Philipp Rauch, Josef Kas, Christoph A. Naumann. Fibroblasts Sense Substrate Viscosity. Submitted and currently out for review.

Michael J. Murcia, **Daniel. E. Minner**, Gina-Mirela Mustata, Kenneth Ritchie, and Christoph A. Naumann. (2008) Design of Quantum Dot-Conjugated Lipids for Long-Term, High-Speed Tracking Experiments on Cell Surfaces. *J. Am. Chem. Soc. 130* (45), p. 15054-15062.

CONTRIBUTED RESEARCH PRESENTATIONS

(*indicates presenting author)

Oral Presentations

Minner, D.E.*, Rauch, P., Kas, J., Naumann, C.A. (2010) Fibroblasts sense changes in substrate viscosity. ACS 239th National Meeting, San Francisco, CA.

Siegel, A.P.*, **Minner, D.E.**, Murcia, M.J., Tackett, L., Elmendorf, J.S., Ritchie, K., Naumann, C.A. (2010) raft recruitment processes if membrane proteins studied in planar model membranes. ACS 239th National Meeting, San Francisco, CA.

Minner, D.E.*, Murcia, M.J., Naumann, C.A. (2007) Ultra-thin quantum dot coatings for the single molecule fluorescence tracking of phospholipids and proteins. University of Leipzig.

Minner, D.E.*, Murcia, M.J., Oh, K., Ritchie, K., Naumann, C.A. (2007) Design of quantum dot-conjugated phospholipids and membrane proteins for single molecule tracking studies. ACS 233rd National Meeting, Chicago, IL.

Poster Presentations

Minner, D.E.*, Rauch, P., Kas, J., Naumann, C.A. (2010) Fibroblasts sense substrate viscosity. Biophysical Society 54th Annual l Meeting, San Francisco, CA.

Siegel, A.P.*, **Minner, D.E.**, Murcia, M.J., Elmendorf, J.S., Ritchie, K., Naumann, C.A. (2010) Monitoring Submicron and Micron-Size Membrane Compartments using Quantum Dots Monovalently Conjugated to Tracer Molecules. Biophysical Society 54th Annual Meeting, San Francisco, CA.

Minner, D.E.*, Rauch, P., Siegel, A.P., Stelzer, J., Kas, J., Sprowl, G., Harvey, K., Siddiqui, R., Atkinson, S., Naumann, C.A. (2009) Tuning Cellular Mechano-Response Using Biomembrane-Mimicking Substrates of Adjustable Fluidity. Biophysical Society 53rd Annual Meeting, Boston, MA (Poster Presentation).

Wang, P.*, **Minner, D.E.**, Stantz, K.M., Naumann, C.A., Yu, W. (2009) Biocompatible Quantum Dots for Intravital Kidney Imaging. Biophysical Society Annual Meeting.

Minner, D.E.*, Stelzer, J., Koch, D., Naumann, C.A., Kas, J., Harvey, K., Siddiqui, R. (2007) Cell adsorption and motility on biomembrane-mimicking substrates of adjustable fluidity. Local ACS Meeting, Indianapolis, IN.

Minner, D.E.*, Murcia, M.J., Naumann, C.A., Oh, K., Ritchie, K. (2007) Design of quantum dot-conjugated phospholipids and membrane proteins for single molecule tracking studies in model membranes and on cell surfaces. Indiana Microscopy Society 3rd Annual Meeting, Indianapolis, IN.

SOCIETY/RESEARCH CENTER MEMBERSHIPS

American Chemical Society (2007-present)
Biophysical Society (2008-present)
IUPUI Signature Center for Membrane Biosciences (2007-2010)
IUPUI Nanoscale Imaging Center (2006-2010)